ZAAYMAN O.C.D.

TERRAIN PROFILE ROUGHNESS MEASUREMENT AND CHARACTERIZATION

M. ING UP 1989

TERRAIN PROFILE ROUGHNESS MEASUREMENT AND CHARACTERIZATION

by

OSWALD CORNELIUS DANNHAUSER ZAAYMAN

A thesis submitted for the degree of

MASTER IN ENGINEERING

in the Faculty of Engineering

of the

University of Pretoria

November 1988

Abstract

This report deals with an investigation into the measurement and characterization of ground surface roughness, with emphasis on its' influence on vehicles. The roughness of interest is defined, whereafter the results of an extensive literature study are presented. Attention is given mainly to the techniques employed by other authors to measure the ground surface roughness. These techniques were evaluated and the slope integration method, together with the method of reporting the roughness with the Power Spectral Density, were accepted as suitable to develope and implement. A prototype system consisting of a measuring cart and software was established and subjected to acceptance tests. Design changes were implemented on the final measuring system. This system was used in field tests over cross country terrain and the results are discussed against the backdrop of other authors' results. Recommendation are made to improve the measuring system and data representation. It is concluded that the selected slope integration method and the developed hardware performs satisfactorily in measuring and presenting the surface roughness of cross country terrain.

The theory of the mathematical framework used in this work, together with the results of the field measurement, are presented in the appendices.

Acknowledgements

I would like to express my gratitude to the following people for their involvement in this study:

- William Haddad who identified the need and enthusiastically promoted the whole effort through financing and motivation.
- Anton Raath who was as usual always available for sensible guidance and excellent advice,
- Christo Schoeman who developed most of the spectral analysis software and assisted in the mathematics,
- Arnold Albrecht and Jacob Madileng who manufactured the hardware full of initiative and fresh ideas.
- Neville Young who efficiently took care of the electronics.
- Tertia du Toit who patiently handled the typing of the manuscript.
- all my collegues who showed interest and gave advice in passing.
- and lastly, my faithful wife Nicolette who always set my eyes back on the goal.

The Author
November 1988

To Nicolette,

my best friend.

CONTENTS

LIST OF SYMBOLS

a	–	Slope of straight line fit to spatial PSD function.
a_0	–	Mean value of function in Fourier series expansion.
a_k	–	Fourier series coefficient term.
$b^2[\ ]$	–	Bias of an estimate.
b_k	–	Fourier series coefficient term.
d	–	Diameter of wheelset wheel.
ds	–	Distance between samples when measuring profile.
e	–	Exponent of natural logarithm.
$f(x)$	–	Any function of a variable x.
f	–	Frequency [Hz]
f_k	–	Frequency of k'th harmonic
f_o	–	Reference frequency or centre frequency.
f_s	–	Sampling frequency.
f_c	–	Cut–off or Nyquist frequency.
$h(\tau)$	–	A weighting function of time lag τ.
h	–	Time interval between samples.
ι	–	Imaginary value defined by $\sqrt{-1}$.
	–	Index for a series of sample values.
k	–	Number of discrete term in Fourier series expansion.
ℓ	–	Track width.
m	–	Mean output from a device.
n	–	Number of values in discrete sequence { }.
n'	–	Strain hardening/softening exponent.
$p(x)$	–	Probabiliy density function.
r	–	Lag number.
	–	Number of Reversals.
s	–	Wheelbase of measuring wheelset.
t_ι	–	Time value at instant ι.

x	–	Horisontal distance.
$\{x_n\}$	–	Sequence of discrete values of the function x.
y	–	Profile height.
y_r	–	Right hand track profile
y_ℓ	–	Left hand track profile
$\dot{y}$	–	Speed of profile height (vertically).
$\ddot{y}$	–	Acceleration of profile height (vertically).
$\{y_n\}$	–	Sequency of discrete values of the function y.
$\{z_n\}$	–	Sequence of discrete values of the function z.
B	–	Frequency bandwidth.
B_e	–	Effective frequency bandwidth.
	–	Frequency resolution
D	–	Wheel diameter.
	–	Damage value with Miner cumulative damage calculation.
E	–	Modulus of Elasticity of a material.
$E[\ ]$	–	Estimation of some parameter.
F	–	Force.
	–	Dummy frequency.
G_{xy}	–	Cross Spectral Density function.
G_x	–	Power Spectral Density function.
$\hat{G}_x$	–	Estimation of PSD function.
$\tilde{G}_x$	–	Raw unsmoothed PSD.
$H(f)$	–	Frequency Response Function
H_o	–	Frequency Response Function at reference frequency f_o.
$Im(\ )$	–	Imaginary part of a complex number.
K	–	Roughness constant.
K_f	–	Fatigue notch factor.
K_t	–	Theoretical Stress concentration factor.
L	–	Total sample record length [m].
	–	Space lag in ACF calculation for spatial data.
	–	Length of measuring cart from towing hook to wheels.
L'	–	Length of shorter sample length in time averaging procedure.
M	–	Moment of force acting at a distance.
N	–	Total number of samples, sample functions or records.
	–	Any random variable.
N_f	–	Reversals to failure in fatigue analyses and testing.

R	–	Radius of curve in road.
R_x	–	Auto correlation function.
$\dot{R}_x$	-	Estimate for auto correlation function.
Re( )	–	Real part of a complex number.
S_x, S_{xy}	–	Double sided PSD and CSD functions.
T	–	Time interval or length of sampling record in time.
$W(t)$	–	Spectral window function.
W_h	–	Hanning Spectral window function.
W_{eff}	–	Effective track width of a vehicles' tyre.
X_k	–	Discrete Fourier Transform of sequence $\{x\}$
	–	Fourier series coefficient of function $x(t)$.
$X(f)$	–	Input to a linear system.
Y_k	–	Discrete Fourier Transform of Sequence $\{y\}$.
	–	Fourier series coefficient of function $y(t)$.
$y_m, \ddot{y}_m$	–	Translation and Acceleration of moving mass.
$y_p, \ddot{y}_p$	–	Translation and Acceleration of profile with time.
$Y(f)$	–	Output from a linear system.
Z_k	–	Discrete Fourier Transform of sequence $\{z\}$
α	–	Life function of material.
	–	Wheelset swivel angle relative to frame.
β	–	Weibull slope or shape parameter.
	–	Gyroscope roll angle.
δ	–	Delta function.
Δt	–	Time increment.
Δf	–	Frequency increment.
Δx	–	Increment of variable x.
$\Delta\epsilon, \Delta e$	–	Local and nominal strain respectively.
$\Delta\sigma, \Delta s$	–	Local and nominal stress respectively.
ϵ	–	Strain.
	–	Error value.
ϵ_f	–	Monotonic fracture ductility.
ϵ_b	–	Normalized bias error.
ϵ_r	–	Normalized standard error (or random error).
ϕ	–	Phase value of complex quantity.

γ	–	Spatial frequencies [c/m].
	–	Wheelset absolute swivel angle.
γ_{xy}	–	Coherence function.
Γ	–	Gamma function.
λ	–	Wavelength of profile undulation.
μ_x	–	Mean value of record x.
∞	–	Infinity.
π	–	Pi.
σ^2	–	Standard deviation or variance.
σ_f	–	Monotonic fracture strength.
σ	–	Stress.
θ	–	Gyroscope pitch angle.
τ	–	Time lag for ACF calculation.
ν	–	Vehicle or system forward speed.
ω	–	Harmonic frequency $^{2\pi}/T$.
Ψ_x^2	–	Mean square value of sample record x.

Abreviations

ACF	–	Auto Correlation Function.
CCF	–	Cross Correlation Function.
CSD	–	Cross Spectral Density Function.
FRF	–	Frequency Response Function.
FFT	–	Fast Fourier Transformation.
DFT	–	Discrete Fourier Transformation.
JDF	–	Joint Probability Density Function.
MSV	–	Mean Square Value.
PDF	–	Probability Density Function.
Var[ ]	–	Variance of an estimate.

1. INTRODUCTION

Even before the discovery of the wheel, man has been intrigued by the problem of mobility over paved and unpaved terrain. The aim was always the same - movement, progression and mobility. These factors were the source of much thought, ingenuity and also discouragement. The technology boom in the beginning of this century paved the way for more and more complex methods to approach the problem of safe, efficient and comfortable mobility. The ability of vehicles to negotiate a variety of terrains improved considerably from the 1899 "Daimler Steel-Wheeled Automobile" of the Neckarsulm Cycle Works, to the eight wheeled all-terrain vehicles of today like South Africa's latest "Rooikat". The secret lies with a thorough knowledge of the terrain properties for which the suspension, tyres, wheels and also vehicle structure are to be designed. One of these properties is the terrain roughness.

If the roughness of any terrain can be measured and characterised, independent of the vehicle which traverses it, a data bank of such information could be compiled. This data bank would then be available as design and testing input information which can be applied to existing vehicles or even to new vehicles in the design phase. This report proceeds to describe the work performed to develope a method for measuring and characterizing terrain roughness in order to compile such a data bank

2. OBJECT DEFINITION

2.1 AIM

The object of this work is to quantify ground surface irregularities which would induce vibrations into a vehicle structure which may or may not result in fatigue failure or even total collapse of any part of the structure. The data should be in such a format that it may be used as a basis for comparing the roughness of various terrains. It may be argued that what is rough to one vehicle is not rough to another vehicle. This is true, and therefore vehicles are classified in three basic groups viz. light passenger vehicles like cars, mini buses, etc, secondly heavy passenger vehicles and road bound trucks, and thirdly cross country and construction vehicles. Terrain roughness should therefore be differently defined for each category. It may also be noticed that "roughness" as such, may vary with the speed of the vehicle, therefore vehicle speed as an influencing factor in the measuring process should be considered and it is therefore desirable that the actual geometry of the terrain should be obtained.

2.2 TERRAIN CHARACTERISTICS NOT OF INTEREST

The question of mobility in a 'go,no-go' sense is ignored because it is assumed that all terrains in question are passable to all vehicles purposed to traverse these terrains. Any traction problems caused by soil composition or soil condition viz. mud, clay, wet grass, sand, etc. are excluded and it is assumed that structural fatigue or strength problems associated with variation in traction are negligable. Furthermore any obstacles larger than the vehicle wheelbase viz. rivers, embankments, gullies, etc. and also any obstacles which can be bypassed like trees, anthills, craters, etc. are excluded.

2.3 STABLE GROUND ROUGHNESS

In the light of the above exclusions the terrain in question is defined as 'hard' ground. Hard ground roughness can be divided into two types, one type consisting of such irregularities as mentioned above, viz. large rocks, tree stumps, stream beds, embankments, small hills, etc. The other type is defined as conditions that "maintain a statistically uniform character over reasonably large areas changing but gradually with distance" (Core, et al. 1965). These kind of irregularities are also defined as being 'stable' over large areas and hence the name of stable ground roughness. It is the latter ground roughness which is primarily of importance in this work.

An effort will be made not only to measure and characterize stable ground roughness but to include certain elements of the first type of hard ground roughness like large rocks, tree stumps and smaller ant hills. A suitable method to measure the profile of stable ground roughness as well as these objects should therefore be devised.

3. THEORY

Having defined the nature of the ground roughness of interest the next step would be to identify the rough ground which would pose a hindrance to vehicle locomotion. This involves a selection process which, according to Bekker (1969), consists of two elements, viz. selecting "terrain association areas" and then devising a method of sampling these areas. Terrain association areas are those areas exhibiting more or less the same soil types and surface characteristics. Such areas have been identified to a great extent by geologists but, being subjective to their own aims and purposes, these selections are not of real value to the engineer who is interested in surface characteristics inducing vibrations into vehicle structures. This has the result that certain judgement is to be applied in identifying terrain association areas and this judgement should be based on some knowledge of vehicle behaviour. The work of sampling terrain associated areas is therefore immensily reduced if one can sample only one area as being representative of all associated areas.

A sampling process is however also involved when obtaining the characteristics of a sample area. Samples of the surface characteristics should be made over this area, which would be the population according to estimation theory (See appendix A). These samples should in turn exhibit statistical properties which are descriptive of the sample areas to a certain level of confidence. This will be discussed later and also in appendix A & B.

The surface characteristics of interest in an identified area are therefore the geometrical properties of obstacles like lengths, heights, angles, thickness and distribution. These properties should be measured, or at least its' influence on a vehicle traversing the terrain should be obtained. Three approaches to this problem were found in the literature, viz.-

- having the actual physical dimensions of the surface profile available;
- having data available of an accelerometer mounted on the axle of a fifth wheel;
- having strain data of a vehicle component available.

It can be observed that the first approach is independent of vehicle type or speed and is desirable in certain applications when a comparison of the roughness of terrains are to be made. The second approach would have the vehicle forward speed as a variable, which would have to be accomodated in the output data. The third approach would have the vehicle type, tyre type, speed, etc. as influencing factors, which would need to be eliminated or compensated for in arriving at a description of the terrain roughness. This data is however very useful if only the specific vehicle is under scrutiny.

The various methods of obtaining this data will be discussed in chapter 4, but a discussion on the parameters involved will now follow.

3.1 MEASURING SURFACE PROFILE GEOMETRY

The output from the measuring device is the actual profile geometry expressed in a set of coordinates, the height y_l above an arbitrary reference plane, at every horizontal position x_l, spaced an equal distance, ds, apart.

Figure 3.1

3.1.1 Sampling

For a measurement to be representative of a given terrain the length of the sample measured should be of adequate size so that the properties of the terrain can be derived from the sample properties. (See appendix A). The sample size is largerly determined by the method of PSD calculation as described in appendix C. The smallest wavelength required in the measured data determines the sampling frequency, which is a measure of the horisontal distance between samples of the profile height. The total number of these sample points needed to form a sample record necessary for the PSD calculation determines the sample length. The sample size or length should also be of such a size that the assumption of stationarity is confirmed (See Appendix A). In other words it must be ensured that all necessary roughness properties are prevalent in the selected sample. The methods of sampling include random walks over the terrain, dividing the terrain into segments, measuring along perpendicular lines, etc. Wendenborn (1965) suggested 75 meter sample lengths as the absolute minimum for country terrains. The Waterways Experimental Station used 50 feet (15m) sample areas (Bekker 1969). Bulman (1979) suggested 200m lengths and Laib (1977) used 50m lengths.

3.1.2 Frequency bandwidth of measurement

It is necessary to define the bandwidth of wavelengths that should be measured. This is determined by the bandwidth of vibrational frequencies which would be imposed on a vehicle suspension, because the relation between the wavelength and these frequencies is the vehicle's forward speed. The vibrational frequencies affecting both human response as well as the vehicle structure should therefore firstly be defined. Bekker (1979) fixed these frequencies between 0.5

and 20 Hz and Raasch (1979) defined the bandwidth between 0.5 and 10 Hz. The following table illustrates the wavelength bandwidth used by the various investigators:

Investigator	Wavelength bandwidth [m]		
Bekker (1969)	0.01	–	30
Raasch (1979)	0.1	–	150
Crolla & Maclaurin (1986)	?	–	20
Ohmiya (1986)	0.3	–	20
Hunter (1979)	0.25	–	?
Wendenborn (1965)	?	–	30

It is obvious that the lower limit would be dictated by the resolution of the measuring device. It would also be suitable to limit the smaller wavelengths to the length of the rubber tyre footprint. The only problem would be to define the specific tyre for which the profile is measured.

3.1.3 Measuring both tracks of a vehicle

A vehicle traversing rough ground is subjected to roll movements which impose torsional strains into the vehicle structure. These roll movements result from the difference in elevation of the profile at certain transverse positions. Bekker (1969) asserts that "measuring these two profiles may be an expensive refinement that might not pay for itself in terms of improved accuracy".

Ohmiya (1986) investigated the correlation between his seperate measured profiles of the two tracks of a vehicle with the coherence function (Appendix B). He found that no correlation exists between the two tracks and this means that the transverse track profile is also accepted to be random. Other investigators considered the possibility of using a two dimensional power spectral density to characterize a two track country road (Cebon & Newland; Cote, Kozin & Bogdanoff, 1963).

3.1.4 Distortion of the ground by vehicle tyres

Measurement should possibly be done in the vehicle's track because the profile is never the same after a vehicle has passed over it. It also might not be far from the truth to assume that the profile experienced by a vehicle is the distorted one of the vehicles' track. Laib (1977) employed his measuring device in this manner and Buiman (1979) mentioned the same aspect.

3.1.5 Data representation and classification

For the detail of the mathematics to be discussed in this paragraph the reader is referred to appendix A,B, C and D.

The surface profile, as illustrated in figure 3.1, is assumed to be an ergodic, stationary, random process which exhibit Gaussian sample functions. Like with most natural phenomena, this has been proven to be an erroneous assumption in a strict mathematical sense, but this assumption is necessary in order to make any calculation effort worthwhile and sensible. (Sayles & Thomas, 1978).

The roughness of any surface is a function of the size of the irregularities together with their wavelength, or alternatively their frequency of occurence per unit distance. The property which would illustrate these parameters is the power spectral density (PSD) (See appendix B & C). A spatial PSD curve is shown in figure 3.2 when plotted on logarithmic axis.

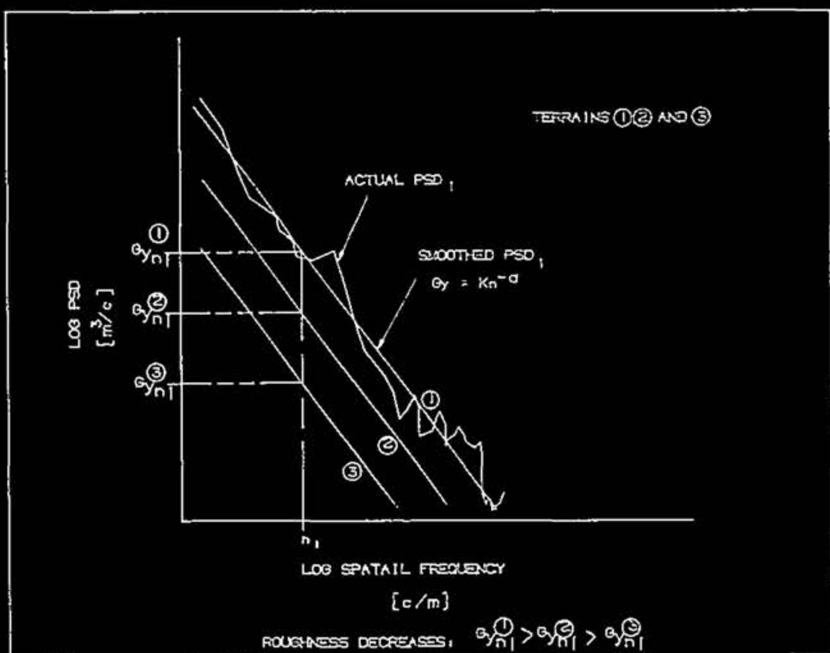

Figure 3.2 PSD (with straight line fitted to the curve)

If a straight line is fitted to the data points, employing the least squares technique, the resulting equation reveals the measure of roughness of the terrain (Appendix D):

$$G_x(\gamma) = K\gamma^a \qquad (D2)$$

K is called the roughr ss constant and is the value of the straight line PSD at a reference frequency of 0,1c/m. The slope is given by the value of a. The procedure for smoothing the initial PSD, in order to fit the straight line to the data, is set out clearly in ISO/TC 108. This international standard also gives the classification of road roughness, by means of the value of K, and is illustrated in figure 3.3

Van Deusen (1969) concluded from his work on lunar surfaces that natural random surfaces follow a power law, viz. the amplitude falls off at the square of the spacial frequency. Sayles & Thomas (1978) confirmed this fact with their investigation on surfaces ranging from virgin terrain to ball bearing surfaces. It is also illustrated by the value of the slope, 'a', which was usually found to be −2. Table 3.1 gives the values of 'a' as calculated by Van Deusen for various surfaces and table 3.2 shows those calculated by Wendenborn (1965).

The value of 'a' in equation (D2) has since then been accepted to be −2, and this was also adopted in the international standard ISO/TC/108. It can therefore be predicted for any natural surface that the slope of the straight line, fitted to the spacial PSD, would be approximately −2.

Surface	K	a
Paved Road	$1.2x10^{-5}$	2.1
Unpaved, with gravel	$1.1x10^{-5}$	2.1
Unpaved, waved	$3.7x10^{-6}$	2.4
Unpaved, rough	$2.0x10^{-6}$	3.8
Virgin, cross–country	$1.6x10^{-3}$	2.0

Table 3.1 Van Deusen values of slope 'a'. (n in cycles/ft).

Surface	K	a
Country road	$1x10^{-0.48}$	2.33
Field road	$1x10^{-0.46}$	2.24
Freshly ploughed field	$1x10^{2}$	0.38
Furrowed field	$1x10^{1.37}$	1.15

Table 3.2 Wendenborn values of slope 'a'. (n in cycles/m).

FIGURE 3.3 ISO/TC 108 ROAD ROUGHNESS CLASSIFICATION

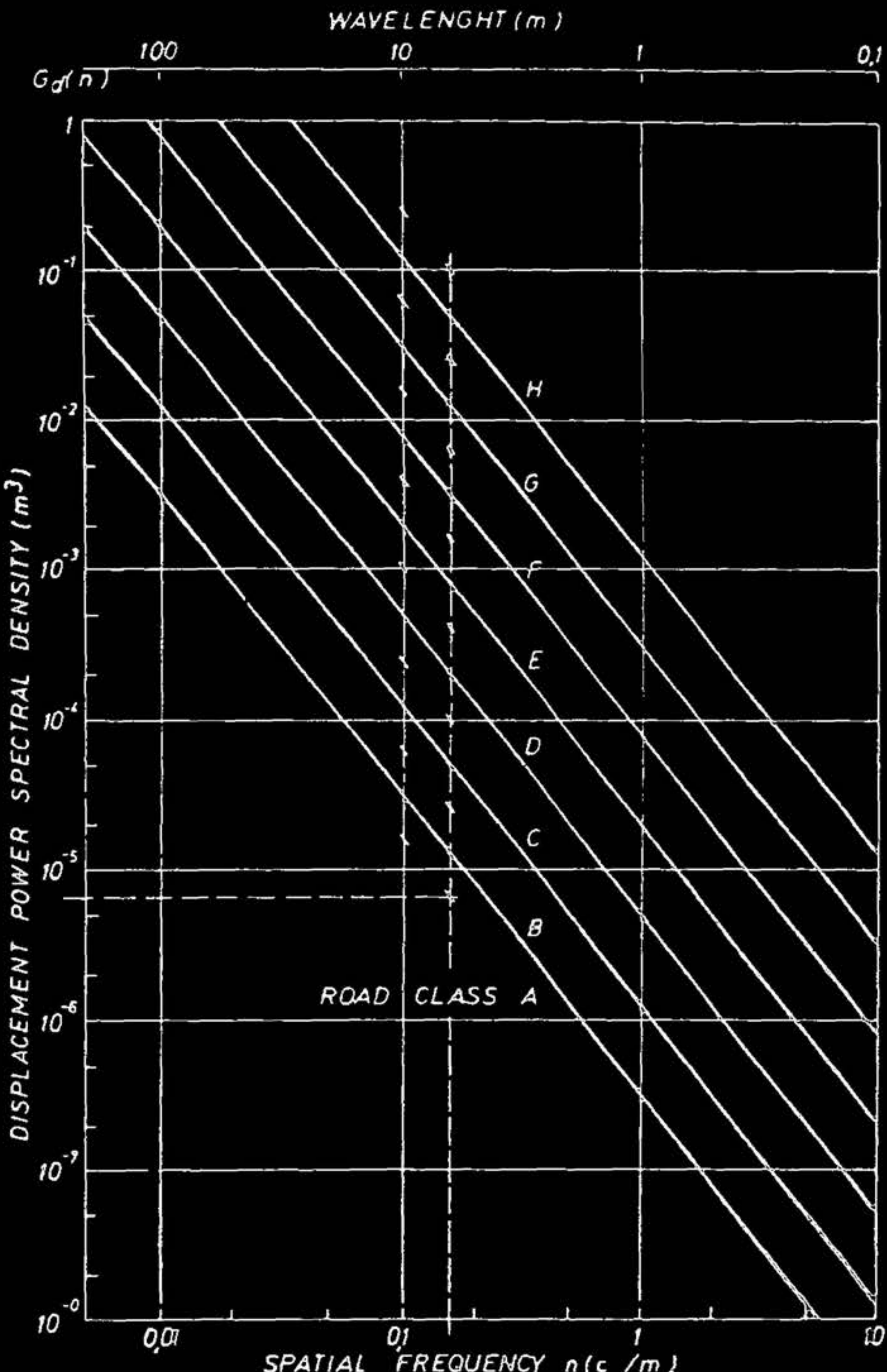

3.2 MEASURING THE ACCELERATION OF A PROFILE FOLLOWING WHEEL

The output from the measuring device is a signal of the vertical acceleration, as a function of time, measured on the axle of a wheel which follows the profile while moving forward at a speed v. The acceleration can also be measured on a damped mass fixed onto the wheel axle.

The same considerations concerning sampling, bandwidth, distortion of the ground by rubber tyres, etc. which was discussed in paragraph 3.1 apply to this measuring method and the reader is simply refered to that paragraph. The difference comes obviously with the data processing in order to arrive at the same representation format as before, viz. the spatial PSD.

3.2.1 Data processing and representation

The acceleration signal can either be integrated twice to obtain the actual ground profile as a function of time, as was done by Laib (1977), or a much easier way would be to do some transformations in the frequency domain. For the detail of the mathematics discussed in this paragraph the reader is referred to appendix E. With the transformation principle, the spatial PSD is calculated via the acceleration PSD from the acceleration data (equation E10). The PSD which is calculated from the acceleration signal is called the acceleration PSD and it's unit would be $[(m/s^2)^2/Hz]$. Note that the frequency is the time frequency in [Hz]. Because these accelerations are measured on the axle, or anywhere else except directly on the profile itself, the acceleration PSD for the profile must be calculated through the frequency response function of the system between the profile and the accelerometer. (See appendix B equation (B21)). Hereafter the acceleration PSD of the profile is transformed to the spatial PSD by incorporating the vehicle forward speed, which should be constant throughout the measuring process.

The result would be a spatial PSD as illustrated in figure 3.2. Classification of the terrain roughness proceeds exactly as for the previous method, viz. utilizing the methods of ISO/TC 108.

3.3 MEASURING THE STRAIN HISTORY OF A VEHICLE COMPONENT

In this case a strain or load history on a vehicle component is analyzed. Attention is focused on the fatigue life of the vehicle structure and how the terrain roughness influences this life. The criteria is, therefore, the amount of damage imparted to the vehicle structure by the rough terrain or road. The strain or load signal is analyzed with respect to the size of the amplitudes occuring in the signal and this is done using appropriate amplitude counting techniques developed for fatigue damage calculation procedures.

A clear distinction needs to be made between two applications of the fatigue cycle counting algorithms found in the literature. Because of the ability of these algorithms to reveal the number of cycles contained in any random signal, this property is also used to find the number of occurences of the amplitudes of a surface profile. This would directly indicate the length of the profile measured and is done because the spectral analysis described in the previous two paragraphs furnishes no information regarding the length of the sample measured. This fact would become clear with investigation of the methodology of the spectral analyses procedures and the cycle counting algorithms. For a detail description of the fatigue cycle counting and damage calculation method, the reader is refered to appendix F.

In order to find a vehicle's response to a given terrain profile, it is usually necessary to instrument critical or suitable components. 'Suitable components' implies chassis parts subjected to torsional and bending load modes, suspension or axle displacements and accelerations. 'Critical components' are usually engine mountings, suspension links, wheel hubs and stub axles, springs, etc. In order to get an adequate picture of vehicle response, it would be necessary to have quite a number of monitoring positions, the minimum being at least three, being the front and back axle vertical displacement and the relative displacement of the left and right hand wheels. (Murphy (1982)).

When investigating the loads on critical components, the criteria is the amount of damage inflicted by the random loading on the component, with the assumption that fatigue damage is cumulative. Usually a plot is generated of size of amplitudes vs the number of occurences. From this data the damage calculation is done which results in a figure indicating life spent or remaining life. (See Helfman, Collins 1981, Osgood 1982).

With a surface profile, the plot of amplitude size vs number of occurences is directly used as characteristic of the profile. A typical example of such a plot is the level crossed and the range pair plot of the counted cycles. Contrary to the PSD roughness characterization, a one figure classification of the profile roughness is not possible with this method.

This method of surface characterization is however severely vehicle dependent and is usually employed when a specific vehicle is developed or investigated. Some vehicle manufacturers have employed this method to design and build test tracks for testing of a definite vehicle configuration. The following chapter describes some of these techniques in detail.

4. METHODS FOR MEASURING SURFACE ROUGHNESS

In the previous chapter the principles involved with the basic approaches to measuring ground roughness were discussed. What follows is a critical discussion of the actual measuring devices employed by investigators in this field. Every method is judged according to the following aspects of importance:

(a) Cost.
(b) Vehicle independency.
(c) Post-processing of data. (To be kept to a minimum).
(d) The existence of a suitable reference plane.
(e) Whether the measuring technique incorporates various vehicle load modes, especially torsion.
(f) Whether the distortion of the ground because of the vehicle's weight and wheels is incorported.
(g) The role of vehicle forward speed.
(h) Resolution.
(i) Influence of measuring instruments on the accuracy of the data.
(j) Accuracy.

4.1 LEVEL, TAPE AND YARDSTICK

This is the oldest and most primitive method but it might still be the most accurate. In principle the elevation y(x) of the ground profile is directly measured relative to an arbitrary reference plane:

Figure 4.1 Level, tape and yardstick method

With the yardstick the elevation y is measured at predetermined positions x + Δx, measured with the tape. Increment size, Δx, is chosen with accuracy and purpose in mind and may be from 50mm up to 10 feet (3000 mm) apart (Bekker 1969).

4.1.1 Advantages

(a) Excellent accuracy, especially with decrease in size of increments, Δx.
(b) Instrument influence very small.
(c) Totally vehicle independent.

4.1.2 Disadvantages

(a) Extremely time consuming.
(b) Data available on clip board – processing time consuming.
(c) Measure unwanted long wavelengths and trends.

4.2 SLOPE INTEGRATION METHOD

The properties ℓ and θ (see figure 4.2) are measured in small increments from a continuous profile. The profile co-ordinates are then calculated as follows:

$$y - y_0 = \int_0^s \sin\theta \, dl \qquad (4.1)$$

$$x = \int_0^s \cos\theta \, dl \qquad (4.2)$$

This method was developed by the University of Michigan in 1961 and subsequently used by several other researchers. (Ohmiya, 1986).

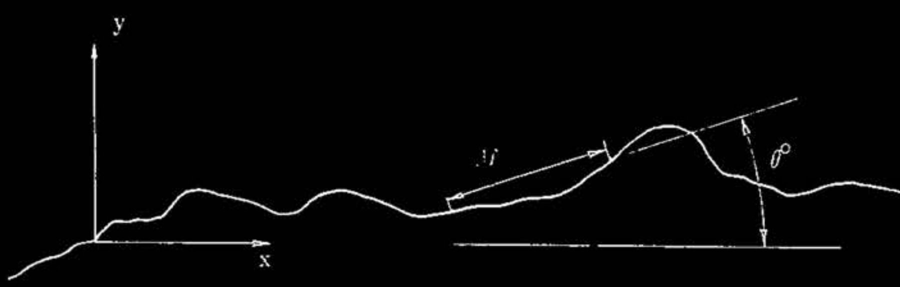

Figure 4.2 Slope integration method parameters

4.2.1 Hardware : University of Michigan (Bekker 1969)

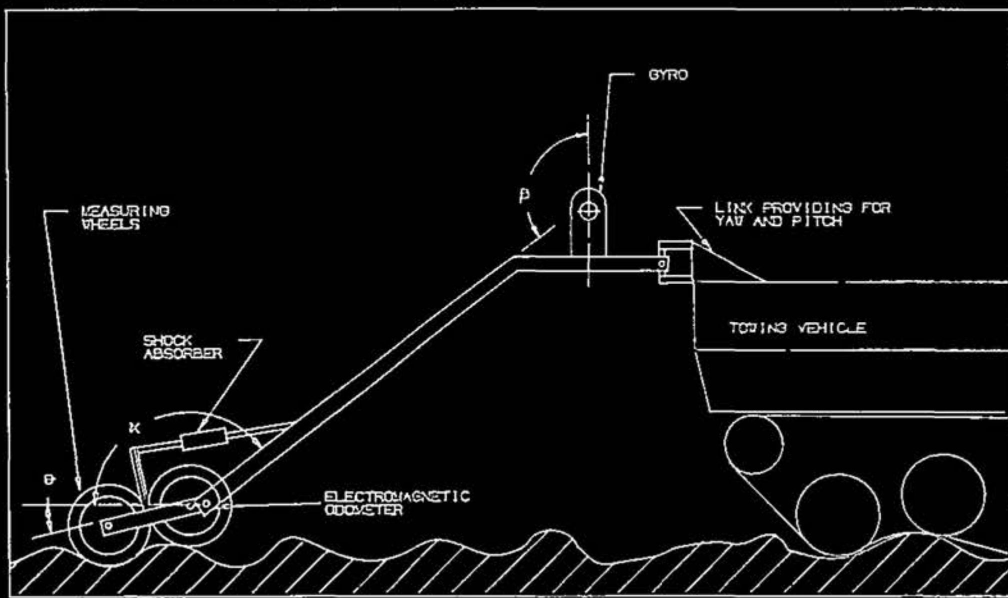

Figure 4.3 University of Michigan profilometer

An electromagnetic odometer measures the distance ℓ while a syncrosystem measures the angles α and β. The angle θ is obtained by:

$$\theta \quad = \quad 90° - (\beta - \alpha)$$

4.2.2 Hardware : Ohmiya (1986)

Ohmiya constructed his device in such a manner that the gyroscope was mounted direcly onto the swiveling wheelset and thus the angle θ was measured directly by the gyro. The distance ℓ was measured by the electromagnetic proximity sensor which was mounted beside one of the wheels and triggered by spokes on the wheel.

4.2.3 Advantages

(a) Fast and uncomplicated.
(b) Gyro gives a good absolute reference plane.
(c) Accuracy is good.
(d) Output data is in useful format.
(e) Vehicle independent.
(f) Distortion of ground by vehicle is included if measurement is done in the vehicle's track.

4.2.4 Disadvantages

(a) Measure only one vehicle track per pass – no torsional load information.
(b) Resolution limited by wheelbase of wheelset.
(c) Expensive equipment.
(d) Measures long wavelength and trends.

4.3 USING ACCELEROMETERS

4.3.1 General Motors Corporation Profilometer (Spangler & Kelly 1964)

The principle behind this system is to measure the relative displacement between the profile following wheel and a sprung mass, as well as the acceleration of the mass. The acceleration signal is then integrated twice and if combined with the measured displacement gives the road profile.

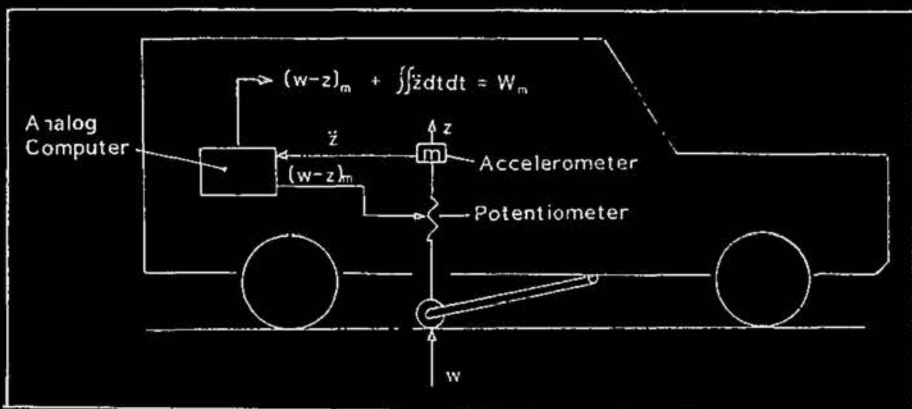

Figure 4.4 GMR Road Profilometer

4.3.1.1 Advantages

(a) Fast and uncomplicated.
(b) Profile available as an analogue time signal on magnetic tape.

4.3.1.2 Disadvantages

(a) Not suitable for rough terrain (Designed only for roads).
(b) Limited to wavelengths the size of the vehicle i.e. reference platform not so stable.
(c) Dependent on another source for horisontal displacement measurement. (Vehicle's odometer).
(d) Constant vehicle speed required.

4.3.2 Laib's method (Laib 1977)

Dr Laib of Hungary used an unsprung mass (10 kg) on a small 100 mm diameter measuring wheel, with an accelerometer mounted on the mass. (See figure 4.5).

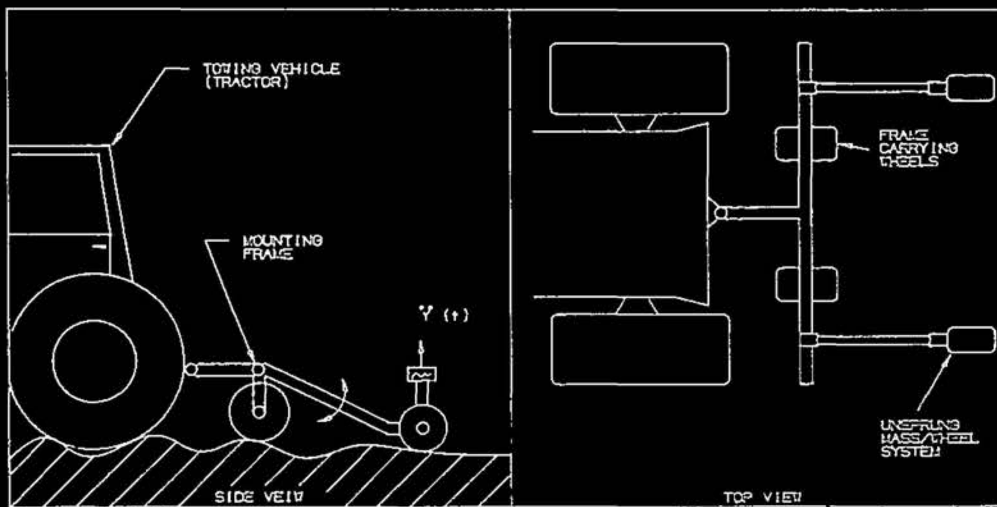

Figure 4.5 Laib's measuring device

The acceleration signal was stored digitally and the profile was obtained by digitally integrating this signal twice. From this data the power spectral density (PSD) was determined. He did not use a spatial PSD but left the data in time frequency.

4.3.2.1 Advantages

(a) Fast and very simple.
(b) Measures in the vehicle's track – incorporates distortion of the ground by the tyres.
(c) Suitable for medium rough terrains like ploughed lands, etc.
(d) Vehicle independent.

4.3.2.2 Disadvantages

(a) Horisontal distance measured by vehicle travel. (Odometer or time/distance).
(b) Constant vehicle speed is required and this might be difficult to obtain on very rough ground.
(c) Sensitivity of accelerometer might present a problem at low speeds.

4.3.3 Hunter's Method (Hunter 1979)

AGM Hunter of Scotland used a method where he towed a light metal frame with a rigid wheel (diameter 588 mm) over the profile of a ploughed land. The vertical acceleration of the wheel axle was measured.

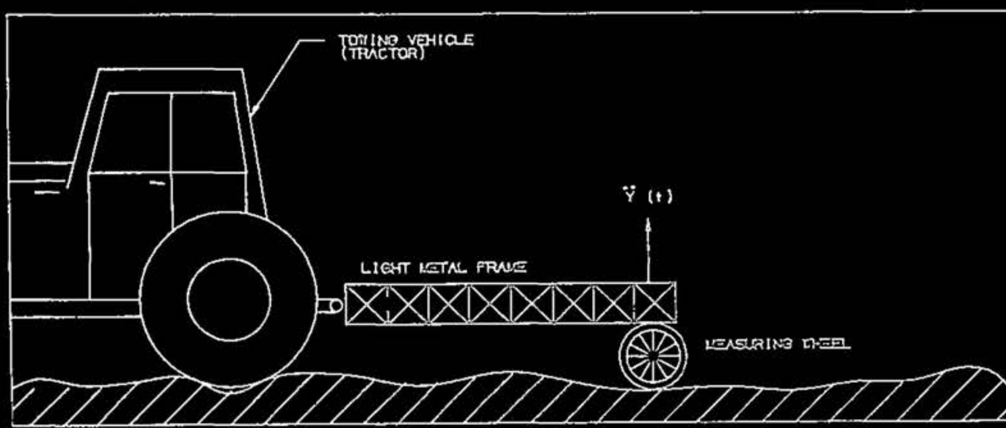

Figure 4.6 Hunter's measuring device

He used the technique of transforming the acceleration PSD to the spatial PSD. (See appendix E). The data was therefore never available as the coordinates of the profile.

4.3.3.1 Advantages

(a) Fast and uncomplicated.
(b) Inexpensive instrumentation.
(c) Accuracy is good.
(d) Vehicle independent.

4.3.3.2 Disadvantages

(a) Hard ground results in wheel bouncing because of light frame.
(b) Large wavelengths are omitted.
(c) Constant vehicle speed is required.

4.3.4 Fujimoto's Method (Fujimoto 1983)

Fujimoto used a pneumatic rubber fifth wheel towed at constant speed behind a light truck. An accelerometer was mounted on the wheel axle and a PSD was obtained with the help of the transformation process described in appendix E.

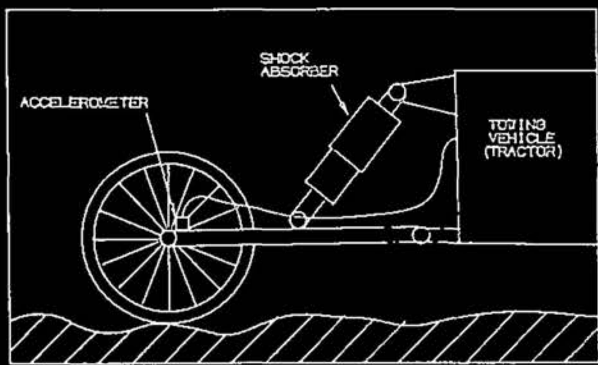

Figure 4.7 Fujimoto's measuring device

4.3.4.1 Advantages

(a) Fast and uncomplicated.
(b) Inexpensive instrumentation.
(c) Vehicle independent.

4.3.4.2 Disadvantages

(a) Non–lineariy of rubber fifth wheel.
(b) Same as 4.3.3.2.

4.4 FATIGUE CYCLE COUNT AND CUMULATIVE DAMAGE CALCULATION METHODS

4.4.1 Opel Kadett's Method (Helfman)

In order to monitor different critical positions, 24 transducers, which included displacement transducers and strain gauges, were fitted onto a vehicle. The measured signals were evaluated with the help of the level crossed and range pair counting methods (see appendix F). Data for 5 different tracks were thus analyzed, and for each transducer the 5 tracks distributions were plotted on the same paper (see figure 4.8). One track was chosen as the reference for comparison.

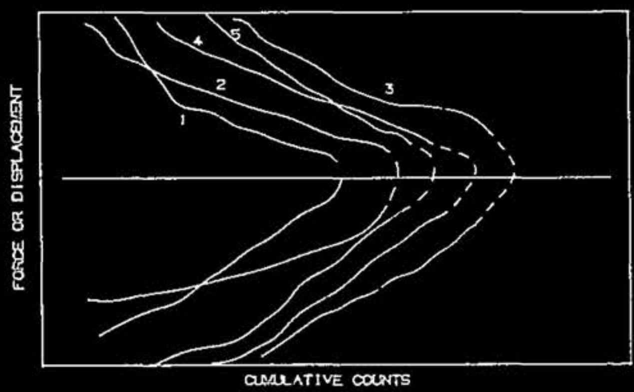

Figure 4.8 Level crossed histograms of one transducer's data for each of 5 tracks

Every distribution was shifted along the "Cumulative counts" axis until the deviation from the reference distribution became a minimum. The value of the deviation was linked to the specific track as a single number correlation for the specific transducer's data. A mean correlation figure for all 24 channels were calculated and this was used as the comparative number for a track.

4.4.1.1 Advantages

(a) Include all modes of vehicle structural loading.
(b) Distortion of ground by tyres included.
(c) No reference plane required.

4.4.1.2 Disadvantages

(a) Cumbersome data processing with so many channels of data.
(b) Vehicle dependent.
(c) No indication of terrain profile is given.

4.4.2 Freightliner Corporation's Method (Murphy 1982)

Murphy utilized the response histograms, explained in appendix E, to obtain a desired sequence of routes on a test track in order to simulate a transcontinental trip of a big transport truck.

The truck was instrumented as follows:

(a) An accelerometer on the front axle.
(b) An accelerometer on the cross member between the two back axles.
(c) Linear potentiometers which were connected in such a way as to give the difference in displacement of the two front wheel suspension units.

The output from these three transducers were analyzed with rainflow counting and plotted in the form of the response histogram. The data from the test track was also plotted and the different curve fit coefficients were compared. Test track data exhibiting unwanted large accelerations were eliminated from further consideration. The plots for the test track incorporated multiple passes at various speeds. Thus a suitable selection of test track route sequences were chosen to represent the transcontinental trip. The total length of these sequences were 2.61 miles.

4.4.2.1 Advantages

(a) Less data to process than with the previous method.
(b) Include torsion loading of vehicle's frame.
(c) Include distortion of ground by tyres.

4.4.2.2 Disadvantages

(a) Vehicle dependent and simulation requires passes over the same profile but at various speeds.
(b) Comparing 3 channels of data simultaneously.
(c) Vehicle speed required to remain constant or fixed for each route.

4.4.3 Ford Motor Company's Method (Smith, et al. 1979)

The purpose was to design a synthetic test track simulating a specific gravel road called the Silver Creek Road. 25 Channels of strain gauge data, covering the complete structure of a F250 pick–up truck, were used to match the cumulative fatigue damage imposed by the gravel road to that of the replacement test track.

A one figure value for the cumulative damage at a certain position on the vehicle was obtained for the road at certain time intervals spaced over three years. (See table 4.1). A strain based, Neuber type fatigue model employing Miner's rule for damage calculation was used (See appendix F). The α life curve equation (F5), was used together with the stress intensity factor, K_f, to determine damage values. All these values were then fitted to a Weibull distribution (see appendix F) thus producing one unique distribution of damage over a period of time for each of the 25 positions on the vehicle. This procedure is illustrated in table 4.1 and figure 4.9. Similar data was obtained for certain events (cobblestones, potholes, etc) at proving grounds accessible to Ford MC and this data was reduced to a cumulative damage number per pass of each event. Relative 50 % median values for the distributions of data at each position on the vehicle for Silver Creek Road were set as the target values, setting as limits the historical range. The purpose was therefore to mathematically combine events from the proving grounds until the severity value for every position monitored on the vehicle falls within the historical damage limits on Silver Creek Road or, that the final severity for all positions is as close as possible to the median value of each distribution for each position.

Every permutation of combination of events was tested to this criteria until satisfied. Thus the final product was a damage equivalent route made up of X passes of event A, Y passes of event B, etc.

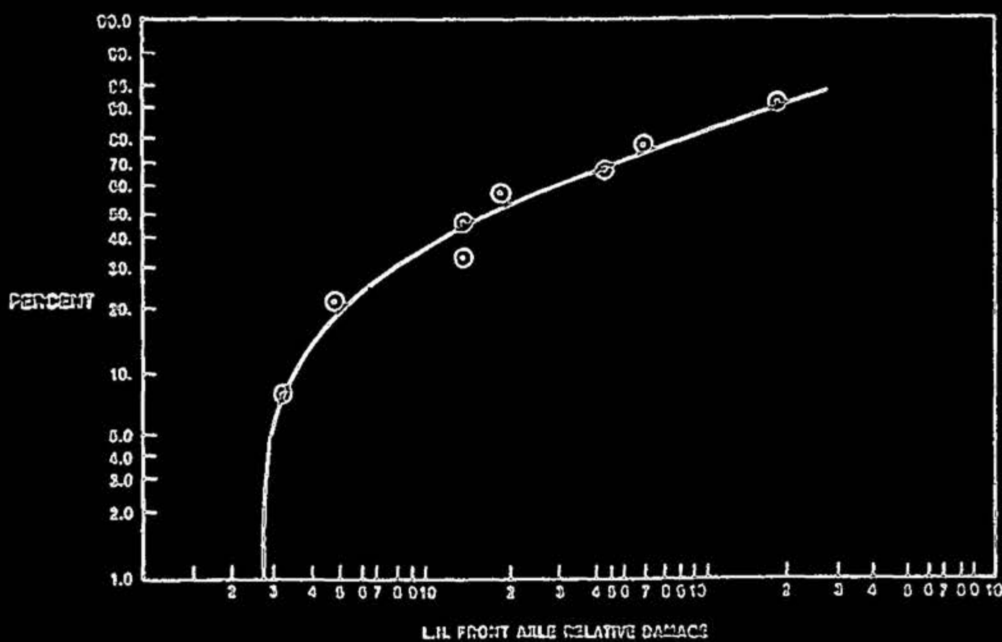

Figure 4.9 Silver Creek Road Relative Fatigue Damage Weibull Distribution

Table 4.1: Relative cumulative fatigue damage for F–250 front axle on Silver Creek country road

Month/Year	Relative damage
7/7	4.61
11/74	169.49
4/75	68.02
5/75	14.6
11/75	42.02
12/75	13.76
5/77	17.83
8/77	3.01

Smith noticed that the "final replacement road may not look or feel like the original road because the damage is duplicated with relative short high damage content events".

The route was verified by testing five Ford light trucks on it comparing incidences of damage with historical testing on the Silver Creed Road. The occurance of damage at certain mileages were consistant and no new damages were recorded.

4.4.3.1 Advantages

(a) Most accurate for one specific test vehicle.
(b) Include all modes of vehicle structural loading.
(c) Include distortion of terrain by tyres.

This method seems to be quite accurate in the light of the fact that all 25 channels of data were compared simultaneously.

4.4.3.2 Disadvantages

(a) Huge amount of data to be processed.
(b) Vehicle dependent by being isolated in its application to the measured vehicle.
(c) No indication of road profile is given and the simulation route may not even remotely resemble the actual terrain.

4.4.4 Method used by LGI (Report no VLG 87/064)

A medium truck had to travel a severe gravel road twice a day and developed cracks in the corners of the bin. A strain gauge was fitted at this position to determine the strain history during the ride. The purpose was to simulate the specific strain history by driving over certain sections of a simulation test track.

A range pair count was done on the strain gauge data from the gravel road as well as the various sections of the test track. A certain sequence of the sections was chosen by visually studying each section's range pair histogram, bearing in mind how it would influence the summation of all the section's data. The data of the selected combined sequence was then analyzed with range pair counting and the resultant histogram was again compared with the gravel road's histogram. The process was continued until satisfactorily visual correlation existed between the desired and the mathematically generated histogram.

The results were verified by driving an undamaged vehicle over the generated sequence of track sections. The same type of fatigue damage occured at the same location after several rounds of this route.

Although this method was very simple and proved to be accurate, it is necessary to notice that the sequence of sections would only simulate the load on one specific position of one specific vehicle.

4.5 OTHER METHODS

4.5.1 Photometric method (Raasch 1979)

This method is based on the human ability of spatial vision or depth perception. Depth perception resolution can be improved by widening the distance between the eyes. This can be done for instance with air photgraphs if a piece of countryside is photographed from two different positions in the air. The resulting picture, if viewed through a stereoscope, would appear three dimensional. This "appearance" can be controlled so that it can accurately represent the actual surface to scale, and is thus used to obtain a model of the terrain surface. With the necessary equipment the surface texture can be measured by adjusting a marker above the model in the field of vision horisontally in the x and y axis just by operating a crank wheel, and in the vertical direction (z–axis) by means of a foot pedal. The operator sees the marker as a point in space and is to bring it to register with the various points on the model's "surface". The movement of the marker is plotted on rolling paper but digitizing equipment is also available to facilitate storage of a digitized version of the profile on computer disc. The resolution possible is 20cm between points, depending on the terrain, vegetation, etc.

4.5.1.1 Advantages

(a) Covers a wide range of wavelengths, 0 1 – 150m, without limitations of instrumentation.
(b) High resolution possible.
(c) Does not affect soil or terrain condition.

Raasch mentions some more advantages over the measuring wheels methods viz, no restriction in the long wavelength range, wheels deforming terrain, damage to vegetation, etc. but these are either not an advantage or not important in this work.

4.5.1.2 Disadvantages

(a) Altitude resoluting.
(b) Vegetation impairs measurement – this is the greatest disadvantage of this method which also disqualify it from consideration. (One does not want to measure the height of thick grass as being the ground profile).
(c) Expensive equipment.

4.5.2 Chrysler's terrain profilometer (Bekker 1969)

Chrysler used two vehicles as stationary marking points for a horisontal reference. (See figure 4.10). A wire was stretched between the vehicles and a cart running along the wire sensed the ground profile.

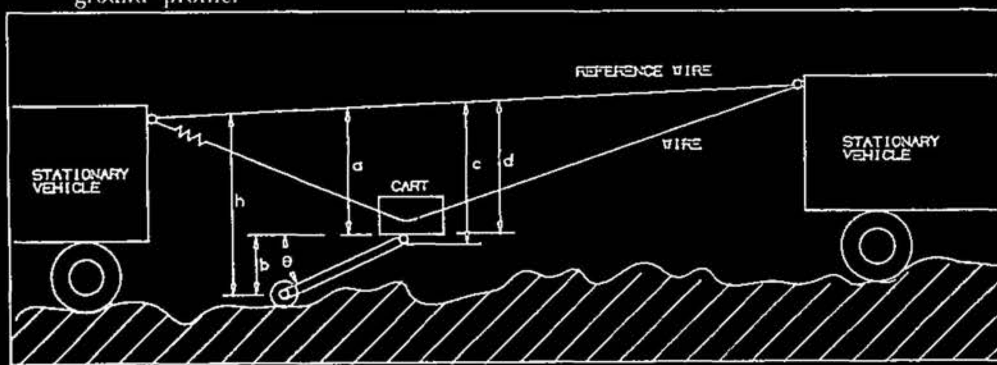

Figure 4.10 Chrysler's profilometer

Distances are measured with displacement transducers. The angle θ is measured by a potentiometer of which the output voltage is proportional to sin θ. The following calculations are done to obtain the ground profile height, h:

$$b = e \sin \theta \qquad (4.3)$$

$$H = \frac{c}{2} + \frac{d}{2} + e \sin \theta \qquad (4.4)$$

It is performed by a simple voltage circuit giving as output an analogue signal of h as a function of the horisontal distance.

4.5.2.1 Advantages

(a) Vehicle independent.
(b) No complicated data processing.
(c) Good reference plane – platform stable.
(d) Inexpensive.

4.5.2.2 Disadvantages

(a) Cumbersome equipment.
(b) Torsion of vehicle frame not included. (If parallel measurements are not done).
(c) Distortion of ground by tyres not included. (If measurement is not performed in a vehicle track).
(d) Sample length is restricted by length of reference wire.

4.5.3 Laser Profile Measuring Device (Bulman 1979)

Bulman used the device as pictured in figure 4.11. The profile following wheel could be exchanged so as to investigate the enveloping effect of different tyres and the compressibility of the soil.

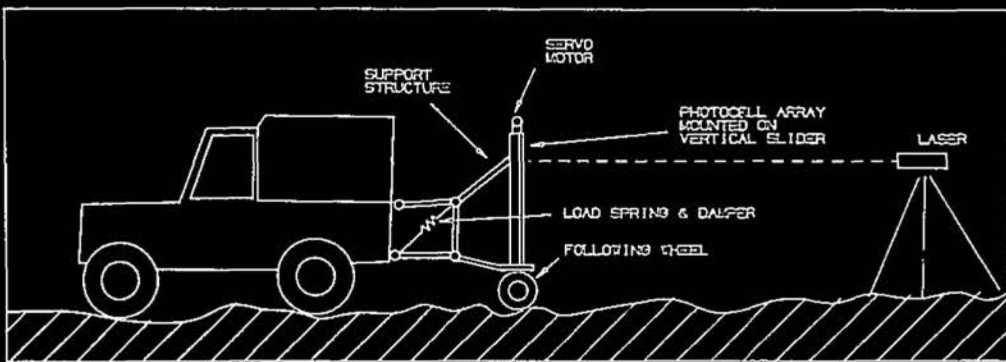

Figure 4.11 Laser profile measuring device

The position of the light beam on the array of photocells is sensed and thereby giving the vertical movement of the wheel, which is following the ground profile. Because the array is only 1m long and the vehicle might deviate vertically more than this over rough terrain, a servo motor keeps the array aligned with the light beam. The position of the array above the wheel is then added continously to the position of the light beam on the array.

4.5.3.1 Advantages

(a) Relative stable reference platform.
(b) Includes distortion of ground by tyres and vehicle weight.

4.5.3.2 Disadvantages

(a) Constant vehicle speed required.
(b) Limitations of equipment to relative straight, flat profile.
(c) Vehicle dependent: Suspension is an influencing factor.
(d) Does not include torsion of vehicle frame.

4.5.4 As proposed by University of Michigan Transportation Research Institute (Gillespie 1984)

The U of M represented the United States in an international study to correlate methods of measuring road roughness. Although the emphases was on roads and not cross country terrains, we include the method for completeness.

The device is depicted in figure 4.12. It is similar in principle to the device developed by the CSIR (Van der Merwe, et al, 1980), and is essentially a mechanical integrator. The rod passes through a hole in the body above the rear axle and is fixed onto the axle. The movement of the axle is then transferred onto the rod. The cumulative movement of each up and down stroke of the rod is used to give a single value of roughness related to the distance travelled. An international index was developed which specifies roughness numbers as well as required road speed, etc.

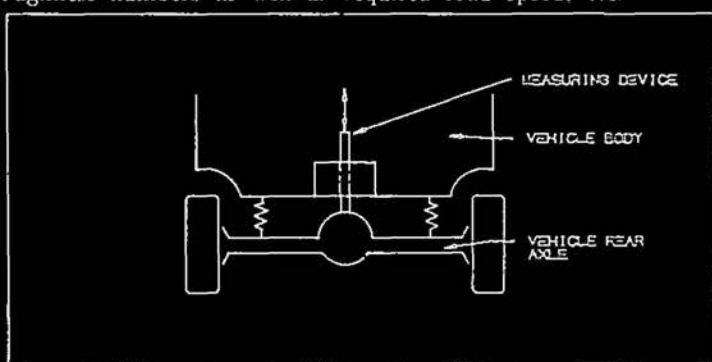

Figure 4.12 U of M and CSIR roughness measuring device

The CSIR used a stiff steel wire rolled around a drum with some kind of odometer on the drum. The translation of the axle is transferred to a rotation of the drum which is then integrated.

The measurement obtained by this method is called "average rectified slope" measured at a certain speed. The roughness number is expressed as inches per mile or meters per kilometer, where the inches or meters denote the total up and dowr movement of the rod.

The roughness index (also called the Quality Index (QI)) numbers range from 0 -- 18 m/km. Gravel roads with potholes and transverse and longitudinal erosion gulleys have an index between 13 – 18. Travel speeds on these roads are limited to below 50 km/h.

This standard has been accepted among road engineers and all efforts by those concerned indicate that it may be adopted worldwide because of its simplicity. The method was, however, developed specifically to give a simple numbered index for the condition of roads internationally, and in this respect it succeeds in its purpose. Because of the output format of the measurement it would obviously not be of any use in the field of fatigue, vehicle dynamics, etc.

5. THE PROTOTYPE MEASURING SYSTEM

5.1 CONCEPT

The concept of the slope integration method was adopted and employed in this study, the primary reason being the problem of keeping the vehicle's speed constant over very rough terrain, or alternatively measuring the vehicle speed and compensating for it afterwards in data processing, which is required for the acceleration method. This method therefore compares unfavourably to the more simple and modular slope integration method because of the effort involved to measure, or compensate for the speed of the vehicle parallel to the mean of the surface irregularities.

A further reason is that the actual profile dimensions can be used successfully in ride simulation, both on a computer vehicle model as well as in the laboratory, with the vehicle mounted on servo hydraulic actuators. The vehicle's forward speed is consequently the only variable which would need to be selected at will in the simulation process. The method of analyzing load histories of components was rejected because of its dependency on the type of vehicle and the limited application of the measured data.

The idea of a two wheeled device was implemented in order to obtain the two tracks of a vehicle and consequently being able to investigate the transverse stationarity. It would also result in knowledge of the torsional loading on a vehicle frame during movement over a rough terrain. In order to confirm the design it was decided to build a prototype device first, which would be small enough to be towed by a light passenger vehicle. Design changes could be implemented on the final version which would follow after qualification of the complete system on the prototype model.

5.2 DESCRIPTION OF THE SYSTEM

The design of the experimental device is shown in figure 5.1 and 5.2 and the completed device is shown in figures 5.3 to 5.8 at the end of this paragraph. The system comprizes a hardware side and also an instrumentation and software side. The hardware consists of the two wheeled cart having a small single wheel following the left hand track of the vehicle and a wheelset following the right hand track of the vehicle. The wheelset is constructed in such a way that there are always at least two wheels following the ground in the track profile. The pivot movement of the wheelset with respect to the cart frame is measured by a potentiometer giving as output the angle α between the wheelset frame and the cart frame (figure 5.2). A proximity switch, mounted on the wheelset, is triggered by a notched plate, attached to one of the wheels, with the result that a pulse is generated every 'ds' meter during movement.

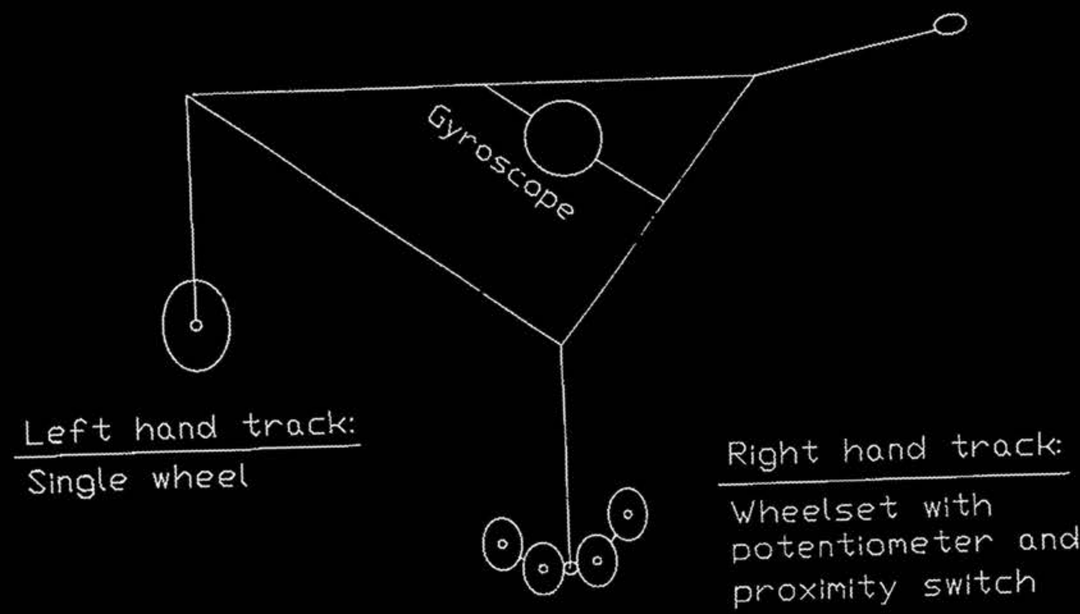

FIGURE 5.1

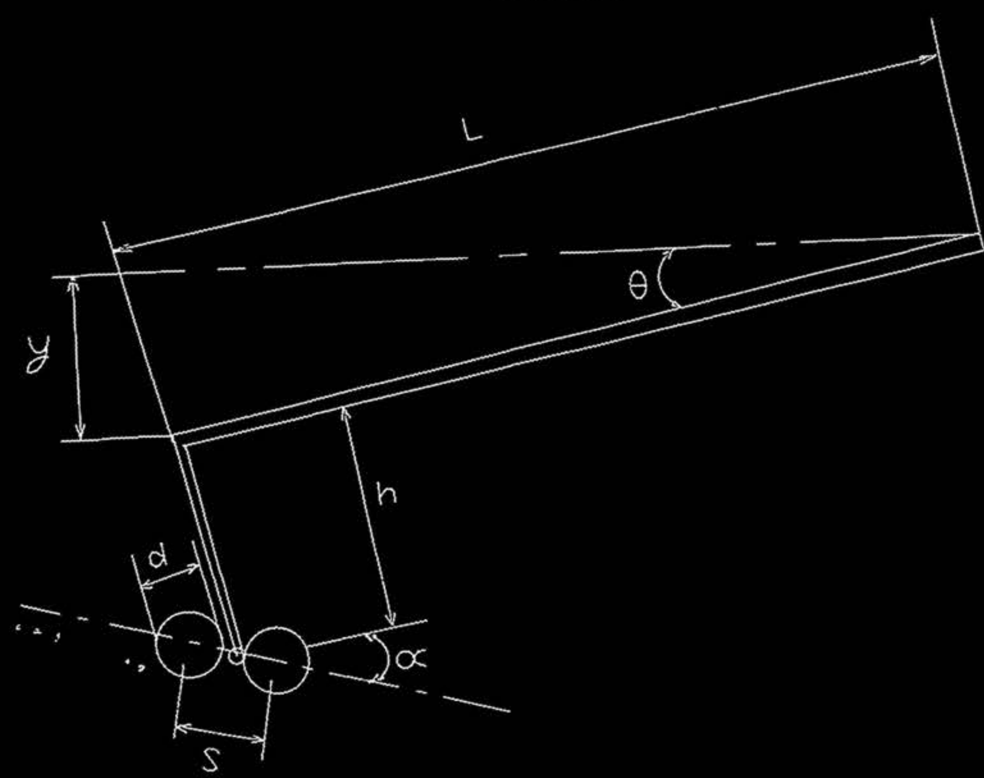

FIGURE 5.2

This gives the sloped distance which the cart has covered. In order to ensure that this wheel constantly turns, eventhough it might not be in contact with the ground, the front and rear running wheels were connected by a chain and sprocket system. (It proved, however, to be a mistake, and will be discussed later on.) A gyroscope mounted on the cart frame measures the pitch angle θ and roll angle β which the frame makes with the absolute horizontal plane as it moves behind the towing vehicle. The output signals from every transducer are stored on an FM tape recorder.

After these signals have been transferred to a digital computer, calculations are performed on them to give the coordinates of the profile. The value of θ, β and α are sampled everytime the pulse occurs in the signal of the proximity switch. These pulses are, as mentioned earlier, always a fixed distance 'ds' apart and the coordinates, x and y of the measured profile can be calculated as follows:

The angle γ which the wheelset would make relative to the absolute horisontal can be calculated simply by

$$\gamma_i = \theta_i + \alpha_i \qquad (5.1)$$

The righthand track profile height is then given by

$$y_{ri} = y_{r(i-1)} + ds \sin \gamma_i$$

and the lefthand track by (5.2)

$$y_{li} = y_{ri} + \ell \sin \beta_i$$

where ℓ is the track width.

For both tracks the horisontal displacement is given by

$$x_i = x_{i-1} + ds \cos \gamma_i \qquad (5.3)$$

The coordinates are then converted to only the value of the height, y, at equally spaced horisontal distances. The result is an array of height values, y, starting at horisontal distance x = o.

The software developed for these calculations need only be adapted for the increment distance 'ds' as well as the calibration curves of the angles θ, β and α, if a new wheelsize is implemented.

A wiring diagram of the complete hardware side is shown in appendix I.

5.3 REQUIREMENTS AND CONSIDERATIONS

The subsequent discussion refers to figure 5.2.

5.3.1 Length L should be such that the angle θ is measureable by the gyroscope and falls inside the resolution and accuracy specifications of the gyro.

5.3.2 y is the height of the smallest obstacle with wavelength of s. This is to be determined by tests and the wheelsize should be dictated by it as explained in 5.3.3.

5.3.3 The wheelsize of the wheelset should be such that the complete range of possible wavelengths is included in measurement. Care should be taken that the large obstacles do not stall the cart and that small obstacles are not bridged. Hence wheelsize directly influences resolution and accuracy.

5.3.4 Wheelbase s should tend towards the wheeldiameter d.

5.3.5 The width of the running surface of the wheelset should approximate the width of the "average" tyre in the category of interest. This can be obtained by using two small wheels running side by side in the wheelset.

5.3.6 A compromise should be made between the requirement of soft rubber wheels to dampen high frequency shocks and the requirement that the rubber should be hard enough so that the frequency response function between the ground and the axle could be approximated by one.

5.3.7 The loading on the wheels should be such that the ground pressure of the average vehicle in the category concerned is approximated.

5.3.8 In the light of the decision to cater only for light passenger vehicles, the wavelength of obstacles and irregularities of interest are bounded at the lower end by approximately 0.05m. This is because the enveloping effect of pneumatic tyres acts as a filter of vibrational inputs to the vehicle structure. At the high end it is bounded by approximately 20 m. The height of any abrupt obstacle should not be higher than approximately 100 mm. (ISO/TC 108).

5.3.9 A restriction is imposed on the maximum inclination of any large obstacle by the maximum possible swivel angle, α, of the wheelset. This angle in its' turn is restricted by the geometry of the design. The result would be that sharply inclined obstacles will be smoothed and measured as being smoother than in reality.

5.3.10 A certain amount of consideration should be given to the effect on the measuring system of grass tussocks spread among the obstacles on the terrain. The ground contact pressure should be such that these are flattened and measured as the vehicle sees them. Slippage of the wheels over the grass should be prevented.

5.3.11 The assumption is made that the profile which a vehicle "sees" or experiences, is the deformed profile after the vehicle has travelled over it. This is true for the rear wheels but not for the front wheels depending on the soil type and hardness. This assumption is, however, justified against the definition of the properties of the surfaces of interest, viz, hard ground roughness. The profile measuring wheels are therefore allowed to run in the tracks of the vehicle.

5.4 DETAIL DESIGN OF THE MEASURING CART

5.4.1 <u>Frame</u>

Refer to figure 5.2.

The angle θ is determined by the length L of the frame and the height y of the smallest obstacle of interest. The height y is actually also determined by the smallest possible wavelength s that will be accurately measured by the system.

For light commercial and passenger vehicles on rough terrain or dirt roads the smallest obstacle of interest would also dictate the wheelsize of the measuring system. A practical wheelsize was taken to be 75 mm diameter, therefore the lower limit of wavelengths which would be measured accurately is 0.075 m. The value of y was therefore decided to be approximately 15 mm.

$$\therefore \quad L = \frac{y}{\sin \theta} \tag{5.4}$$

But gyroscope accuracy = 0,83 % of 90°

and gyroscope resolution = 0,2 % of 90°

$$\Rightarrow \quad \theta \geq 0{,}75^\circ$$

$$\therefore \quad L \leq \frac{0.015}{\sin(0.75^\circ)}$$

$$L \leq 1{,}150 \text{ m}$$

5.4.2 Wheelsize

Wheelset configuration:

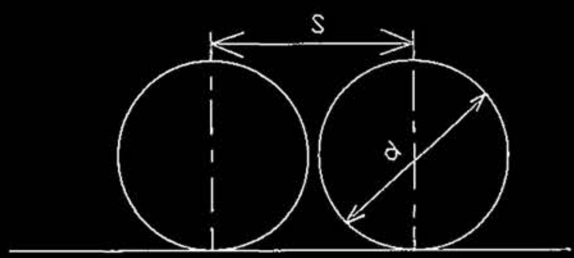

$d = s$

The smallest wavelength that will be measured accurately depends largely on the size of the obstacle:

It is clear in the figure above that the wavelengths are the same although the amplitudes differ. Wavelengths that will be measured accurately are therefore larger than d, depending on the shape of the obstacle. For simplicity it is assumed that the shape is always favourable and the lower limit wavelength is taken to be d and therefore $s \approx d$.

Assume a wavelength smaller than d:

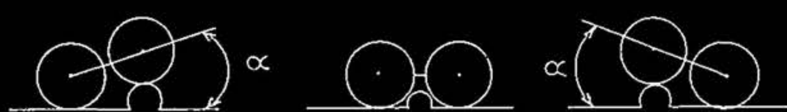

The resulting measurement of α would be as shown below while θ would be measured to be constantly zero.

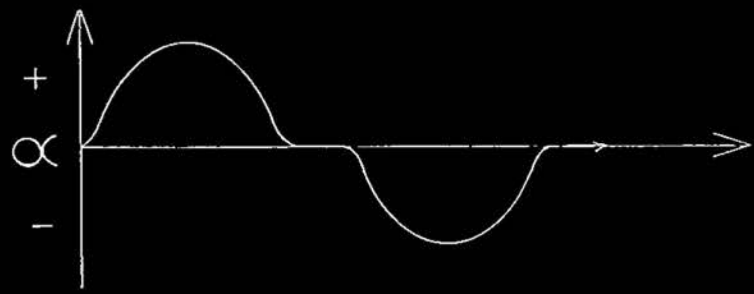

If this value of α is employed in equations 5.1 & 5.2 the result would be an obstacle measured as having a wavelength of s, which is approximately equal to d:

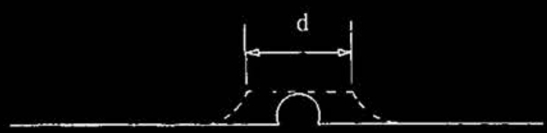

5.4.3 Configuration of wheelset

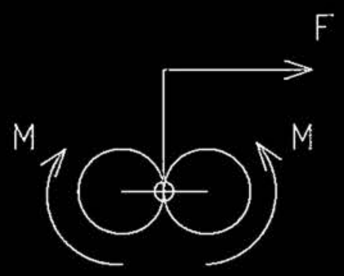

Out of a few alternatives the configuration for the wheelset, in terms of swivel point, was selected to be as illustrated above. In this configuration the weight on the wheels would act as a suspension thus eliminating the need for such a system. A moment M is constantly generated by the reaction force of the ground on the wheels.

In order to accomodate large obstacles the following concept was adopted:

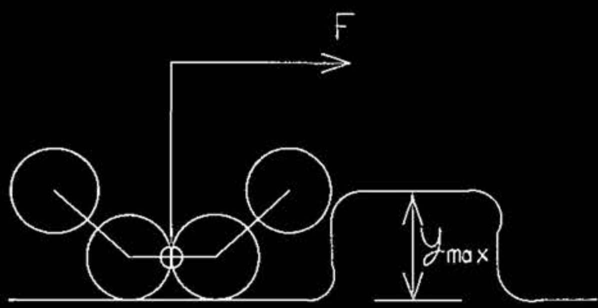

Where y_{max} would be approximately 1.5d. The higher amplitude limit is therefore also dictated by the wheelsize.

In order to accomodate the tyre width, the concept of two wheels running side by side to simulate the effective tyre width was added to the design:

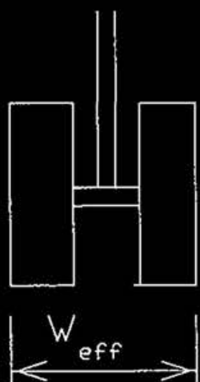

$W_{eff} \approx 80$ mm for the 155SR13 tyre used

In the light of these two factors, that of large obstacles and tyre width, it would be necessary to provide at least three measuring wheelsets. A smaller wheelset would cater for commercial passenger vehicles with a certain tyre size. The tyre diameter would determine the largest obstacle which can be taken on by the vehicle. For trucks operating on off–road conditions another wheelset would have to be available with larger wheels resulting in an increase in lower limit wavelength but also an increased capability for measuring larger obstacles. For larger wheeled cross country vehicles, like six wheeled military vehicles and construction machinery, a still larger wheelset would have to be used, typically in the region of 200 mm diameter, with the result that higher obstacles can be measured but with a sacrifice of resolution in the lower wavelengths. This sacrifice would not be serious because a large wheel is in any case insensitive to smaller obstacles. This statement is not completely true but would have to be accepted for practical reasons, otherwise a method would have to be devised which will be able to measure wavelengths from 50 mm as well as obstacle heights of 500 mm accurately.

5.4.4 Ground contact pressure

According to Bekker (1962), the equation for calculating the ground contact pressure of a pneumatic tyre includes such parameters as the mean vertical pressure within the tyre carcass, soil strength parameters, etc. This results in a complicated calculation of which the result is largerly determined by choice of tyre and soil type.

For calculating the contact pressure of solid rubber wheels, such as those used on the wheelset, the parameters are the real contact area, tyre deflection in the center and elastic constant of the rubber. These parameters can be obtained without any difficulty but what is still required are the soil deformation and soil strength parameters. As it would not be possible to cater for all types of soils, and in the light of the decision to measure only hard ground roughness, it was decided to find the correct contact pressure empirically. The weight on the wheelset should also be such that constant contact with the ground is ensured and no bouncing occurs. A compromize would therefore be necessary between enough weight to ensure constant ground contact and not too much weight as to result in incorrect contact pressure. This would have to be optimized during the planned field tests of the system. With the current design the ground was assumed to be hard and undeformable and the weight of the cart was made such as to function as a suspension system and keep the wheels of the wheelset constantly in contact with the ground.

5.5 SOFTWARE

In addition to the calculations necessary to give a set of profile heights at equally spaced horisontal distances (see paragraph 5.2), software had to be developed to perform the following:

5.5.1 Calculate the Power Spectral Density (PSD) according to the procedure described in appendix C, paragraph 5. An existing subroutine was adapted to make use of profile data because this function is usually calculated for time data.

5.5.2 Smooth the PSD according to the procedure described in ISO/TC 108 and explained in appendix D, paragraph 2. This smoothing is to be done to simplify the process of fitting a straight line to the data, which was done with the least squares technique.

5.5.3 Calculate the roughness constant after ensuring the slope has a value of –2 (see paragraph 3 earlier). This was obtained by varying the frequency limits between which the straight line was fitted to the data points. ISO/TC 108 suggests between 0.1 and 2.8 c/m which proved to be sufficient.

5.5.4 Various plotting software was adapted to provide for the format as required by the profile data, viz, spatial frequency, etc.

The detail of the mathematics employed in this software is discussed extensively in the appendices and a guideline for the use of the software is contained in appendix J.

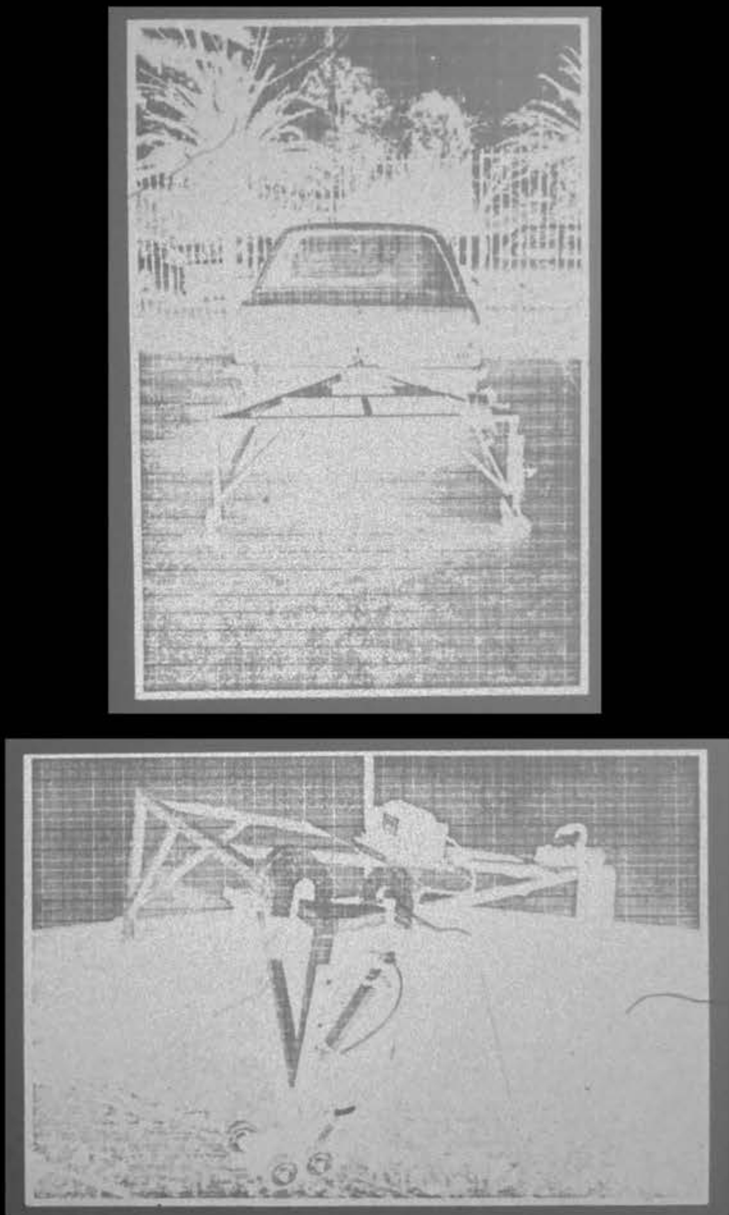

FIGURE 5.3: The Measuring Device

FIGURE 5.4: The Gyroscope

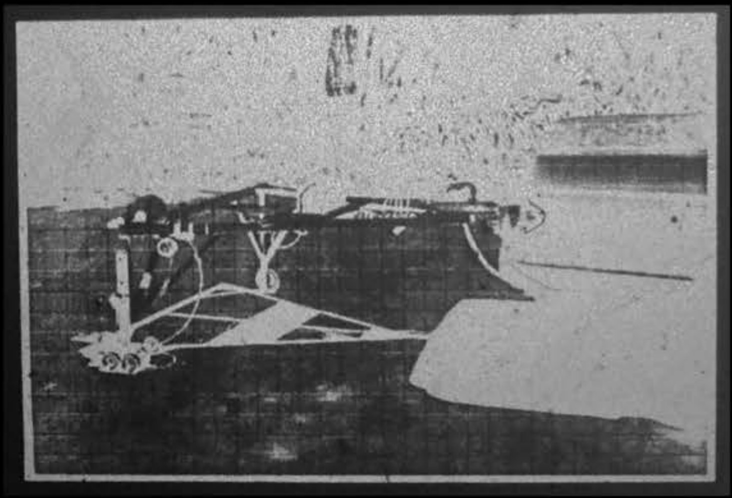

FIGURE 5.5: The Measuring Device on Towing Vehicle

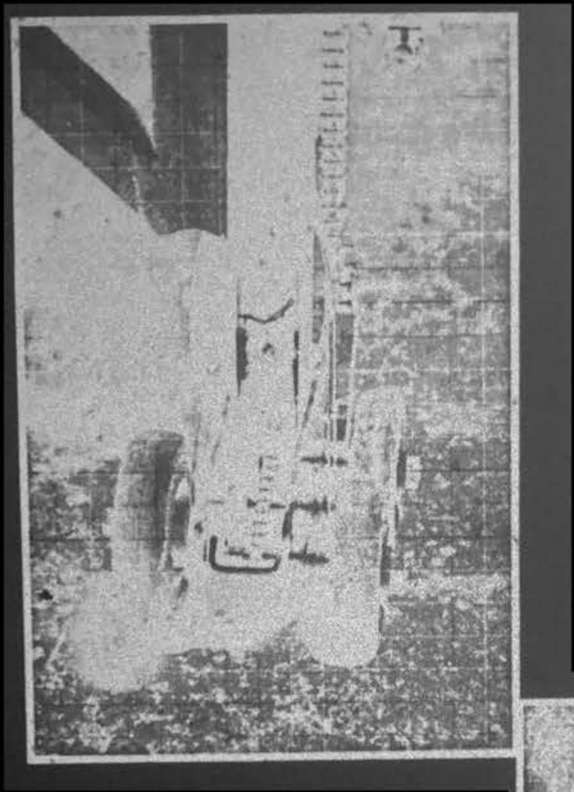

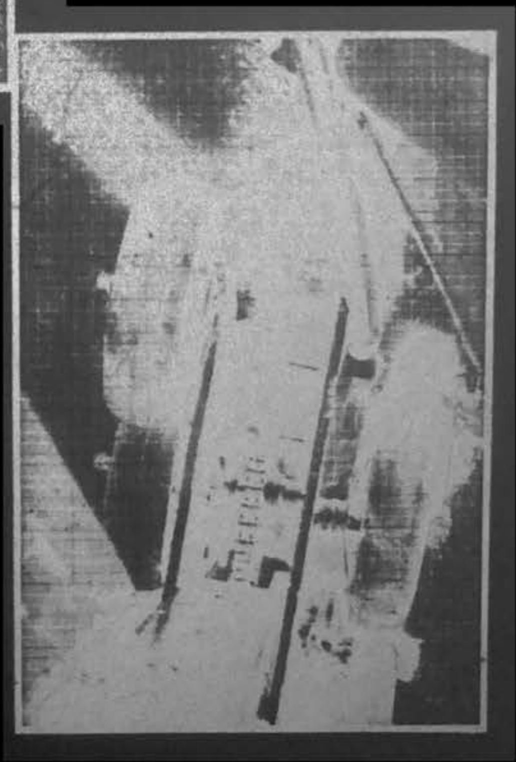

FIGURE 5.6: Wheelset detail

Notice chain/sprocket system which connects the lower two wheels. This was discarded later on when proved to be a mistake.

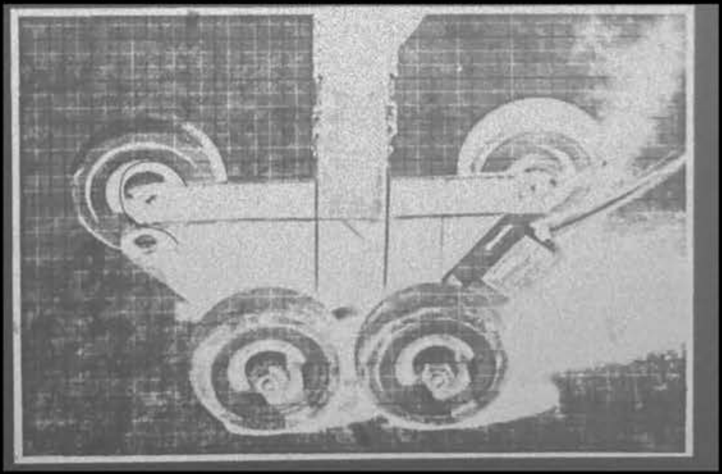

FIGURE 5.7: The wheelset configuration

Notice chain & cable system which transfers rotation of wheelset to potentiometer.

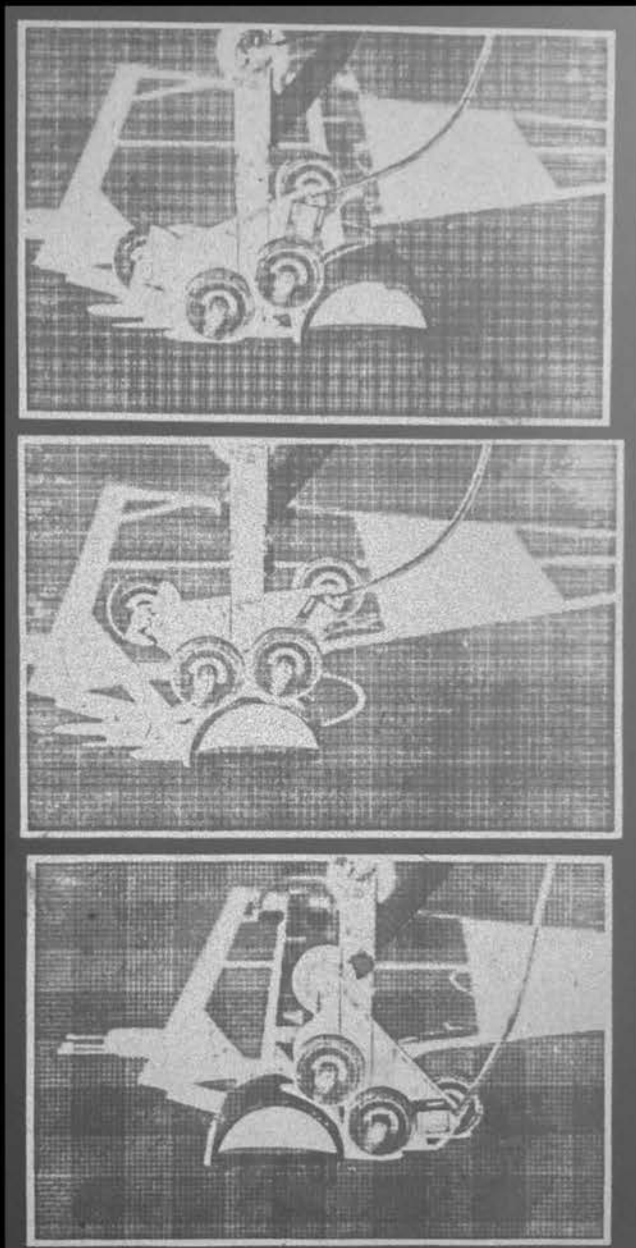

FIGURE 5.6: The wheelset movement as it negotiates an obstacle

6. QUALIFICATION TESTS

6.1 The first series of tests were done to debug the hardware and ensure sound mechanical functioning. The following synthetic obstacles were used for all tests:

Square obstacle
(a) 20 x 20 mm
(b) 30 x 30 mm
(c) 50 x 50 mm

Half round obstacles (radius)
(a) 25 mm
(b) 37,5 mm
(c) 55 mm
(d) 70 mm
(e) 125 mm
(f) 155 mm

These obstacles are only of academic importance and are employed to investigate design principles and theory. A real profile was used however, to qualify the accuracy of the device.

The results from the tests over the synthetic obstacles proved the following points:

6.1.1 The largest square obstacle should be smaller than the wheel radius (37,5 mm).

6.1.2 The largest round obstacle is in the range of 125 mm otherwise slippage of wheels occur.

6.1.3 More weight is needed on the wheelset to ensure constant ground contact.

6.1.4 The ground following wheels of the wheelset should be disconnected because they do not turn at the same speed when climbing an obstacle. This resulted in a false downward slope in all the measurements.

6.1.5 The optimum sample frequency for analogue to digital conversion was found to be 128 Hz by investigating sample points per pulse of the proximity switch. The pulse signal from the proximity switch was also filtered with a 64 Hz low pass filter and the other signals from the gyro and potentiometer were filtered by a similar 8 Hz low pass filter.

6.1.6 Unwanted transient vibrations occured on the gyro roll signal caused by bumps and also vibrations transmitted from the towing vehicle. Although the instrument was mounted in it's original rubber mountings, it proved to have too much damping for this application. A stiffer mounting was devised which improved the results but would obviously decrease gyro life expectancy.

6.1.7 Towing speed should be as low as possible, typically around 0.1 to 0.2 m/s, so that bouncing, sudden jerks and shocks, do not occur.

6.1.8 It is essential that the gyro be started in an absolute horizontal position. The zero value signals in this position are used in subsequent computor calculations as calibration values. If a value for an angle is assumed to be zero, but does not represent an actual zero angle, a false slope is induced into the calculated profile.

6.2 The second series of tests were made to prove the adherence to the initial specifications of the measuring system:

6.2.1 Obstacles smaller than the wheel diameter are not measured with any reasonable amount of accuracy. See figure K.1, in appendix K, where a square obstacle of 8 x 8 mm was incorrectly measured to have a wavelength of approximately 70 mm. (Please note that horizontal and vertical scales are not the same.)

6.2.2 The lowest obstacle to be measured is determined by gyroscope resolution which is 0,2 % of 90°, and according to equation 2.4 it gives a minimum obstacle height of 3 mm. A 3 mm plate was measured and the result is shown in figure K.2 where the distorted shape can be seen.

6.2.3 The smallest obstacle to be measured with reasonable accuracy is the halfround obstacle with radius the same as the wheel radius i.e. 37,5 mm. A comparison to the actual shape is shown in figure K.3. A smaller 20 mm radius half round obstacle was measured as having a triangular shape as shown in figure K.4. This is severely influenced by the length of the sampling distance, ds. The principle is that of the Nyquist or cut–off frequency where the accuracy is influenced by the number of sample points per wavelength. In order to measure a wavelength of 37.5 mm accurately, at least two sample points are to occur during its' traversing.

6.2.4 Small square obstacles of size 20 x 20 mm and 30 x 30 mm were measured to have the shape as shown in figure K.5 and K.6. The downward slope in figure K.6 is due to the fact that the wheelset jammed behind the obstacle during which time the front and rear wheels are lifted into the air simultaneously until the front wheel is able to climb the obstacle.

6.2.5 A sloped step obstacle was created and the measuring system proved itself capable of measuring it's shape quite accurately as shown in figure K.7.

6.2.6 Figure K.8 shows the comparison between the actual profile of a simulation concrete rough track, as obtained by measuring the profile height with dumpy level and yardstick every 40 mm, and also by the measuring cart. The stretch of road was 8 meters long with obstacle heights of approximately 150 mm. The phase difference which can be seen between the curves can be ascribed to two possible reasons:

(a) The fact that the profile was measured every 40 mm with the dumpy level method and every 39,2 mm with the measuring device which results in a 160 mm phase shift because when plotting the two profiles it is assumed that both are measured at the same incremental distance.

(b) The probable error with the dumpy level method because the measuring tape was not stretched absolutely horizontal over the obstacles when the incremental distances were measured.

6.2.7 With every measurement it was found that the lefthand track, or channel 2, is definitely not measured with the same accuracy as the right hand track. This is mainly due to two reasons:

6.2.7.1 Gyroscope roll resolution and accuracy

6.2.7.2 Susceptibility of the gyro to vibrations in the transverse or roll direction purely because of it's mounting configuration.

7. THE FINAL MEASURING CART

7.1 DESIGN CHANGES

In order to produce a workable measuring cart a first prototype was subjected to the qualification tests as described in the previous chapter and the necessary design changes were implemented in a model which will be called the final measuring cart. The reader is refered to paragraph 5.4 for the discussion which is to follow. The final device is shown in figures 7.1 to 7.7.

7.1.1 Frame

The frame was made to be adjustable in order to cater for a wide range of towing vehicles:

Length: L = 2000 mm.
Track width: B = 1400 – 2100 (adjustable).
Height: H = 950.
Towing hook height was made adjustable from 500mm to 1400mm.

7.1.2 Wheelsize

Wheelset wheels: 150 mm diameter (This is therefore also the lower wavelength limit).
Single wheel: 250 diameter.
The proximity switch was made to generate pulses every 0.039 meters.

7.1.3 Configuration of the wheelset

The extra two top wheels, which were adopted in the prototype to cater for large obstacles, were rejected and the inclination and height of the larger obstacles are simply limited by the size of the wheelset wheel.

The two wheels running side by side to accomodate tyre width were also found to be superfluous and rejected in the final design. This was motivated by the fact that the extra possible measuring width is only an asset with narrow projecting obstacles but is of no use with narrow indentations or holes in the measured profile.

7.1.4 Ground contact pressure

During the field tests with the final device, an observation of the ground pressure was made. It soon became clear that the crushing effect of the device's wheels under it's own weight was about the same as that of the light four wheel drive towing vehicle. This was observed over large grass tussocks and earth clods.

7.1.5 <u>Software and instrumentation</u>

The software employed with the system, as well as the instrumentation, remained unchanged except for a change in the calibration curves of the angles θ, β and α, the value of 'ds' and the value of the track width, ℓ. These changes are to be implemented in the program before analysis.

7.1.6 <u>General</u>

At the pivot point of the wheelset, two face to face tapered roller bearings were installed to prevent any other movement other than the required swiveling. The swivel angle was increased to just under 90° by making all protruding bolts and nuts flush with the swivel arm.

The chain and cable system for transfering the swivel movement of the wheelset to the potentiometer was replaced by a single chain over the sprockets.

All necessary instrumentation was shielded from the sun.

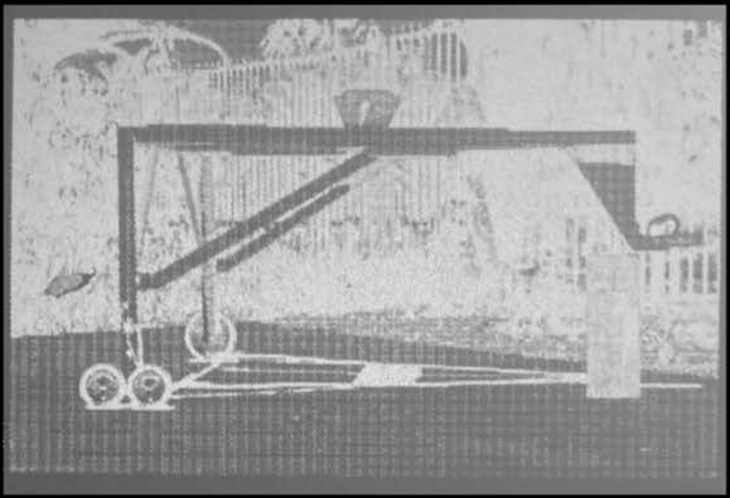

FIGURE 7.1 The Final Measuring Device.

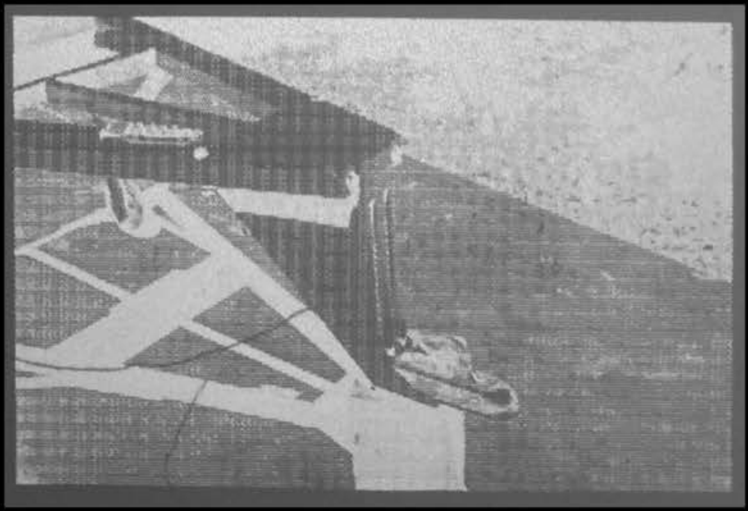

FIGURE 7.2 The Adjustable Towing Hook.

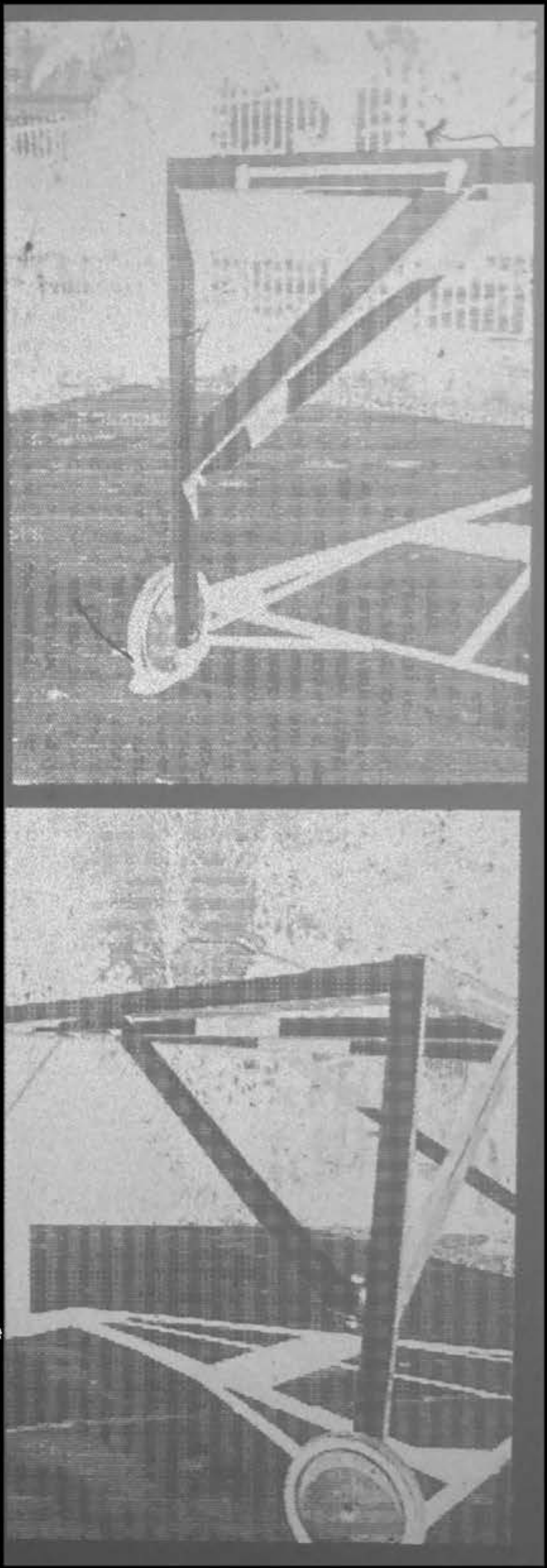

FIGURE 7.3

Two views of the adjustable track width.

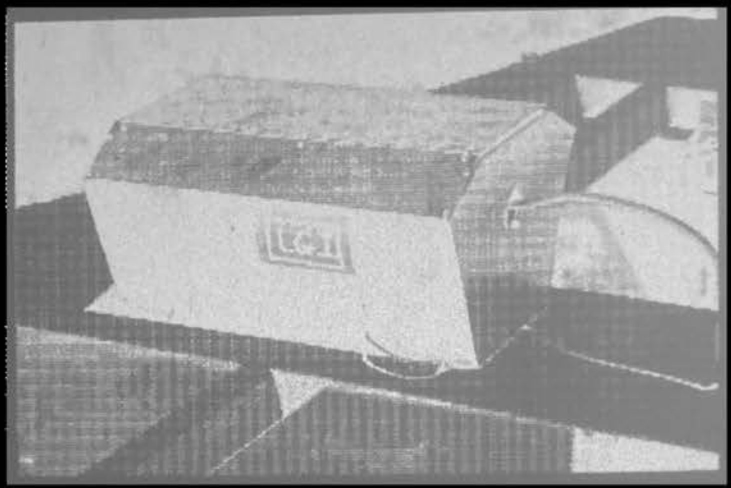

FIGURE 7.4 The Gyroscope was shielded from the sun with a small roof

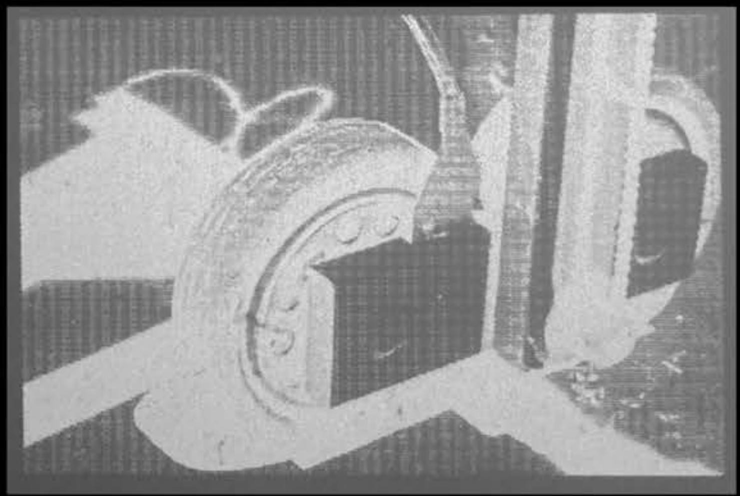

FIGURE 7.5 The Proximity Switch trigger plate can be seen mounted on the wheel.

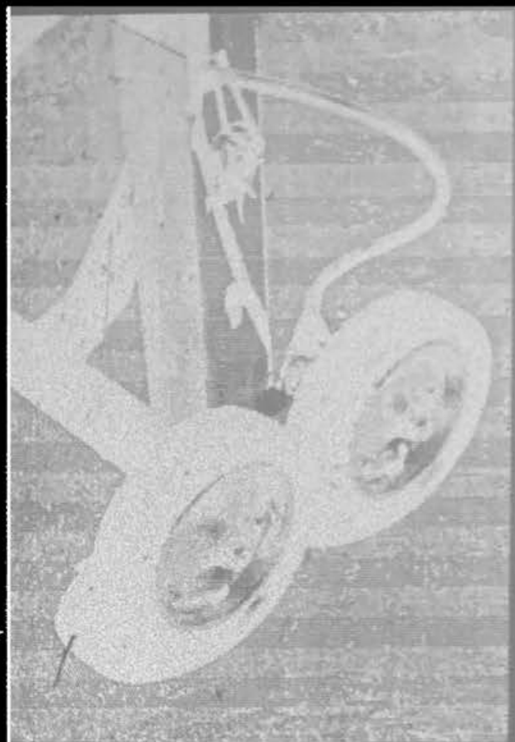

FIGURE 7.6

The wheelset with the potentiometer mounted inside the leg.

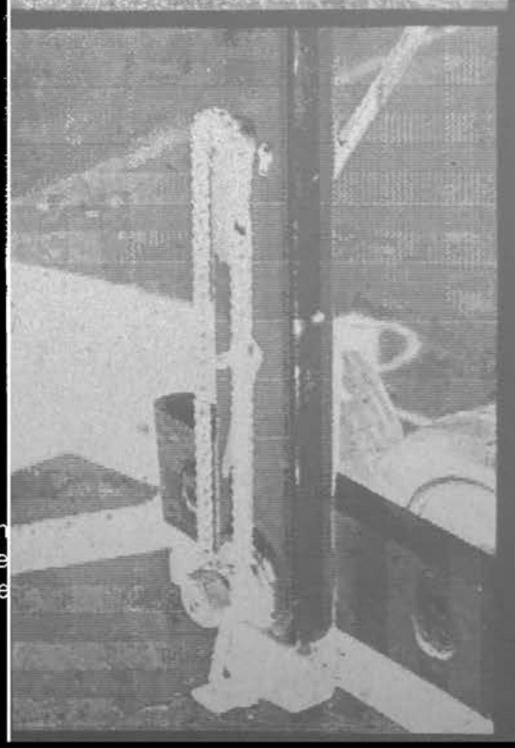

FIGURE 7.7

The chain sprocket system (uncovered) which transfers the rotation of the wheelset to the potentiometer.

8. FIELD TEST

8.1 AIM

The aim of the field tests was to verify the terrain characterization process. In order to achieve this, three terrains of obvious difference in roughness where surveyed with the final measuring device and the data analyzed. The characterization process would be accepted if a definite difference in the PSD's for the three terrains could be observed. The calculated roughness constant, K, (see appendix D) should be a distinct one figure characterization for a specific terrain.

The three measured terrains are described as follows:

(a) Dirt road – A stretch of gravel track with small lose pebbles. The track is such that a 4x4 bakkie could travel it comfortably at 60 km/h. It is illustrated in figure L1 which is the measured profile.

(b) Belgian paving – A stretch of synthetic track made up of large bricks while exhibiting also bumps and holes. It is rougher than the ground road. The Belgian paving is illustrated in figure L2.

(c) Rough track – A stretch of concrete rough terrain obtained by copying existing natural terrain. It is illustrated in figure L3.

8.2 RESULTS

The result of the measuring process is illustrated in figure L1, L2 and L3 where the profiles of the three terrains, as measured by the measuring system, are depicted. Low frequency wavelengths and trends were removed from the data as far as possible with a polynomial and linear trend removal process.

The smoothed PSD's for each terrain are depicted in figures L4 to L9. Channel 1 implies the righthand track or the wheelset side of the cart, whereas channel 2 is the lefthand track or the single wheel side of the measuring cart. To illustrate the effect of the frequency smoothing process, the unsmoothed PSD's for the rough track are included in figure L10 and L11.

The calculated value for the roughness constant, K, as well as the slope, a, for each terrain is contained in table 8.1

Table 8.1: Roughness of measured terrains

Terrain	Right wheel track		Left wheel track	
	K	a	K	a
<u>Dirt Road</u>				
(1) 0.17 –1.9*	3.76×10^{-5}	-1.12		
(2) 0.2 –2.0*			30.9×10^{-5}	–2.02
<u>Belgian Paving</u>				
(1) 0.4 –1.9*	82.67×10^{-5}	–1.8		
(2) 0.37 –1.9*			90.9×10^{-5}	1.94
<u>Rough Track</u>				
(1) 0.25 –2.5*	537×10^{-5}	–2.02		
(2) 0.35 –5.0*			193×10^{-5}	–1.95

*The frequency limits in c/m between which a straight line was fitted to the data. Number in brackets indicates channel number.

8.3 DISCUSSION

It should be remembered that the calculation of the smoothed PSD's illustrated in figure L4 to L9 is influenced by a variety of factors. These need to be stated clearly and any interpretation should be made while bearing them in mind, because the smoothed PSD is crucial in the calculation of the roughness constant, K.

Firstly, the effect of aliasing (explained in appendix H) during initial measurement should be considered. This will usually result in a relatively flatter PSD. It is obvious from the PSD's of all three terrains that the upswing in the tail ends of the curves might be caused by this. The bump at the frequencies 5 – 6 c/m in the PSD for the Belgian paving is however due to the harmonic irregularity of the 100mm paving brick used to construct the track. It might prove to be necessary to investigate the matter of aliasing in more detail before confident interpretations can be made. Hunter and Smith (1980) did a study into this matter and their results can be found in their paper.

It is obvious that frequencies higher than the cut–off frequency should be ignored: These are the frequencies higher than approximately 13 c/m, and they also do not appear in the curves.

The second important aspect to remember is the trend removal process. It did happen that the polynomial fit with least squares sometimes proved to be insufficient and low frequencies were therefore included in the data. The elimination of low frequencies or large wavelengths are surely dependent on the vehicle size and type for which the terrain is surveyed. This process should therefore be handled with sound judgement and common sense. The amount of attention being paid to the low frequency range should therefore be determined by the specific purpose for which the data is collected.

A running average method for eliminating low frequencies was not applied to the data even though some authors suggested it. The reason was that this process would eliminate frequencies in the range of interest. This could however be investigated further.

The third aspect to consider is the success of the frequency smoothing technique (see appendix C). It is evident from the PSD's of the three terrains that the curves might still be a little too rough in order to make a confident deduction from it in terms of the frequency content of the data. This applies specifically to the detection of harmonic components in the terrain. Such components are, for instance, definitely present in the profile of the Belgian paving (See figure L2), but can be observed only with some difficulty in the PSD for this terrain. The possibility also exists that frequencies of interest to vehicle locomotion may be eliminated by the frequency smoothing process (Kozin, Cote & Bogdanof, 1963).

The accuracy of the calculated PSD's is given by the expression for the complete normalized error in appendix G:

$$\epsilon_r = \frac{1}{\sqrt{B_e L}} \qquad (G10)$$

For the average sample length of L = 80 m and a frequency resolution of $B_e = 1/(1024)(0.039)$ the error is in the order of 70 %, but if expression (G11) is used, derived for the change in frequency resolution because of the frequency smoothing process, the average value for the changed frequency resolution is found to be 0.1152 . The error given by equation (G10) is then calculated to be 32.9 %. As mentioned in appendix G, this error can be reduced by making the estimate more consistent (employing a larger number of samples) and by utilizing a frequency smoothing process which gives a coarser frequency resolution. These two aspects need to be investigated further.

It is definitely necessary to consider the vibrations induced into the measuring cart during terrain surveying. These vibrations cause false slopes to be measured by the gyroscope as this instrument is extremely sensitive to vibrations. The measuring cart's stiffness rubber wheels and gyroscope mountings all play a major role in controlling these vibrations. It was obvious during measurement that the gyroscope tends to vibrate at a damped natural frequency during traversing of certain terrains. The sharp peaks at approximately 0.8 c/m in all the PSD's are most probably due to this. A stiffer gyroscope mount resulted in premature failure of the instrument and this shows the compromise necessary in stiff mountings for accurate measurement and soft mountings for instrument protection.

Figures L4 to L9 as well as table 8.1 indicate that the terrain characterization method with the PSD and roughness constant, K, is successful. The position of the curves differ relative to each other, which is an indication of the difference in roughness as predicted by the ISO/TC 108. Inspection of the calculated values for the roughness suggests that the rough track can be classified as an E or F terrain, according to ISO/TC 108, the Belgian paving as a D or E terrain whilst the smoother dirt road is a C or D terrain. These values compare favourably with terrains classified in a similar manner by Ohmiya (1986). To make a clear distinction between the PSD's of the various terrains would require some experience though. It should also be noticed that some curves seems to be too flat due to the aspects mentioned earlier on. This is evident from the values for the slope, a, in table 8.1, which are on the average lower than −2. A major reason for this can be the unwanted vibrations experienced by the gyroscope as mentioned earlier.

The measuring cart itself performed much better than its' predecessor. This is largely due to more attention having been paid to tolerances and clearances, sturdier wheel construction, more rubber on the wheels, etc. The large vibrations noticed in the measured roll data with the prototype model were reduced. This can be noticed in the relatively smoother profiles generated for the left hand track by the final system. (See figures L1, L2 and L3).

9. CONCLUSION AND RECOMMENDATIONS

A workable measuring device was created which would need only minor modifications in order to be applicable to a large variety of terrains. The system is completed by the software which was developed to give a set of profile heights for a measured terrain. This measuring system performed satisfactorily under the tests to which it was subjected but could still easily be improved upon in order to reduce some of the existing problems.

The profile characterization software, i.e. to calculate the PSD's and roughness constant, is successful but would need experience and care to use. The theory discussed in the first few appendices illustrates the fact that there is more than one way of obtaining a PSD and obviously there are some other possibilities for data preparation and analysis. These should not be seen as alternatives but rather as complementing or improving the present work.

Some recommendations and suggestions need to be made and these are discussed under seperate aspects of the work:

9.1 THE MEASURING DEVICE

9.1.1 Investigate the possibility of manually towing the device while, say, two meter cables connect the device to a vehicle which carries the power supply and recording equipment. This might improve the controllability in terms of towing speed, especially over rough terrain, where it is very difficult to maintain a slow enough towing speed. Too high towing speed results in too fast pulses from the proximity switch which may be missed during analog to digital conversion of the time data.

9.1.1 Soft, pneumatic, detachable road wheels fitted to the device would help a great deal in moving of the device between measured terrains.

9.1.2 The frequency response behaviour of the cart needs to optimized in order to eliminate all vibrational frequencies generated from the measured terrain and the towing vehicle.

9.2 INSTRUMENTATION

9.2.1 A stock of at least two more gyroscopes is required as the treatment this instrument recieves during measurement is way over its' design limits and hence results in an exceptionally short lifetime. The other alternative is to invest in a higher quality gyroscope but the high cost/high risk implications would make this impractical.

9.3 DATA ANALYSIS FOR ROUGHNESS CHARACTERIZATION

9.3.1 The assumption of stationarity and ergodicity of the profile should be investigated. Some authors have made extensive investigations into this aspect (Kozin, Cole & Bogdanoff, 1963, Bekker, 1969, etc) but a definable method of assessing this assumption when doing field measurement should be developed as a complement to the present work.

9.3.2 A detail study of the aliazing effect of the measuring wheelset should be undertaken. The influence of aliazing, in the conversion of the 'analogue' profile to the 'digital' set of profile heights, on the resultant PSD for a terrain is expected to be considerable and a means of reducing, or a least quantifying it, is necessary. The work of Hunter & Smith (1980) might be useful in this regard.

9.3.3 An investigation into more effective trend removal methods should be made, including perhaps a moving average method.

9.3.4 The error in the estimated PSD needs to be reduced by utilizing larger sample lengths and by finding a more effective frequency smoothing technique.

9.4 GENERAL

9.4.1 For light rough terrains and roads the accelerometer method (see paragraph 3.2 and appendix E) would be more practical. This measuring system should be developed as an integral part of the existing one which would create the possibility of covering these 'not–so–rough' terrains faster during measurement. A device similar to the one discussed in paragraph 4.3.2 could be integrated with the current device. Additional software is required, however, to perform the calculations described in appendix E.

9.4.2 No record of the length of the measured terrain is stored in the calculated PSD. An extensive investigation is required into using fatigue cycle counting methods, in combination with the PSD, to determine the number of undulations in a stretch of terrain and thereby creating a reference for the length of terrain which was measured, that can be used in lifetime simulation of vehicles or vehicle components. Although studies into this aspect have definitely been made (Murphy, 1982, Kaneshige, 1969, etc) it is again perhaps necessary to develope a method cooperating with the existing profile measuring system. A study of amplitude probability distributions (Van Deusen) or rainflow counting techniques to be employed instead of, or in addition to, the PSD profile characterization would be required. Care should be exercised not to lose frequency information which is of importance in computer model ride simulation and suspension component testing.

In conclusion it is noticed that the system described in this report offers an excellent baseline for further studies and investigations. It also succeeds in its' purpose of being a successful tool in measuring and characterizing the profiles of rough terrain surfaces.

APPENDIX A

PRINCIPLES OF THE ESTIMATION THEORY

Because it is much more easier to vizualize any phenomenon as a function of time than as a function of any other variable, the theory presented here are all based on processes which are functions of time. With minor modifications here and there they would apply exactly to any process or phenomenon which is a function of any other variable.

Consider a random process with output value x which is a funtion of time. Because the process is random it is impossible to predict the value of x at any time t in the future. It is though, possible to find the probability that the value of x will be between certain limits at time t. This is the basis of the estimation theory. This theory is used to estimate statistical properties, which characterizes the random process with any chosen level of confidence and they include the mean, variance, power density spectrum, etc.

When the random process is observed for a certain finite time interval T, a sample record or function x(t) is obtained representing the process concerned. It is obvious therefore that the complete process is made up of an infinite number of these sample records but it is not possible to observe them all. If a large number, say N, of these functions can be collected though, it would be "enough" to represent the random process sufficiently for estimation purposes. This collection of sample functions is called an ensemble, denoted by $\{x(t)\}$, and is an approximation of the random process.

To be able to describe the properties of the random process at any instant say t_1, the average of the value at t_1 of all the sample functions is calculated. This is called the ansemble average $E[x]$ and is illustrated in figure A1. This is also called the mean value μ_x or first moment of the random process at time t_1:

$$\mu_x(t_1) = \frac{1}{N} \sum_{k=1}^{N} x_k(t_1) \qquad \text{(A1)}$$

The values of all the sample functions at t_1 together form the first-order probability distribution whereas additional values at t_1 form the i-th order probability distributions. A probability distribution can be described by a function which in turn is called the probability density function. If a random process is said to be Gaussian all the probability distributions must be Gaussian and therefore the density functions must all be of the form depicted in figure A2, and be described by the following relation:

$$p(x_k) = \left[\frac{1}{\sqrt{2\pi}\;\sigma}\right] e^{\frac{-(x_k - \mu_x)^2}{2\sigma^2}} \qquad \text{(A2)}$$

Th. standard deviation or variance is defined as follows.

$$\sigma^2 = \frac{1}{N} \sum_{k=1}^{N} \left[x_k(t_1) - \mu_x\right]^2 \tag{A3}$$

and is simply the mean square value around the mean.

The correlation between values of the random process at two different times t_1 and $t_1 + \tau$ can be computed by taking the ensemble average of the product of these two values. This is called the joint moment or auto correlation functior and is given by

$$R_x(t_1,t_1 + \tau) = \frac{1}{N} \sum_{k=1}^{N} x_k(t_1)x_k(t_1 + \tau) \tag{A4}$$

Two additional concepts are now defined namely, stationarity and ergodicity. A random process is said to be stationary if all possible moments are independent of absolute time t and only dependent on the time seperation τ between the points. In other words if the first moment, viz the ensemble mean value (A2), is calculated at time t_1 it will have the same value if calculated at any other time t_i. The same for the second moment, R_x, with the only condition that τ does not change with each calculation. This implies that the statistical properties of the random process do not vary with time (or space, or any applicable variable other than time). A weakly stationary process is a process in which only the first and second order probability distributions are invariant with time. For practical situations an assumption of stationarity is made even though the process is weakly stationary and therefore a verification of weakly stationarity implies stationarity.

A process is said to be ergodic if it is stationary and additionally, the time average of the values in one single sample function does not differ when calculated over any other sample function. Instead of therefore describing the system by ensemble averages of the sample function, the mean and autocorrelation is calculated over say, the single sample function k, only. The mean value and autocorrelation are therefore given by

$$\mu_x(k) = \frac{1}{T}\int_0^T x_k(t)dt$$

$$R_x(\tau,k) = \frac{1}{T}\int_0^T x_k(t)x_k(t + \tau)dt \tag{A5}$$

In other words the time average and autocorrelation of the sample are the same as the ensemble average autocorrelation and any sample function therefore completely represent the random process. Ergodicity therefore implies stationarity but not visa versa. All the necessary statistical properties of an ergodic random process can therefore be obtained from one single sample function.

Take a process which is stationary. To estimate some parameter, simply called p, which can be the mean, average or power density, a finite segment of a single sample function is used. There are therefore T values of $x(t)$ where $0 \leq t \leq T-1$ which will be used to estimate p. Because x and t are in themselves random variables and the estimate $\hat{p}$ of p is a function of these variables, $\hat{p}$ is also a random variable and possess it's own probability density function of which the form and shape will be determined by the composition of the estimator and the form of the probability density functions of the random variable $x(t)$ depicted in figure A2. The estimator used to estimate p is "good" when the probability is high that $\hat{p}$ will be close to the true value of the desired parameter. A probability density function of an estimate which is "narrow" (curve A in figure A3) implies a better estimator than the less "narrow" function (curve B in figure A3). This aspect can also be characterized by the confidence interval. This concept is not discussed in detail here and can be found in the appropriate literature. It is sufficient to note that for the same level of confidence the probability of $\hat{p}$ being close to p is higher for a "good" estimator than for a "not–so–good" one.

Two estimators are usually compared by their bias and variance. The bias is defined as the true value of the parameter minus the expected value of the estimate:

$$\text{bias} = p - E[\hat{p}] \qquad \text{(A6)}$$

An unbaised estimator's probability density function have it's centre on the true value of the estimate, therefore the bias = 0. Similarly an estimator is said to be consistent if the bias and variance, which is defined as in (A3), tend towards zero if the number of observations increases. The estimate therefore becomes more accurate if a larger number of values in a sample record of the random process is employed. Furthermore an estimator is said to be efficient if the mean square error, given by

$$E[(\hat{p}_t - p)^2],$$

is smaller than the mean square error of any other estimator. These three concepts viz bias, variance and efficiency define the "goodness" of an estimator.

To be able to make these deductions for a specific random process it is necessary to know the probability distribution of the variables $x(t)$. This is obviously not possible with most natural phenomena and therefore a Gaussian distribution for these variables is assumed. It was also done during this study and this assumption validates the application of the theory discussed.

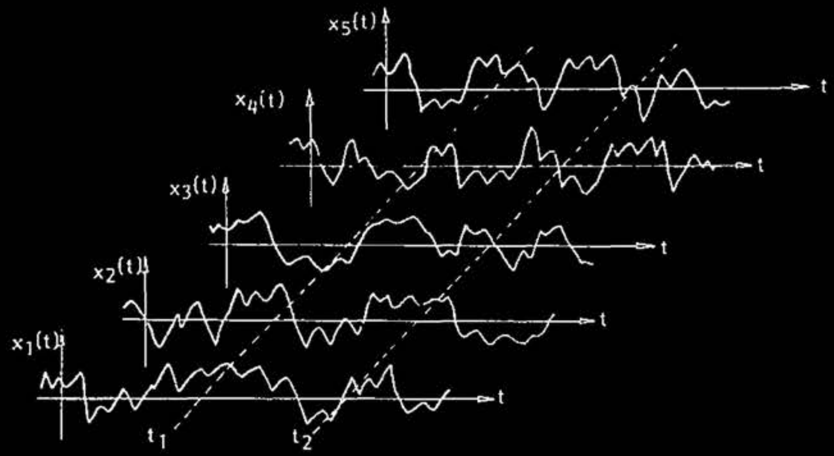

Figure A1 The Concept of Ensemble Averaging

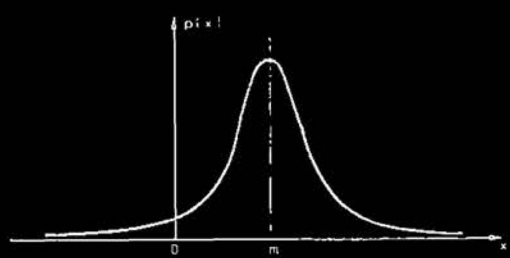

Figure A2 Probability Density for Gaussian Process

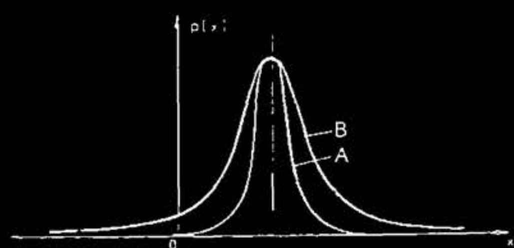

Figure A3 The 'goodness' of an estimator

APPENDIX B

DESCRIPTIVE PROPERTIES OF RANDOM DATA

For the following discussion a certain random process is assumed to be ergodic, therefore stationary and exhibiting Gaussian sample functions (See appendix A). Because of these assumptions it is not necessary to observe a large number of sample function in order to calculate the properties of the process but these can be obtained from a single sample function. Although random data in discrete form was used with the work discussed in this report, for the sake of simplicity and clarity, the relations derived here are for continuous data. The detail calculations for some of the properties, employing discrete data points, are contained in appendix C.

According to Bendat & Piersol (1971) four main types of statistical functions are used to describe the basic properties of random data:

Mean square value (MSV)	–	indicates general intensity of data
Probability Density Function (PDF)		furnished information of the properties of the data in the amplitude domain
Autocorrelation Function (ACF)	-	furnished information of the properties of the data in the time domain
Power Spectral Density Function (PSD)	-	furnished information of the properties of the data in the frequency domain

The ACF and PSD supply basically the same information concerning the data because they are only fourier transforms of each other. The use of either one of the two is determined by the format required by the user for a specific application.

The functions mentioned above are used to describe properties of single random processes and in order to describe the joint properties of two or more random processes three main types of statistical functions were devized viz. Joint Probability Density functions (JDF), Cross Correlation function (CCF) and Cross Spectral Density function (CSD). The joint properties are sometimes required where, for example, the profile heights of the left and right hand track of a rough country road are to be investigated and the degree of influence is to be established which the undulations on the right hand track have on the undulations on the left hand track at the same, and also future, positions on the road.

After discussing all of these properties, attention will be turned to the response properties of linear systems, as this theory is very much applicable to the work discussed in this report.

1. PROPERTIES OF A SINGLE RANDOM PROCESS

1.1 MEAN SQUARE VALUE

For a sample time record x(t), observed over time 0 to T, the mean square value is given by

$$\Psi_x^2 = \frac{1}{T} \int_0^T x^2(t)dt \qquad (B1)$$

The square root of this being called the root mean square or rms. The average of all values in the sample record is denoted by the mean value μ_x and is given by

$$\mu_x = \frac{1}{T} \int_0^T x(t)dt \qquad (B2)$$

which is similar to (A5).

The mean square value around the mean is called the variance and, in equation form, is given by

$$\sigma_x^2 = \frac{1}{T} \int_0^T [x(t) - \mu_x]^2 dt \qquad (B3)$$

1.2 PROBABILITY DENSITY FUNCTION

This function describes the probability that the data will assume a value within some defined range at any instant of time. Because x(t) is random, the values cannot be predicted in advance but a sample time record could be recorded, say starting at time t_0, for an interval T and in the light of the assumption of ergodicity, we may use the statistical characteristics of this sample record to predict what the value of x(t) may be at any instant t where $-\infty < t < \infty$. The probability that x(t) assumes a value within the range x and $(x + \Delta x)$, may be calculated by the ratio t_x/T where t_x is the total time that x(t) falls within the designated range.

$$\text{Prob}\,[x < x(t) \leq x + \Delta x] = \frac{t_x}{T} \qquad (B4)$$

If Δx is small the PDF can be defined as

$$p(x) = \lim_{\Delta x \to 0} \frac{1}{\Delta x} \left[\frac{t_{x+\Delta x}}{T} - \frac{t_x}{T}\right] \qquad (B5)$$

1.3 AUTOCORRELATION FUNCTION

This function indicates the influence of values of the data at one time on the values at a future time. The definition for the ACF was given for an ensemble average by equation (A4). For an observation time T of a sample history the ACF is given by (A5) which is

$$R_x(\tau) = \frac{1}{T}\int_0^T x(t)x(t + \tau)dt \qquad (B6)$$

where $R_x(-\tau) = R(\tau)$ and $R_x(\tau)$ have a maximum at $\tau = o$. It is important to note at this stage the relation between the MSV and the ACF of $x(t)$:

$$\Psi_x^2 = R_x(o) \qquad (B7)$$

This function has a maximum at $\tau = o$ and is an even or symmetric function. It is used in the calculation of the PSD as is illustrated in appendix C and also in the following paragraph.

1.4 POWER SPECTRAL DENSITY FUNCTION

This function describes the general frequency composition of the data in terms of the spectral density of its mean square value. Various methods exist to calculate this function and a few of those will be discussed in detail later on in other appendices. It is though necessary to explain the PSD calculation in context with the other functions mentioned above. As mentioned earlier the PSD, G_x, is the fourier transform of the auto correlation function.

$$G_x(f) = 2\int_0^\infty R_x(\tau)e^{-j2\pi f\tau}\, d\tau \qquad (B8)$$

This results in a one–sided PSD which is defined for frequencies in the interval $(0,\infty)$, the two–sided PSD being defined for the interval $(-\infty, \infty)$. The mean square value of $x(t)$ is equal to the total area under a plot of the power spectral density function vs frequency. Therefore

$$\Psi_x^2 = \int_0^\infty G_x(f)df \qquad (B9)$$

and a more appropriate name for PSD is mean square spectral density. A detail discussion of the PSD follows in appendix C.

2. JOINT PROPERTIES OF RANDOM DATA

2.1 JOINT PROBABILITY DENSITY FUNCTION

This function indicates the probability that two seperate sample records will simultaneously assume values within some defined pair of ranges at any specific time. In other words it describes the probability that $x(t)$ would assume a value between x and $x + \Delta x$ while at the same time $y(t)$ assumes a value within the range y and $y + \Delta y$.

Hence

$$p(x,y) = \lim_{\substack{\Delta x \to 0 \\ \Delta y \to 0}} \frac{1}{\Delta x \Delta y} \left[\lim_{T \to \infty} \frac{t_{xy}}{T} \right] \qquad \text{(B10)}$$

during an observed interval T with t_{xy} indicating the time that $x(t)$ and $y(t)$ fall within the respective ranges.

The JDF is used, among other things, to relate the probability of occurence of a event to the probability of occurence of another event. In other words, what is the likelyhood of an event if the likelyhood of another correlated event is known.

2.2 CROSS CORRELATION FUNCTION

This function, in turn, describes the general interdepedence of the values of two sample records. It is defined in a similar fashion as the ACF but instead utilizes two sets of random data, x and y. The value of x at time t is compared to the value of y at time $t + \tau$.

$$R_{xy}(\tau) = \frac{1}{T} \int_0^T x(t)y(t + \tau)dt \qquad \text{(B11)}$$

As opposed to the ACF R_{xy} does not necessarily have a maximum at $\tau = 0$, nor is it an even function.

2.3 CROSS SPECTRAL DENSITY FUNCTION

Because the PSD is a fourier transform of the ACF, the CSD is defined as the fourier transform of the CCF. But as the CCF is not necessarily symmetric, the CSDF function is usually a complex number. The CSD can be described as being the average product of x(t) and y(t), within a frequency band f + Δf, devided by Δf. The CSD has the following form:

$$G_{xy}(f) = /G_{xy}(f)/e^{-j\phi_{xy}(f)}$$

$$\text{with} \quad /G_{xy}(f)/ = \left[(Re(G_{xy}))^2 + (Im(G_{xy}))^2\right]^{1/2}$$

$$\text{and} \quad \phi_{xy}(f) = \tan^{-1}\left[\frac{Re(G_{xy})}{Im(G_{xy})}\right] \qquad (B12)$$

The coherence function γ_{xy} is mostly used in practical situations:

$$\gamma^2_{xy}(f) = \frac{/G_{xy}(f)/^2}{G_x(f)G_y(f)} \qquad (B13)$$

When $\gamma_{xy} = 0$ at a specific frequency it means that x(t) and y(t) are uncorrelated at that frequency, where as if $\gamma_{xy} = 1$ the two sample records are said to be fully correlated at that frequency. This is a valuable quantity to calculate if the correlation between the profile heights of two parallel tracks on. a road are to be investigated.

3. <u>FREQUENCY RESPONSE PROPERTIES</u>

In addition to the properties above by which random data is characterized . the need exists to discuss some principles of the dynamic behaviour of systems. In addition to the assumption of ergodicity, stationarity and Gaussian sample function, two further assumptions are made concerning the random data involved in this report namely that the systems involved have constant parameters and are linear. Constant parameters imply a system having properties which are constant with time. Linearity implies the system has response characteristics which are additive, that is, the output to a sum of inputs are equal to the sum of outputs produced by each input individually. It also implies the response characteristics are homogeneous. These two terms are explained as follows:

Additive:	$f(x_1 + x_2) = f(x_1) + f(x_2)$
Homogeneous:	$f(cx) = cf(x)$

If a real system exhibit non–linear characteristics in certain extreme areas, it is assumed that the system always operates in the linear area so as to make the theory discussed here applicable.

With any input to a system, as defined above, the output will occure after a certain time lag, τ. This dynamic characteristic is described by a weighting function $h(\tau)$ which is the output of the system to any unit input applied time τ before. For any input $x(t)$ the output of the system $y(t)$ is given by the convolution integral defined in general as

$$h * x \quad = \quad \int_{-\infty}^{\infty} h(\tau)x(t-\tau)d\tau$$

and more specific

$$h * x \quad = \quad y(t)$$

therefore

$$y(t) \quad = \quad \int_{-\infty}^{\infty} h(\tau)x(t-\tau)d\tau \qquad \text{(B14)}$$

The lower limit of integration changes because a linear system responds only to past inputs that is,

$$h(\tau) \quad = \quad 0 \text{ for } \tau < 0.$$

The frequency response function (FRF) of a linear system is defined as the fourier transform of the weighting function $h(\tau)$ (see Kaplan p216)

$$H(f) \quad = \quad \int_{\infty}^{\infty} h(\tau)e^{-i2\pi f\tau}d\tau \qquad \text{(B15)}$$

A constant parameter linear system cannot cause any difference in frequency but only in amplitude and phase. Another important property of $H(f)$ is obtained by taking the fourier transform of both sides of (B14).

$$Y(f) \quad = \quad H(f)X(f) \qquad \text{(B16)}$$

where $Y(f)$ and $X(f)$ are the Fourier transforms of the output $y(t)$ and input $x(t)$ respectively. Because of (B15) the FRF is a complex quantity which can also be written as

$$H(f) \quad = \quad /H(f)/e^{-i\phi(f)} \qquad \text{(B17)}$$

where /H(f)/ is called the system gain factor and (f) the system phase factor. The system gain factor indicates the difference in amplitude of the input and output while the phase factor indicates the phase shift induced by the system.

If (B14) is rewritten for a pair of times t and t + (τ) the product y(t)y(t + τ) is given by

$$y(t)y(t+\tau) = \int_0^\infty\int_0^\infty h(\epsilon)h(\eta)x(t-\epsilon)x(t+\tau-\eta)d\epsilon d\eta$$

and in terms of the auto-correlation, this can be written as

$$R_y(\tau) = \int_0^\infty\int_0^\infty h(\epsilon)h(\eta)R\ (\tau + \epsilon - \eta)d\epsilon d\eta \qquad (B18)$$

With the knowledge of Fourier transforms as well as the relationship defined by (B8) the following equation is obtained if the Fourier transform of both sides of (B18) is calculated:

$$S_y(f) = /H(f)/^2S_x(f) \qquad (B19)$$

With similar manipulations for the cross-correlation properties the following is obtained

$$S_{xy}(f) = H(f)S_x(f) \qquad (B20)$$

Note that (B19) contains only the system gain factor while (B20) contains phase information as well. For one-sided PSD functions these two equations can be rewritten to be

$$G_y\ (f) = /H(f)/^2G_x(f) \qquad (B21)$$

$$G_{xy}(f) = H(f)\quad G_x(f) \qquad (B22)$$

where x indicates input and y output. It follows that the output mean square value is given by

$$\Psi_y^2 = \int_0^\infty G_y(f)df = \int_0^\infty /H(f)/^2G_x(f)df \qquad (B23)$$

according to the definition that the MSV is the area under the curve of spectral density vs frequency (B9).

APPENDIX C

CALCULATION OF POWER SPECTRAL DENSITY

It is deemed necessary to discuss in some detail three basic methods of calculating the PSD of a random history. As in the previous appendices the data is again assumed to be ergodic, Gaussian random processes and therefore statistical properties can be calculated from the time average and mean of a single sample record.

Analogue frequency analyzers operate on the principle of a narrow frequency bandwidth "scanner", the output of which is the mean square value of the amplitude at the frequency enclosed in the range. Calculation of the PSD in this manner is called the Filter–squaring–averaring method. Additional methods, more suitable for digital computors, are the PSD estimation via correlation estimates and PSD estimation via FFT computations. Each of these methods will be discussed seperately and a summary made at the end explaining the specific method used to estimate the PSD during the work described in this report.

1. FILTER SQUARING–AVERAGING METHOD

As mentioned above, an analogue frequency analyzer is an instrument which is essentially a variable narrow–band frequency filter with an rms meter to display the output. A spectrum analyzer is a similar instrument except that it has more accurate filters and precisely calibrated filter bandwidths.

Suppose the filter in the spectrum analyzer have the theoretical FRF (see Appendix B) as depicted in figure C1.

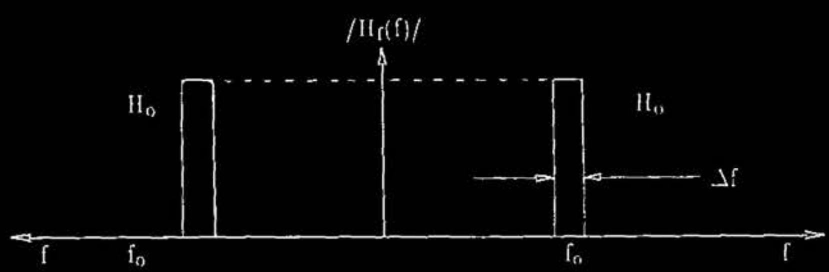

Figure C1

Assume an input x(t) is a sample function obeying the assumptions mentioned above and the output from the filter in the spectrum analyzer is y(t). This output is squared and the time average calculated from (B1):

$$\Psi_y^2 = \frac{1}{T}\int_0^T y^2(t)dt \tag{C1}$$

From (B23), if assumed that T cannot reach infinity, (C1) can also be approximated by

$$\Psi_y^2 = \int_0^\infty /H(f)/^2 G_x(f)df \tag{C2}$$

and with $\Delta f << f_o$ in figure C1 and calling $H(f_o) = H_o$ this relationship can be further approximated by

$$\Psi_y^2 \simeq H_o^2 \Delta f G_x(f_o) \tag{C3}$$

If (C3) is turned around, the value of the spectral density at the specific frequency f_o, is approximated by

$$G_x(f_o) \simeq \frac{\Psi_y^2}{H_o^2 \Delta f} \tag{C4}$$

It should be noted that the output from analogue frequency analyzers or spectrum analyzers produce the one–sided PSD as in the above equation. The mean square value calculated over the bandwidth Δf is therefore normalized by deviding it with Δf. In this manner the influence of Δf is reduced.

But the FRF in figure C1 is theoretical and applies to an infinite averaging time with $T = \infty$. This is not at all practical and such an instrument usually have a finite average time T which results in the fact that spectral values are estimated from short pieces of data and it cannot be hoped to get accurate results. This problem of limited sample length available for calculating the PSD applies to both analogue as well as digital procedures. Discontinuities at the start and end of the record result in a certain loss of precision. This precision or accuracy depends on the record length T and the bandwidth B of the narrow band filter. This can be seen in the fundamental equation to determine the standard deviation σ of the the estimation

$$\sigma = \frac{m}{\sqrt{BT}} \tag{C5}$$

where m is the mean output from the analyzer.

2. WINDOWS AND SMOOTHING

The concept of spectral window which is used to define the equivalent bandwidth B_e of a spectral calculation is introduced now. The explanation will proceed with the analyses on a sinusoidal history. Refering to figure C2 it is clear that, if an infinite length record was used to calculate the PSD of this history, the result in the frequency domain would be a dirac delta function $\delta(f)$ (to be discussed later in paragraph 4.2).

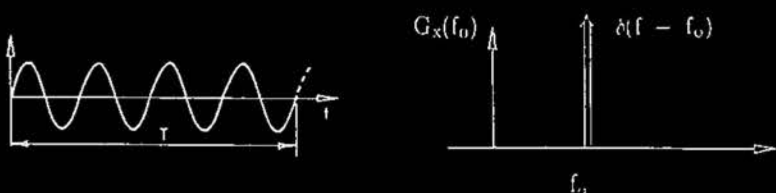

(a) (b)

Figure C2

Because of finite record length the sample can start and end at any value of the sinusoidal history, with the result that parts of wavelengths, hence frequencies, are included in the PSD. If the sample length is perfectly the size of n wavelengths,then obviously there would be no problem. This concept is illustrated in figure C3.

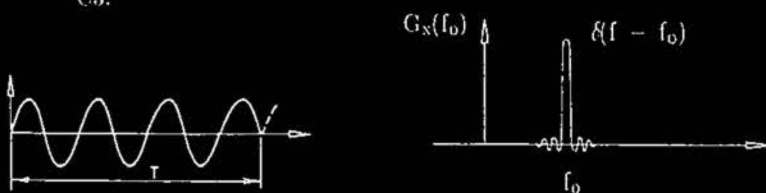

(a) (b)

Figure C3

The resulting PSD is of the shape shown in figure C3(b). The small fluctuations adjacent to the main peak is called leakage and is because of the spurious frequencies included due to the effect illustrated in figure C3(a). This leakage is obviously the cause of an inaccurate PSD and the aim would therefore be to elliminate or reduce leakage in the PSD estimation. It would not be possible to start the sampling record always precisely on the start and end of a wavelength but if the leakage magnitude can be reduced to many times smaller than the main peak, a more accurate PSD would result.

Taking the sample record shown in figure C4(a) and multiplying it with some function, say W(t), so that the result would be figure C4(b), the effect of uncompleted wavelengths at the start and end of the record would be eliminated. The function W(t) is called a window function. Because the signal is made zero at the end points, the original data will be corrupted. With application of a window function, periodicity of the history is assumed with a period T, the record length.

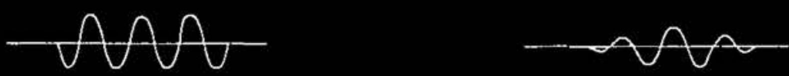

(a) (b)

Figure C4

The effects of different window functions being imposed is illustrated in figure C5. If no window is used it implies in actual fact the imposition of a rectangular window (figure C5(a)). The Hanning and Cosine windows are used with continuous histories such as steady periodic or random vibration. The requirement for a good window would be that, for the perfect case where the record length starts precisely at the beginning of a wavelength, as well as for the worst case where the record length is a complete half wavelength too long or too short, the resulting leakage on the PSD should not differ to much in size and frequency. The width of the spectral peak should also be as narrow as possible and thereby approximating the delta function. The window function obeying these requirements sufficiently is the Hanning window which was therefore used for the work in this report.

The application of a window function on the PSD is also called smoothing and, if the window function is multiplied in the time domain transformation to the frequency domain would imply a convolution integral with the resulting smoothed or estimated PSD defined by

$$\dot{G}_x(f) = \int_0^\infty W(F-f)G_x(F)dF \qquad (C6)$$

where F is a dummy frequency and W(F) the weighting function which satisfies the condition of the delta function, viz:

$$\int_0^\infty W(F)dF = 1$$

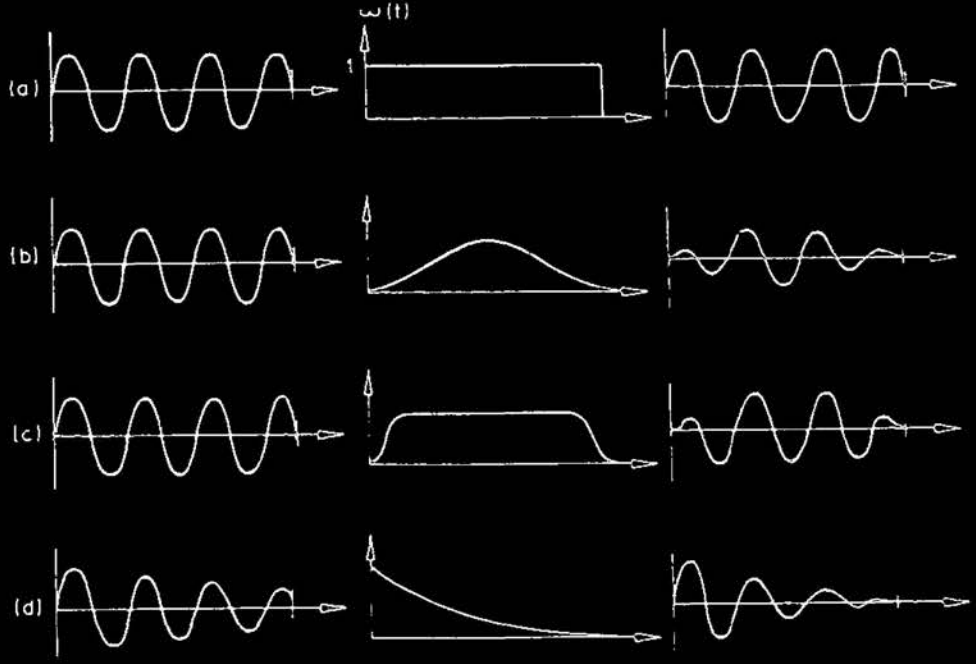

Figure C5: Different types of window functions

(a) Rectangular
(b) Hanning
(c) Cosine Taper
(d) Exponential

The window function can either be applied to the data in the frequency or time domain, the result would be the same. The width of the function determines the band of frequencies over which the averaging is performed. For a rectangular window the effective bandwidth B_e is the full width of the function, whereas with the Hanning window, which rises and falls off gradually, the effective bandwidth can be calculated as follows:

$$B_e = \frac{1}{\int_0^\infty W_h(f)df} \tag{C7}$$

with the Hanning window defined by

$$W_h(t) = 1 - \cos\left[\frac{2\pi t}{T}\right]$$

$$\therefore \quad W_h(t) = 2\sin^2\left[\frac{2\pi t}{T}\right] \quad \text{for } 0 \leq t < T$$

$$\text{and} \quad W_h(t) = 0 \text{ everywhere else}$$

The effective bandwidth B_e is also called the frequency resolution or resolution bandwith. The narrowest possible value for B_e would be $1/T$.

B_e can be seen as the narrow bandwidth of an analogue spectrum filter with a centre frequency f which can be varied over the total frequency range of interest. This bandwidth should not be confused with the bandwith of frequencies contained in the infinite length history.

When the data is a random history, the theory above would apply exactly if the assumption is made that the data is periodic with period T. Multiplying the true data with the window function would in effect imply multiplying every harmonic component in the history which can be obtained by Fourier analyses, by the window function. This would result in a narrow band PSD for every harmonic, or spectral line, in the total PSD. This total PSD would then consist of discrete spectral lines which were calculated by averaging over the narrow band frequencies B_e situated symmetrically around the frequency of the spectral line. This concept is explained in more detail in paragraph 4 later on.

To avoid the loss of data during window application, due to the fact that windowed data are zero near the boundaries, overlap analysis can be performed. Overlap can be intuitively assessed and it is basically defined as the size of the step to the next sample record on which to perform analyses. In this instance a distinction needs to be made between the total sample record used to obtain the statistical properties of a infinite random history and the smaller sample record which is again a subdevision of the total sample record. A PSD is calculated for every smaller record and the average of these PSD's is accepted as the PSD of the complete record, and therefore as the PSD of the random history. This process is called time averaging and will be discussed again later on. Subdividing the initial record into smaller records is done in the time domain before windowing, with the result that values in the original data which are made zero or nearly zero by windowing, are not changed with the next step in the analysis, depending on the measure of overlap. The PSD of a signal are therefore calculated by stepping through the signal with a record of size T calculating the smoothed PSD of every sample record. The step size is any one of T/2, T/3 or T/4, the accuracy of the PSD increasing with the smaller step size. The average PSD of all the samples is then taken as the PSD of the complete signal or history. The above process is illustrated in figure C6.

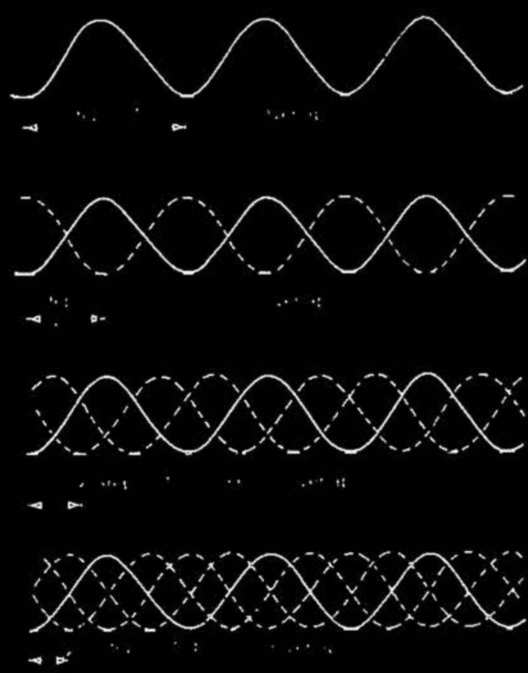

Figure C6

3. ESTIMATING THE PSD FROM AUTO–CORRELATION ESTIMATES

This is the classical method which is called the "Blackman – Tukey" method after the men who developed it. From appendix A the relation between the PSD and the ACF is mentioned again:

$$G_x(f) = 4\int_0^\infty R_x(\tau)\cos 2\pi f\tau d\tau \tag{C8}$$

The equation to use with discrete random series on a digital computer in order to give the value of the PSD at frequency f, is given by

$$\tilde{G}_x(f) = 2h\left[\dot{R}_0 + 2\sum_{r=1}^{m-1}\dot{R}_r\cos\left(\frac{\pi r f}{f_c}\right) + \dot{R}_m\cos\left(\frac{\pi m f}{f_c}\right)\right] \tag{C9}$$

where the parameters are defined as follows:

$\tilde{G}_x(f)$ – raw unsmoothed estimate of the PSD
h – time interval between sample values
$\dot{R}_r$ – estimate of ACF at lag r
m – maximum lag number
$f_c = 1/2h$ – cut off frequency

The autocorrelation estimate are first to be obtained for discrete values by

$$\dot{R}_r = R_x(rh) = \frac{1}{N}\sum_{n=1}^{N-r} x_n x_{n+r} \tag{C10}$$

where r is the lag number and N the total number of samples used. The maximum time displacement of the estimate is given by $\tau_m = mh$.

The value of $\tilde{G}_x(f)$ should only be calculated at discrete frequencies numbering m + 1 calculated by

$$f = \frac{k f_c}{m} \qquad k = 0,1,2,\ldots,m$$

The index k is called the harmonic number and the PSD is therefore estimated at m/2 independent spectral lines.

Because the data was analyzed with a rectangular window (see paragraph 2 above) it is necessary to do smoothing so as to eliminate the side lobe fluctuations. As said earlier the Hanning window or weighting function is used for this and it is defined by

$$W_{h_r} = W_h(rh) = \frac{1}{2}\left[1 + \cos\left[\frac{\pi r}{m}\right]\right] \qquad (C12)$$

for $r = 0, 1, 2, \ldots, m$

$W_{h_r} = 0$ at $r > m$

The final smoothed PSD $\hat{G}_x(f)$ are given for the harmonics, k, by utilizing (C11), (C9) and (C10).

$$\hat{G}_k = \hat{G}_x\left[\frac{k f_c}{m}\right] = 2h\left[\hat{R}_0 + 2\sum_{r=1}^{m-1} W_{h_r}\hat{R}_r\cos\left[\frac{\pi r k}{m}\right]\right] \qquad (C13)$$

4. ESTIMATING THE PSD FROM FFT COMPUTATIONS

4.1 DIGITAL CALCULATION OF THE FAST FOURIER TRANSFROM (FFT)

The Discrete Fourier Transform (DFT) is to be explained before discussing the FFT because the FFT is essentially a computer algorithm to calcula a DFT.

If $x(t)$ is a periodic function with period T (as is the assumption for PSD calculation) then $x(t)$ can be written as a Fourier series

$$x(t) = a_0 + \sum_{k=1}^{\infty}\left[a_k\cos\left[\frac{2\pi kt}{T}\right] + b_k\sin\left[\frac{2\pi kt}{T}\right]\right] \qquad (C14)$$

where $a_k = \frac{2}{T}\int_0^T x(t)\cos\left[\frac{2\pi kt}{T}\right]dt \qquad (C15)$

and $b_k = \frac{2}{T}\int_0^T x(t)\sin\left[\frac{2\pi kt}{T}\right]dt$

In complex notation (C14) can be defined in a single equation by utilizing the Euler relation

$$e^{\iota x} = \cos x + \iota \sin x$$

$$\therefore \quad \cos x = \frac{1}{2}(e^{\iota x} + e^{-\iota x})$$

and $\quad e^{-\iota x} = \cos x - \iota \sin x$

$$\therefore \quad \sin x = -\frac{1}{2}(e^{\iota x} - e^{-\iota x})$$

Therefore the Fourier series can be written as

$$x(t) = a_0 + \frac{1}{2}\sum_{k=1}^{\infty}\left[(a_k - \iota b_k)e^{\iota\frac{2\pi kt}{T}} + (a_k + \iota b_k)e^{-\iota\frac{2\pi kt}{T}}\right]$$

and by making $X_k = a_k - \iota b_k$ the equation becomes

$$x(t) = a_0 + \frac{1}{2}\sum_{k=1}^{\infty}\left[X_k e^{\iota\frac{2\pi kt}{T}} + \overset{*}{X_k} e^{-\iota\frac{2\pi kt}{T}}\right] \qquad (C16)$$

where $\overset{*}{X_k}$ denotes the complex conjugate of X_k. Because a_o is the average or offset value of $x(t)$ it is removed seperately and therefore (C16) can be written as

$$x(t) = \frac{1}{2}\sum_{k=-\infty}^{\infty} X_k e^{\iota\frac{2\pi kt}{T}} \qquad (C17)$$

But if only discrete time values are known, instead of a continuous time function $x(t)$, they can be represented by the discrete series $\{x_n\}$, $n = 0,1,...N-1$ where $t = n\Delta t$ and $\Delta t = T/N$. If now the discrete form of the coefficients a_k and b_k are employed to redefine X_k then (C17) may be written as

$$X_k = \frac{1}{T}\sum_{n=0}^{N-1} x_n e^{-\iota\left\{\frac{2\pi k}{T}\right\}n\Delta t}\,\Delta t \qquad (C18)$$

but substituting $T = N\Delta t$ then (C18) becomes

$$X_k = \frac{1}{N}\sum_{n=0}^{N-1} x_n e^{-\iota\left[\frac{2\pi k}{N}\right]} \qquad (C19)$$

with $k = 0,1,2,....(N-1)$

This is the formal definition of the DFT and the inverse transformation gives every discrete value of $\{x_n\}$, as in (C16), if the time is taken to be the discrete points n.

If the values of x_k is calculated by (C19) N multiplications of the form $x_n \exp\left[-i\left(\frac{2\pi k n}{N}\right)\right]$ are to be performed for each of N values of x_k, bringing the total calculations to N^2. The FFT brings this total number of computations down to Nlog(N) which is a gain of 99,95%. The FFT succeeds in this because it works by partitioning the full sequency $\{x_n\}$ into a number of shorter sequences. The DFT of the shorter sequences are then calculated and combined together to yield the complete DFT of $\{x_n\}$. This process is called the "Cooley–Tukey" method after its developers (Cooley & Tukey, 1964).

The sequence $\{x_n\}$, $n = 0,1,2,...(N-1)$, with N even, is partitioned into two seperate shorter sequences $\{Y_n\}$ and $\{Z_n\}$, as shown in figure C8 where

$$y_n = x_{2n} \text{ and } z_n = x_{2n+1} \text{ with } n=0,1,2,....\left(\frac{N}{2}-1\right) \qquad \text{(C20)}$$

The DFT's of these shorter sequences are given by

$$Y_k = \frac{1}{N/2} \sum_{n=0}^{N/2-1} y_n e^{-i\left(\frac{2\pi k n}{N/2}\right)} \qquad \text{(C21)}$$

$$Z_k = \frac{1}{N/2} \sum_{n=0}^{N/2-1} z_n e^{-i\left(\frac{2\pi k n}{N/2}\right)} \qquad \text{(C22)}$$

with $k = 0,1,2,...(N/2-1)$

Rearranging the summation in (C18) into two seperate sums, similiar to (C21) and (C22), and substituting (C20), the following is obtained

$$X_k = \frac{1}{N}\left[\sum_{n=0}^{N/2-1} y_n e^{-i\left(\frac{2\pi n k}{N/2}\right)} + e^{-i\left(\frac{2\pi k}{N}\right)} \sum_{n=1}^{N/2-1} Z_n e^{-i\left(\frac{2\pi n k}{N/2}\right)}\right] \qquad \text{(C23)}$$

Comparing (C23) with (C21) and (C22) it follows that

$$X_k = \frac{1}{2}\left[Y_k + e^{-i\left[\frac{2\pi k}{N}\right]} Z_k\right] \qquad (C24)$$

for $k = 0,1,2,\ldots,(N/2-1)$, which is the recipe for combining the DFT's of the two shorter sequences Y and Z. The partitioning can actually be done even further by partitioning the two sequences into further sequences and so on, with the only requirement being that the number of samples N in $\{x_n\}$ is a power of 2.

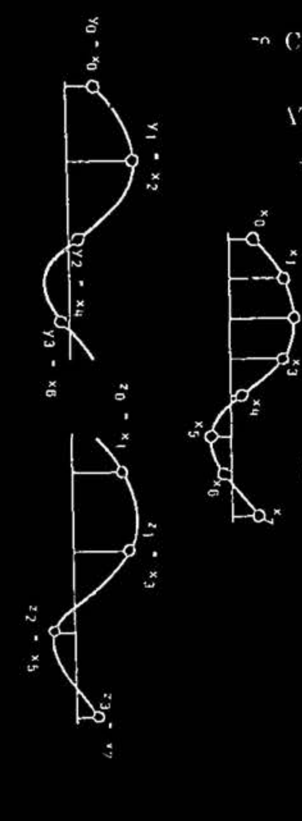

C7: Partitioning the sequence $\{x\}$ into sequences $\{y\}$ and $\{z\}$

ATING THE PSD

metimes necessary to resort back to an analytical explanation is to follow, because keeping to the discrete notation es the discussion unnecessary. It would make no difference ual computations, however.

from the definition of the PSD according to the analogue analyzer, where the power spectral density is defined as square spectral density, a digital similarity is searched for. be the easiest to work with a random history $x(t)$ which ted by its Fourier series as follows

$$(t) = \frac{1}{2}\sum_{k=1}^{\infty}\left[X_k e^{ik\omega t} + X_k^{*} e^{-ik\omega t}\right] \qquad (C25)$$

This is exactly equation (C16) without the mean value a_0 and for simplicity the value $2\pi/T$ is replaced by ω. Here it is clear that the frequency, in Hz, is given by k/T and therefore ω is simply the radian frequency in rad/s. According to (B1) the mean square value (MSV) of this history is given by

$$\Psi_x^2 = \frac{1}{T}\int_0^T x^2(t)\ dt \qquad \text{(B1)}$$

In order to be more correct, T is allowed to approach infinity which implies doing analysis on the complete history and not only a small sample thereof. Substituting (C25) into (B1) therefore gives

$$\Psi_x^2 = \bar{x}^2 = \lim_{T\to\infty} \frac{1}{T}\int_0^T \frac{1}{4}\sum_{k=1}^{\infty}\left[X_k e^{ik\omega t} + X_k^* e^{-ik\omega t}\right]^2 dt$$

$$= \lim_{T\to\infty} \frac{1}{4}\sum_{k=1}^{\infty}\left[\frac{X_k^2 e^{i2k\omega t}}{i2k\omega T} + \frac{2X_kX_k^*t}{T} + \frac{X_k^{*2} e^{-i2k\omega t}}{-i2k\omega T}\right]_0^T$$

which, when the definite integral is solved and T is made to approach infinity, results in the approximation

$$\bar{x}^2 = \sum_{k=1}^{\infty}\frac{X_kX_k^*}{2} \qquad \text{(C26)}$$

The fact that the MSV is equivalent to the Fourier transform squared, can also easily be found from Parseval's Theorem (Kaplan p 151, 244) which states that

$$\int_{-\infty}^{\infty} x_k^2(t)dt = \int_{-\infty}^{\infty} /X_k(f)/^2 df$$

where $X_k(f)$ is the Fourier transform of $x(t)$ and therefore a complex quantity with

$$/X_k(f)/^2 = X_kX_k^*$$

The prove of this theorem is left to the interested reader.

If the discrete form of equation (B9) is employed, the relationship between the MSV and the PSD is found to be

$$\psi_x^2 = \overline{x}^2 = \sum_{k=1}^{\infty} \frac{X_k X_k^*}{2} = \sum_{k=1}^{\infty} G_x(f_k)\Delta f \qquad (C27)$$

where $\Delta f = 1/T$. From this relationship it is clear that the power spectral density can be estimated by

$$\hat{G}_x(f_k) = \frac{X_k X_k^*}{2\Delta f} \qquad (C28)$$

with units [amplitude^2/frequency].

For discrete digital calculations Δf would be the step in frequency to obtain the next discrete spectral line at which to calculate the spectrum value. The value of X_k could be obtained by calculating the FFT of samples taken out of a certain finite time history. The length of the samples should not vary and should be taken as T. The value of Δf is calculated therefore as $\Delta f = 1/T$ and is the narrowest possible value of the resolution B_e.

The PSD for each sample is calculated from the FFT of that sample and the PSD characterizing the complete history is obtained by averaging the PSD's of all the samples. This is the time averaging process mentioned earlier. This procedure also improves the accuracy of the estimate and makes it consistent, that is the accuracy improve with increase in number of samples.

The form of equation (C28) can also be explained by assuming that a random time signal does not consist of a band of continuous frequencies but consists of very discrete frequencies Δf apart. Observing for simplicity only the k'th harmonic lodged in this time signal, which is also assumed to be periodic, it can be given by (C14) that

$$x(t) = a_k \cos \omega t + b_k \sin \omega t,$$

the Fourier transform of which is

$$X(f) = \frac{1}{2}\left[X_k \delta\left[f - \frac{k}{T}\right] + X_k^* \delta\left[f + \frac{k}{T}\right]\right] \qquad (C30)$$

The concept of the dirac delta function, also called the unit impulse function $\delta(f)$, is introduced here. This function is defined as follows

$\delta(o) = +\infty$ and everywhere else $\delta(f) = o$

and the density is $\displaystyle\int_{-\infty}^{\infty} \delta(f)df = 1$

This leads to the following:

$\delta((f = f_k) - f_k) = \infty$ with $\delta(f - f_k) = o$ everywhere else.

$$\text{and} \quad \int_{-\infty}^{\infty} (f - f_k)df = 1 \qquad \text{(C31)}$$

This function is illustrated in figure C8

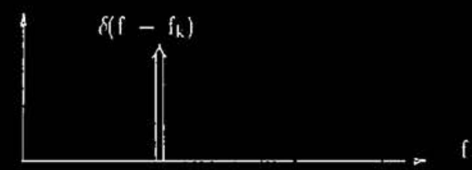

Figure C8

As can be seen from (C31) the area under this function is always unity and the Fourier transform for a single periodic wave, like a sinusoidal wave, is always a dirac delta function. If integration over all the frequencies is done, assuming that there exist no other harmonics except the k'th, then the value of the Fourier transform at the k'th frequency is given by

$$X(f) = \frac{1}{2} \sum_{k=-\infty}^{\infty} X_k \delta\left[\frac{k}{T} - f_o\right]$$

where f_o is the fundamental frequency of the single harmonic history $x(t)$. This equation can be rearranged to give

$$X(f) = \frac{1}{2} X_k \left[\sum_{k=-\infty}^{\infty} \delta\left[\frac{k}{T} - f_o\right]\right]. \qquad \text{(C32)}$$

where the term in brackets is equal to 1.

When working with discrete frequency increments, say Δf, the area of the rectagular pulse should be equal to unity. Refering to figure C9 it follows therefore that the height of the pulse should be $1/\Delta f$. Should Δf becomes infinitely small the height should approach the delta function, therefore

$$\lim_{\Delta f \to 0} \frac{1}{\Delta f} = \delta(f - f_0) \qquad \text{(C33)}$$

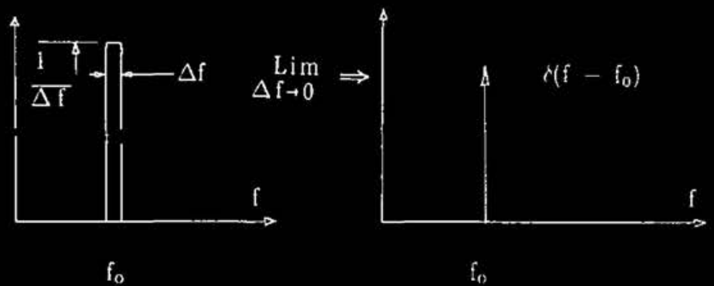

Substituting (C33) into (C32) gives

$$X(f) = \frac{X_k}{2\Delta f} \qquad \text{(C34)}$$

In order to obtain the value of the Fourier transform at the frequency k, it is assumed that only the frequency k is lodged in the history. This is also the principle on which the analogue spectral analyzer operates. The delta function is approximated with a function $\frac{\sin bf}{\pi f}$ having the shape as shown in figure C10, the shape of which is also that of a window function showing the ieakage lobes adjacent to the main peak.

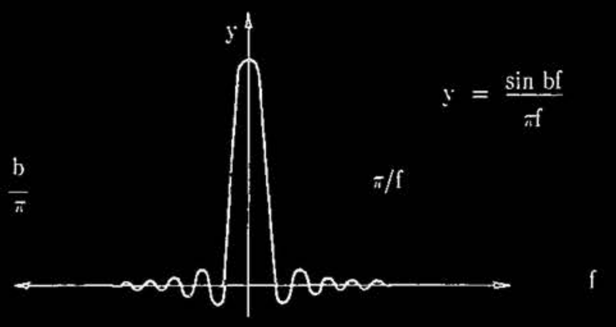

Figure C10

If a different derivation for the mean square value is made it will be seen how the result (C34) can be used to calculate the PSD according to (C28). Starting again from (B1)

$$\Psi_x^2 = \lim_{T\to\infty} \frac{1}{T} \int_0^T x_k^2(t)dt \qquad (B1)$$

Letting the integration be from $-\infty$ to ∞

$$\Psi_x^2 = \lim_{T\to\infty} \frac{1}{T} \int_{-\infty}^{\infty} x_k^2(t,T)dt$$

which, after utilizing Parseval's Theorem as before, can be written as

$$\Psi_x^2 = \lim_{T\to\infty} \frac{1}{T} \int_{-\infty}^{\infty} /X_k(f,T)/^2 df$$

$$\therefore \quad \Psi_x^2(k) = 2\lim_{T\to\infty} \frac{1}{T} \int_{-0}^{\infty} /X_k(f,T)/^2 df \qquad (C35)$$

But it is known that

$$\Psi_x^2 = E\left[\Psi_x^2(k)\right] = \int_0^{\infty} G_x(f)df$$

and therefore together with (C35) it results in

$$G_x(f) = 2\lim_{T\to\infty} \frac{1}{T} /X_k(f,T)/^2$$

which, if the limiting term is ommited, gives an approximation for the PSD

$$\dot{G}_x(f) = \frac{2}{T}/X_k(f)/^2 \qquad (C36)$$

If digital calculation procedures are used, the PSD can be estimated using (C34) and (C36). This is against the background of assuming that the continuous time signal consists of discrete frequencies, which are evaluated as seperate entities as if each one is the only one present in the signal. Thus combining (C34) and (C36), and remembering that $\Delta f = 1/T$, the PSD is estimated by

$$\dot{G}_x(f) = \frac{2\Delta f \quad X_k X_k^*}{4\Delta f^2}$$

$$\therefore \quad \dot{G}_x(f) = \frac{X_k X_k^*}{2\Delta f} \qquad (C28)$$

5. SUMMARY

At this stage it should be sensed that all the above derivations should be summarized. The process of digitally calculating the PSD is thus presented as follows:

5.1 Determine the highest frequency of interest in the data. This is the cut–off frequency, f_c, and all frequencies above this value should be filtered.

5.2 The sampling frequency f_s, is now determined by f_c due to the fact that in order to sample the highest frequency accurately at least two observations need to be made of the signal in this frequency. Therefore $f_s \geq 2f_c$ as explained in appendix H. The time interval between discrete points is therefore $\Delta t = 1/f_s$.

5.3 Determine the number of data points required to calculate a FFT. This should be any value N where $N = 2^n$ and $n = 1,2,3,...$. Normally 1024 data points are used.

5.4 The length of the sample record is now fixed by the relationship $t = N\Delta t$ and the frequency resoluton, B_e is given by $1/T$.

5.5 The accuracy of the estimated PSD can now be determined by equation (C5) which is similar to (G10). If it is not possible to employ the time averaging procedure (See appendix G and par 3.1.1. in the main body of this report) because of the limited amount of data available, the error would be 100 % but can be improved by smoothing of the PSD in the frequency domain (See appendix G). The error can then be calculated by equation (G11).

5.6 Execute the following calculation procedure:

(i) Generate the discrete time series by sampling the various records from the 'infinite' random sequence. (Appendix H).
(ii) Multiply this discrete series with the Hanning window function (Appendix C, par. 2).

(iii) Calculate the FFT's (or more correctly the DFT's) of the sample records (Appendix C, par. 4.1).

(iv) Estimate the spectral coefficients and thereafter calculate the complete spectrum at discrete frequencies according to equation (C28) for each sample record. (Appendix C, par. 4.2).

(v) If *more than one* sample exists obtain the average PSD for all the sample records. (Time averaging, Appendix G).

(vi) If time averaging is not performed, do frequency smoothing by averaging adjacent spectral values (Appendix G) in order to improve the accuracy of the estimate.

The result of the above procedure is a set of coordinates of a smoothed spectrum G(f) between the frequency range 0 to $1/\Delta t$. Plots of typical PSD's are shown in figure C11. Notice the differences in shape which can be utilized to characterize a random waveform simply by its' PSD.

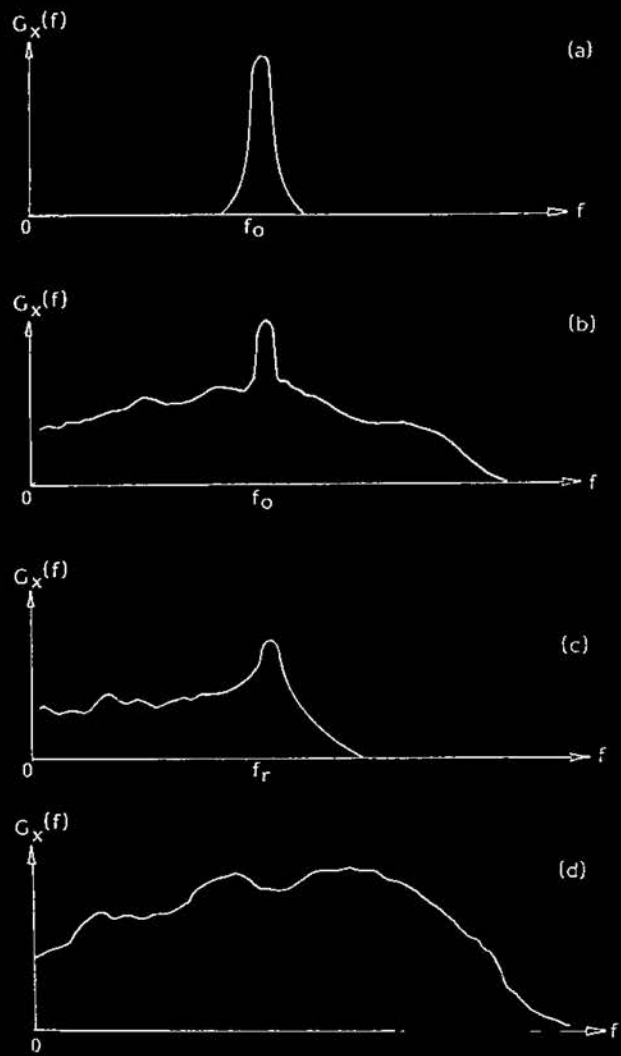

Figure C10: PSD plots for (a) Sine wave, (b) Sine wave plus random noise, (c) Narrow band random noise and (d) wide-band random noise

APPENDIX D

THE SPATIAL PSD

1. DEFINITION OF THE SPATIAL PSD

Although all the theory derived in the preceding appendices are for either periodic or quazi–periodic random sequences, which are functions of time, it is actually applicable to any random sequence which is a function of any other variable. For rough surface irregularities as found on roads, runways, off–road terrain, etc. the spatial PSD is defined. Figure D1 shows the height y of surface undulations, above an arbitrary horizontal reference line, plotted as a function of horizontal distance x along the terrain.

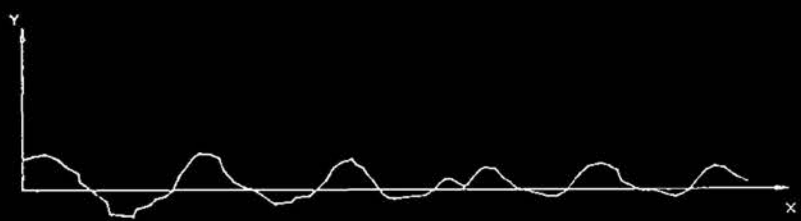

Figure D1

Instead of varying with time, the height is a function of distance and it is clear that long wavelength irregularities correspond to low frequencies in the time dimain, whereas short wavelengths correspond to high frequency disturbances. The time frequency [cycles/second], which was used so far, is now replaced by the spatial frequency [cycles/unit distance] defined as

$$\gamma = \frac{1}{\lambda} \tag{D1}$$

where λ is the wavelength of the undulation. The spectral density of the height variable y is therefore now a function of the spatial frequency which will be defined in SI units namely, cycles/meter, throughout this work. The PSD of a rough surface is thus called a spatial PSD and is given by $G_y(\gamma)$. This quantity is calculated exactly as prescribed in appendix C. There is however a definite shape which is a characteristic of this PSD and this is shown in figure D2.

As can be seen the downward slope is characteristic of the spatial PSD calculated for surface roughnesses. This is consistent with the observation that high frequency surface irregularities have small amplitudes and low frequency irregularities usually have higher amplitudes. This leads to the conclusion that the value of the spatial PSD falls off with the square of the frequency. Therefore, if a straight line is fitted to such curves, as in figure D2, the equation describing this straight line will have the following form

$$G_x(\gamma) = K\gamma^a \qquad \text{(D2)}$$

Where K is called the roughness constant and a is the value of the slope.

2. ROUGHNESS CONSTANT CALCULATION

Confirmation of the validity of equation (D2) is done in section 3.1.5 of the text and for the discussion that follows here a value of -2 for the slope "a" is assumed. Values obtained by the various investigators indicate the suitability of this assumption (Sayles & Thomas 1977).

The constant K is termed the roughness constant and is the value of the PSD at a certain reference frequency. In order to be able to fit a straight line through the PSD log values, it is necessary to smooth the curve. This is not to be confused with the windowing or "smoothing" process of the time data before spectral calculations (see appendix C, paragraph 2). When unsmoothed data is used the high frequency values will be biased by statistical noise and experimental errors, and therefore it is suited to smooth the graph by calculating the mean PSD in a range of frequency bands. This procedure was taken from the ISO/TC 108 and is used in the absence of any other confirmed method. The detail of the smoothing process is contained in the standard but is summarized here for completeness.

The applicable spatial frequency range for natural surface roughness is devided into octave bandwidths and the mean PSD in the following bands are calculated

- Octave bands from the lowest frequency (not zero) up to a centre frequency of 0.0312 c/m.
- Third–octave bands from the last octave band up to a centre frequency of 0.25 c/m.
- Twelfth–octave bands up to the highest frequency.

The applicable frequencies are shown in table D1 taken out of the ISO/TC 108 standard. For simplicity more or less the same notation is employed.

The mean PSD in each bandwidth ι is calculated as follows

$$G_{xs}(\iota) = \frac{T_1 + \sum_{j=n_L+1}^{n_H-1} G_x(j)B_e + \left[n_h(\iota) - (n_H - 0.5)B_e\right] G_x(n_H)}{n_h(\iota) - n_\ell(\iota)} \quad \text{(D3)}$$

where $G_{xs}(\iota)$ = smoothed estimated PSD in band ι

$T_1 = \left[(n_L + 0.5)B_e - n_\ell(\iota)\right] G_x(n_L)$

n_ℓ = lower limit of smoothing band ι

n_h = higher limit of smoothing band ι

$$n_H = \text{INT}\left[\frac{n_h(\iota)}{B_e} + 0.5\right]$$

$$n_L = \text{INT}\left[\frac{n_\ell(\iota)}{B_e} + 0.5\right]$$

B_e = frequency resolution.

(See appendix C par 2)

$\therefore \quad B_e = \frac{1}{L}$ where L is the length of the record.

Therefore $B_e = \Delta f$

Because the value of the PSD at the centre frequency of each band is the sole remaining PSD value in that band, it is necessary to interpolate between these points to obtain the smoothed curve for the complete bandwidth of frequencies. This curve is then used for fitting the straight line which would represent the PSD in such a way that it can be used in characterizing the specific surface.

Equation (D2) can now be rewritten as

$$G_x(\gamma) = \frac{G_x(\gamma_o)\gamma^a}{\gamma_o^a} \quad \text{(D4)}$$

where γ_0 is a reference frequency, determined by the specific surface measured and also the application of the user. According to the ISO/TC 108 standard this reference frequency is 0.1 c/m for on–road surfaces and in order to remain compatible with this international draft standard it was decided to accept this reference frequency as applicable to off–road surface. The roughness constant K is therefore calculated by

$$K = \frac{G_x(\gamma_o)}{\gamma_o{}^a} \tag{D5}$$

where the value of a is –2, and $\gamma_0 = 0.1$ c/m.

TABLE D1: SMOOTHING BANDWIDTHS (ISO/TC 108)

OCTAVE BANDWIDTH

EXP	n_l 1/m	n_c 1/m	n_h 1/m
−9.000	0.0014	0.0020	0.0028
−8.000	0.0028	0.0039	0.0055
−7.000	0.0055	0.0078	0.0110
−6.000	0.0110	0.0156	0.0221
−5.000	0.0221	0.0312	0.0442

THIRD OCTAVE BANDWIDTH

EXP	n_l 1/m	n_c 1/m	n_h 1/m
−4.333	0.0442	0.0496	0.0557
−4.000	0.0557	0.0625	0.0702
−3.667	0.0702	0.0787	0.0884
−3.333	0.0884	0.0992	0.1114
−3.000	0.1114	0.1250	0.1403
−2.667	0.1403	0.1575	0.1768
−2.333	0.1768	0.1984	0.2227
−2.000	0.2227	0.2500	0.2806

CENTRE FRQUENCIES AND CUT–OFF FREQUENCIES FOR PSD SMOOTHING EXPRESSED IN SPATIAL FREQUENCY N.

n_l: Lower cut–off frequency
n_c: centre frequency
n_h: upper cut–off frequency
$n_c = 2ex$

Note:

A small overlap exists between the lowest twelfth octave bandwidth and the highest third octave bandwidth. This overlap maintains the values 0.5:1:2:4 as centre frequences in the twelfth–octave bands. This makes it convenient to calculate the road characterisation (see Annex B.3) immediately from the twelfth octave band smoothing.

TWELFTH OCTAVE BANDWIDTH

EXP	n_l 1/m	n_c 1/m	n_h 1/m
−1.833	0.2726	0.2806	0.2888
−1.750	0.2888	0.2973	0.3060
−1.667	0.3060	0.3150	0.3242
−1.583	0.3242	0.3337	0.3435
−1.500	0.3435	0.3536	0.3639
−1.417	0.3639	0.3746	0.3856
−1.333	0.3856	0.3969	0.4085
−1.250	0.4085	0.4204	0.4328
−1.167	0.4328	0.4454	0.4585
−1.083	0.4585	0.4719	0.4858
−1.000	0.4858	0.5000	0.5147
−0.917	0.5147	0.5297	0.5453
−0.833	0.5453	0.5612	0.5777
−0.750	0.5777	0.5946	0.6120
−0.667	0.6120	0.6300	0.6484
−0.583	0.6484	0.6674	0.6870
−0.500	0.6870	0.7071	0.7278
−0.417	0.7278	0.7492	0.7711
−0.333	0.7711	0.7937	0.8170
−0.250	0.8170	0.8409	0.8655
−0.167	0.8655	0.8909	0.9175
0.000	0.9715	1.0000	1.0293
0.083	1.0293	1.0595	1.0905
0.167	1.0905	1.1225	1.1554
0.250	1.1554	1.1892	1.2241
0.333	1.2241	1.2599	1.2968
0.417	1.2968	1.3348	1.3740
0.500	1.3740	1.4142	1.4557
0.583	1.4557	1.4983	1.5422
0.667	1.5422	1.5874	1.6339
0.750	1.6339	1.6818	1.7311
0.833	1.7311	1.7818	1.8340
0.917	1.8340	1.8877	1.9431
1.000	1.9431	2.0000	2.0586
1.083	2.0586	2.1189	2.1810
1.167	2.1810	2.2449	2.3107
1.250	2.3107	2.3784	2.4481
1.333	2.4481	2.5198	2.5937
1.417	2.5937	2.6697	2.7479
1.500	2.7479	2.8284	2.9113
1.583	2.9113	2.9966	3.0844
1.667	3.0844	3.1748	3.2678
1.750	3.2678	3.3636	3.4621
1.833	3.4621	3.5636	3.6680
1.917	3.6680	3.7755	3.8861
2.000	3.8861	4.0000	4.1172
2.083	4.1172	4.2379	4.3620
2.167	4.3620	4.4898	4.6214
2.250	4.6214	4.7568	4.8962
2.333	4.8962	5.0397	5.1874
2.417	5.1874	5.3394	5.4958
2.500	5.4958	5.6569	5.8226
2.583	5.8226	5.9932	6.1688
2.667	6.1688	6.3496	6.5357
2.750	6.5357	6.7272	6.9243
2.833	6.9243	7.1272	7.3360
2.917	7.3360	7.5510	7.7723
3.000	7.7723	8.0000	8.2344

APPENDIX E

DERIVATION OF SPATIAL PSD FROM PSD'S OF THE TIME DATA

If a vehicle traverses a rough terrain at a certain speed ν, the situation at the wheel can be simplified by a simple spring and damper system as illustrated in figure E1. The translation and therefore acceleration of the mass is a function of the frequency response of the whole system.

Figure E1

Assuming a linear system, the frequency response function is given by

$$H(f) = /H(f)/e^{-\iota\phi(f)} \qquad \text{(B17)}$$

and it is known from (B19) that

$$G_{y_m}(f) = /H(f)/^2 G_{y_p}(f) \qquad \text{(B19)}$$

with $G_{y_m}(f)$ being the PSD of the time signal $y_m(t)$ and $G_{y_p}(f)$ the PSD of the terrain profile at speed ν. The system gain factor is $/H(f)/$ as defined in appendix B.

1. CONSTANT VEHICLE SPEED

If the vehicle forward speed ν, is constant, the relation between the wavelength λ of the terrain profile and the applicable time frequency is the forward speed of the vehicle. The relation between the spatial frequency γ, [cycles/meter], and the time frequency is therefore given by

$$f = \nu\gamma \qquad \text{(E1)}$$

This also means that a time lag, τ, for calculating the ACF for the time signal , is equivalent to the space lag L. by the following

$$\tau = \frac{L}{\nu} \qquad \text{(E2)}$$

The PSD of the time signal is given in analogue form by (B8)

$$G_{y_p}(f) \qquad = 2\int_{-\infty}^{\infty} R_{y_p}(\tau)e^{-i2\pi f\tau}d\tau \qquad (B8)$$

and the spatial PSD should therefore be given by

$$G_{y_p}(\gamma) \qquad = 2\int_{-\infty}^{\infty} R_{y_p}(L)e^{-i\gamma L}dL \qquad (E3)$$

Substituting (E2) and (E1) into (B8) gives

$$G_{y_p}(f{=}\nu\gamma) = 2\int_{-\infty}^{\infty} R_{y_p}\left[\tau = \frac{L}{\nu}\right]e^{-i(\nu\gamma)\left[\frac{L}{\nu}\right]}\frac{dL}{\nu}$$

$$= \frac{2}{\nu}\int_{-\infty}^{\infty} R\quad(L)e^{-i\gamma L}dL \qquad (E4)$$

which is equivalent to writing

$$G_{y_p}(f) = \frac{1}{\nu}\, G_{y_p}(\gamma)$$

It is therefore clear that the relation between the spatial and time PSD's is only the vehicle forward speed which is applied to the spectral value. The horisontal scale need only to be adjusted for (E1).

2. ACCELERATIONS OF MASS IS KNOWN

If the acceleration history, with time, of the mass in figure E1 are available and not the translation with time. the spatial PSD can also be obtained by doing the manipulations set out below. Assuming a unit impulse input to the system then the following applies. The DFT of the translations is given by (C17):

$$y_m(t) = \frac{1}{2}\sum_{k=-\infty}^{\infty} Y_k e^{i\frac{2\pi k}{T}t} \qquad (C17)$$

Differentiate with respect to time results in the speed and acceleration

$$\dot{y}_m(t) = \frac{1}{2} \sum_{k=-\infty}^{\infty} Y_k \left[\frac{\iota 2 \pi k}{T}\right] e^{\iota \frac{2 \pi k}{T} t}$$

and $$\ddot{y}_m(t) = \frac{1}{2} \sum_{k=-\infty}^{\infty} Y_k \left[\frac{\iota 2 \pi k}{T}\right]^2 e^{\iota \frac{2 \pi k}{T} t} \qquad \text{(E6)}$$

which can be rewritten to

$$\ddot{y}_m(t) = \frac{1}{2} \sum_{k=-\infty}^{\infty} \left[-\left[\frac{2 \pi k}{T}\right]^2 Y_k\right] e^{\iota \frac{2 \pi k}{T} t} \qquad \text{(E7)}$$

The term in brackets is the Fourier coefficient of the acceleration signal $\ddot{y}_m(t)$, therefore

$$Y_{k_{y_m}} = -\left[\frac{2 \pi k}{T}\right]^2 Y_{k_{y_m}}, \quad k = 0,1,2,\ldots N-1 \qquad \text{(E8)}$$

With the definition of the PSD of the acceleration signal being

$$G_{y_m}(f) = \frac{2}{T} /Y_{k_{y_m}}/^2 \qquad \text{(C36)}$$

it can be defined in terms of the translation data PSD by

$$G_{y_m}(f) = \left[\frac{2 \pi k}{T}\right]^4 G_{y_m}(f)$$

and with $f = \frac{k}{T}$ it becomes

$$G_{y_m}(f) = (2\pi f)^4 G_{y_m}(f). \qquad \text{(E9)}$$

The spatial PSD can now be computed by using (B21) and (E5) which results in

$$G_{y_p}(\gamma) = \frac{1}{/H(f)/^2} \quad \frac{\nu}{(2 \pi f)^4} \; G_{y_m}(f) \qquad \text{(E10)}$$

APPENDIX F

FATIGUE ANALYSIS THEORY

This subject is obviously not to be covered in detail and the interested reader is refered to the list of references especially Osgood (1982) and Collins (1981). A short summary is however necessary of those aspects of this subject which is applicable to the work discussed in this report.

1. CYCLE COUNTING METHODS

It is quite simple to count the number of cycles in a constant amplitude load signal but when dealing with a random signal, exhibiting a mean value for most of the time, the process gets a bit more complicated. The counting algorithms developed for these cases are based on various approaches and assumptions. The most accurate ones are accepted to be range pair and rainflow counting. (Figure F1 and F4). As can be seen in figure F4 the rainflow counting technique is based on the hysteris stress strain loops experienced by dynamically loaded material. It establishes the size of an amplitude as well as it's mean value and is stored in a matrix where the number of cycles is stored at a position corresponding to a size and mean value. It can therefore be used in consequent accurate fatigue prediction and testing.

The output from the range pair counting method is a histogram depicting amplitude size vs cumulative number of cycles (see figure F1). This format does not include any data of the mean value of a amplitude.

Murphy (1982) used another method to present the rainflow counting data. Accelerations were measured at critical locations and these signals were analyzed with the rainflow method. The data was then stored in the form of a response histogram as shown in figure F5.

The horisontal axis gives the magnitude of the occurence (2 x amplitude) and the vertical axis gives the frequency of occurence of each magnitude per mile. The straight line is obtained by fitting an exponential equation to the data and coefficients of this equation can then be used to characterize the data.

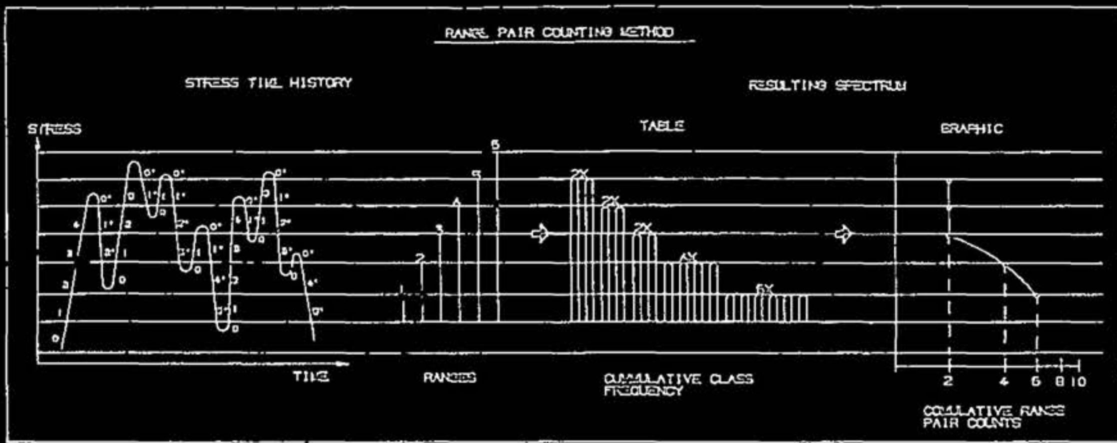

FIGURE F1

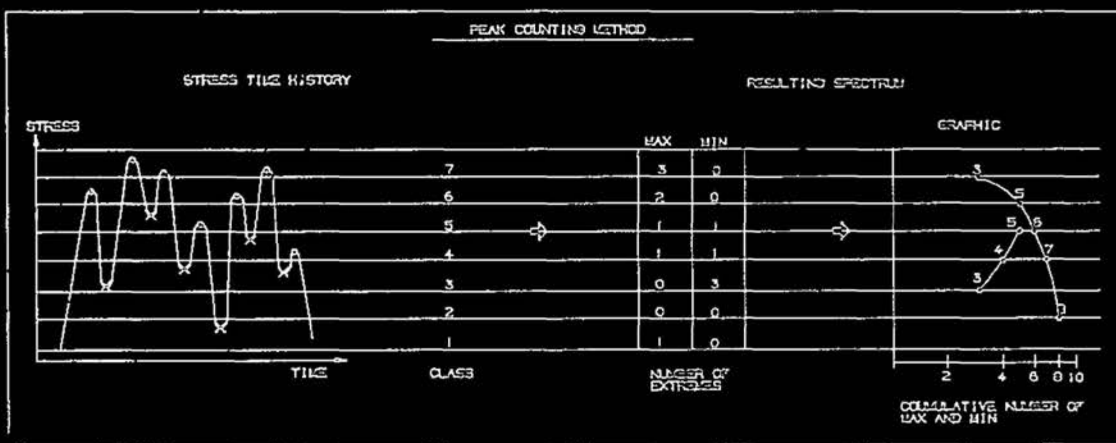

FIGURE F2

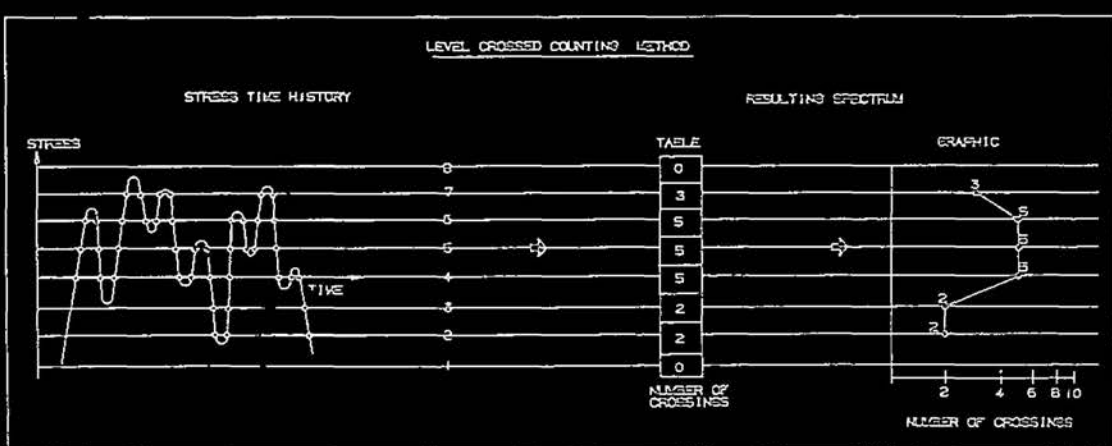

FIGURE F3

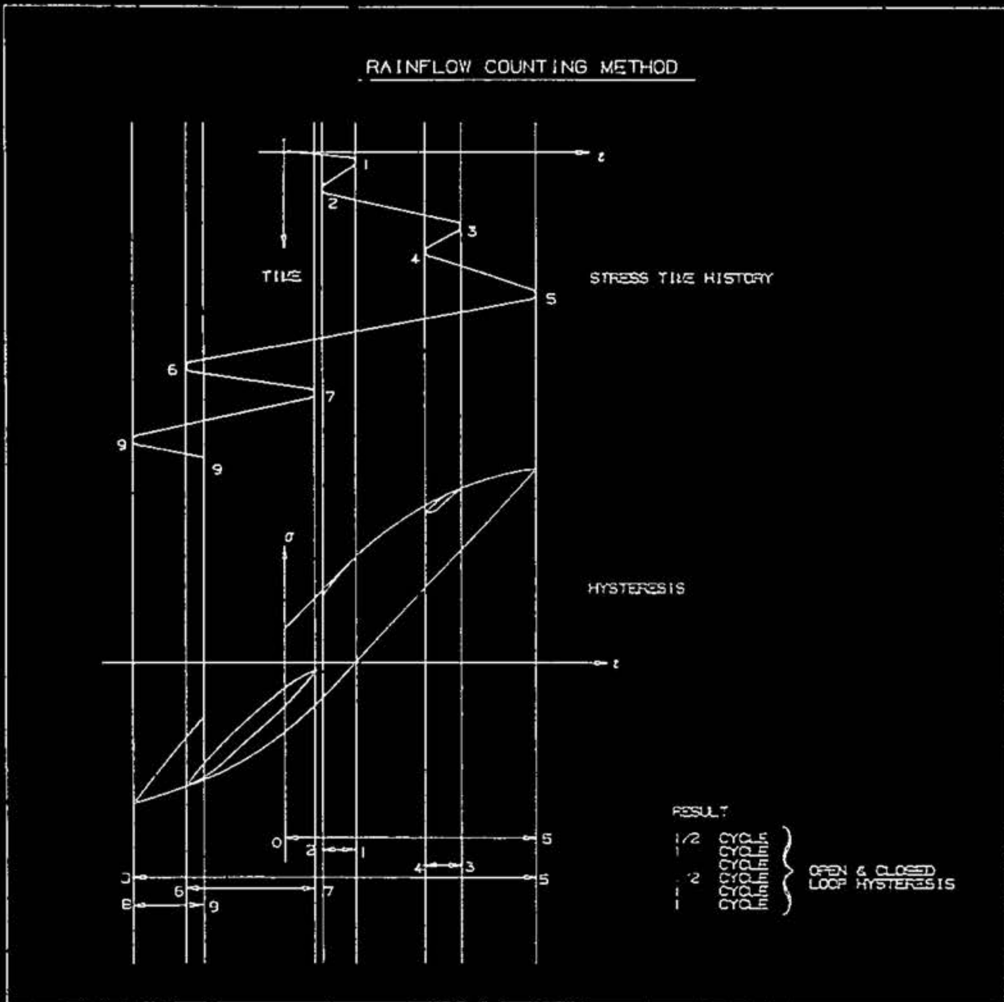
RAINFLOW COUNTING METHOD
TIME
STRESS TIME HISTORY
HYSTERESIS
RESULT
1/2 CYCLE
1 CYCLE
CYCLE
1/2 CYCLE
1 CYCLE
1 CYCLE
OPEN & CLOSED
LOOP HYSTERESIS

FIGURE F4

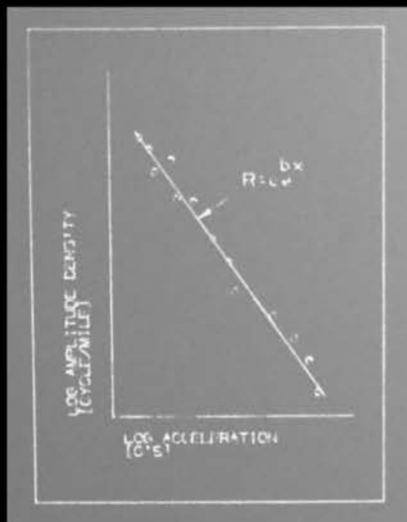

Figure F5: Response histogram of Rainflow counting data

2. DAMAGE CALCULATION METHODS

It is usually required to be able to predict the fatigue life or, at least calculate and predict the damage to any component, with the knowledge of the load cycle it experiences. The various methods available include almost without exception one or more empirical parameter to be determined by laboratory tests. A few of these methods are listed below:

(a) Fatigue SN curve and Goodman diagram. Limited to constant amplitude loading (sine wave).

(b) Miner's Rule for cumulative damage calculation. A load spectrum consisting of sine wave blocks of varying amplitude size is to be used.

(c) The Local Strain Method use cyclic material properties. It accomodates pre–strain, sequence of loading, mean stress effects and employs the results of the rainflow counting technique.

(d) The Nominal Stress Method is primarily concerned with low cycle fatigue and accomodates plastic flow but ignore mean stress effects.

(e) The Fracture Mechanics approach is concerened with crack growth and combined with the local strain approach it also gives an indication of crack initiation.

Local Strain Method

The local stress and strains at the crack root are derived by Neubers' Rule from data on smooth specimens and as it is usually difficult to measure at the crack root the strain gauge data giving the nominal strain on the component is used. The assumption is made that the local damage done on the component is equal to that done by the same loading imposed on an axial test speciment. Validity of a linear summation of damage as well as Neubers' Rule is furthermore assumed.

To include work hardening/softening the cyclic or fatigue properties of the material are included, but because of stabilization during cyclic loading the stable stress strain response is used instead of monotonic values and is given by

$$\frac{\Delta\epsilon}{2} = \frac{\Delta\sigma}{2E} + (\Delta\sigma/\sigma_f')^{1/n'} \qquad \text{(F1)}$$

This relationship is illustrated in figure F6. The fatigue properties in equation (F1) is:

$\frac{\Delta\epsilon}{2}$ = strain amplitude

$\frac{\Delta\sigma}{2}$ = stress amplitude

n' = cyclic strain hardening exponent
(Slope of the log $\Delta\sigma/2$ – log $\Delta\epsilon/2$ plot)

ϵ_f' = fatigue ductility coefficient approximated by the monotonic fracture ductility, ϵ_f

σ_f' = fatigue strength coefficient approximated by the monotonic true fracture strength, σ_f

E = Modulus of elasticity

This data is readily available for most materials or can either be obtained from finite element analysis, or by extrapolating from existing strain data. If no data is available, tests should be done on specimens and the properties above are then derived from plots of the plastic strain, $(\Delta\epsilon p/2)$, and stress $(\Delta\sigma/2)$, versus the reversals to failure, log $2N_f$ (a cycle is two reversals).

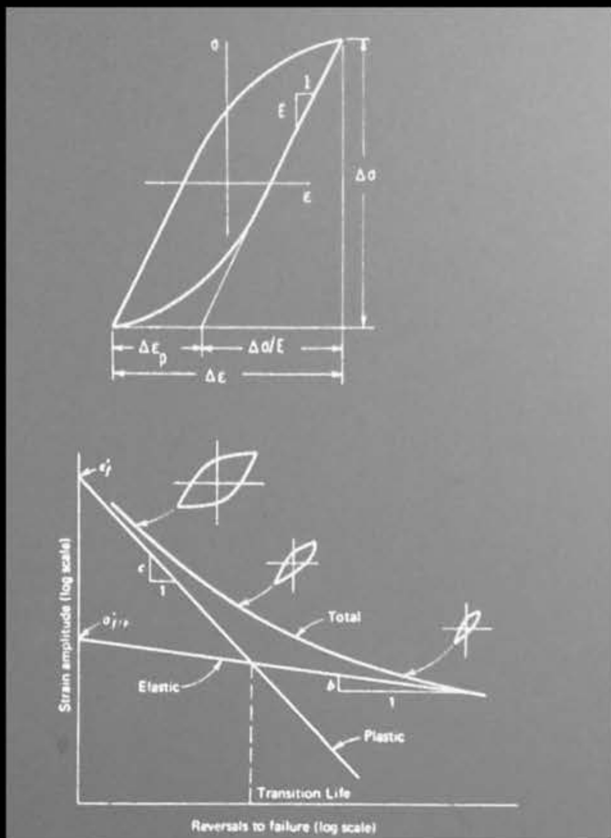

Figure F6: Stable cyclic stress/strain hysteresis behaviour

Additional effects to be catered for are pre–strain, mean stress and geometry effects. For the geometric discrepancy between the laboratory test specimen and the actual component, some emperical expressions had been developed and K_f is defined as the fatigue notch factor.

$$K_f = 1 + \frac{K_t - 1}{1 + {}^{a}/_{r}} \qquad (F2)$$

where K_t is the theoretical stress concentration factor, 'a' is a material constant relating the fatigue life of notched specimens to that of unnotched specimens and r is the number of reversals.

The important thing, however, is to correctly estimate or determine K_f so that the nominal stress and strain values can be related to the local values with Neuber's Rule in the form of

$$\Delta\sigma\Delta\epsilon = K_f^2(\Delta s\Delta e) \qquad (F3)$$

where $\Delta\sigma\Delta\epsilon$ = local stress/strain range
and $\Delta s\Delta e$ = nominal stress/strain range

This relationship can be rewritten with the addition of the modulus of elasticity, E both sides and by taking the square root. it becomes

$$\sqrt{\Delta\sigma\Delta\epsilon E} = K_f \sqrt{\Delta s\Delta e E} \qquad (F4)$$

The α–life function is defined as

$$\alpha = \sqrt{\sigma_{max}\Delta\epsilon E} \qquad (F5)$$

Equation (F4) can therefore also be written as

$$\alpha_{critical} = K_f\alpha_{nominal} \qquad (F?)$$

because it was found that α is independent of the mean stress.

When the nominal strains are elastic it follows that

$$\Delta\sigma\Delta\epsilon = (K_f\Delta e)^2 E \qquad (F6)$$

and because the rainflow counting technique is directly related to the stress strain hysteresis loops experienced by a material (see figure F4). this counting technique is most suitable in determining the correct stress and strain ranges to be used in equation (F6).

A suitable cumulative damage summation which is usually used is the linear rule of Miner:

$$D = \Sigma \frac{r}{2N_f} \qquad (F7)$$

where r is the number of reversals and N_f is determined from the following empirical relations:

$$\frac{\Delta \sigma}{2} = \sigma_f'(2N_f)^b \tag{F8}$$

or

$$\frac{\Delta \epsilon}{2} = \frac{\sigma_f'}{E}(2N_f)^b + \epsilon_f'(2N_f)^c \tag{F9}$$

where b and c are slopes of the respective curves and all the other variables are as defined earlier. These two relationships are usually defined for constant amplitude, completely reversed cycles and therefore pre–strain, mean value, etc. are still to be compensated for.

The linear cumulative damage rule of Miner is usually used because of simplicity and because more complicated ones are still reluctantly accepted in terms of accuracy. One succesful relationship to calculate fatigue life under random dynamic loading was developed by Corten and Dolan (Hofmeister 1959, Collins 1981):

$$N_g = \frac{N_1}{\alpha_1 + \alpha_2\left[\frac{\sigma_2}{\sigma_1}\right]^a + \alpha_3\left[\frac{\sigma_3}{\sigma_1}\right]^a + \ldots + \alpha_i\left[\frac{\sigma_i}{\sigma_1}\right]^a} \tag{F10}$$

where

N_g = Desired answer of cycles to failure
N_1 = Cycles to failure for stressing at σ_1
σ_1 = Maximum applied stress
σ_2 = Second largest applied stress
α_1 = Ratio of cycles N_1 at σ_1 to N_g
α_i = Ratio of cycles N_i at σ_i to N_g
a = A parameter derived from an S–N diagram for the material

Finally, it is necessary to mention shortly how fatigue damage or predicted life can be presented statistically. The Weibull three parameter distribution has been successfully applied where remaining life, damage, strength, etc. are of interest. The Weibull probability density function is given by

$$f(N) = \frac{\beta}{N_a - N_o}\left[\frac{N - N_o}{N_a - N_o}\right]^{\beta-1} \exp - \left[\frac{(N - N_o)}{(N_a - N_o)}\right]^{\beta} \tag{F11}$$

where

N = Random variable namely speciment life, cumulative damage, etc.
N_o = minimum value for random variable.
N_a = characteristic value for random variable.
β = Weibull slope or shape parameter.

For various values of β the Weibull distribution has the shape as depicted in figure F7.

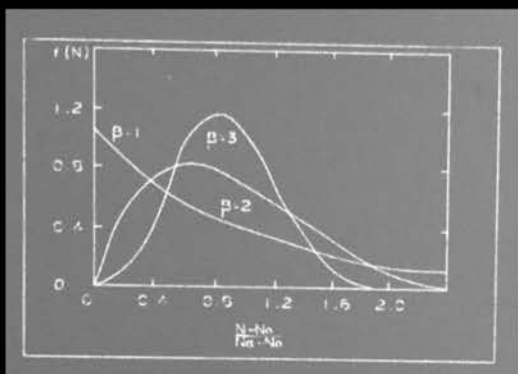

Figure F7: Various Weibull distributions

Fatigue data, be it life cycles or damage values, can be plotted on Weibull probability paper to yield a straight line from whence the slope, β, the characteristic value, N_a, and the minimum value, N_o can be read off directly. The mean and variance can then be calculated to be

$$\mu = N_o + (N_a - N_o)\ \Gamma\ (1+\frac{1}{\beta}) \qquad \text{(F12)}$$

and

$$\sigma^2 = (N_a - N_o)^2 \left[\Gamma\ (1+\frac{2}{\beta}) - \Gamma\ (1+\frac{1}{\beta})^2\right] \qquad \text{(F13)}$$

where Γ is the gamma function. These values can then be used for comparison or reference values or else the median value of the random variable can be read off at the 50% probability point. The median and mean value are not usually the same because the distribution is skewed to the right. (Figure F7).

APPENDIX G

STATISTICAL ACCURACY AND ERRORS

The accuracy of the estimated PSD can be defined in terms of the mean square error

$$\text{rms error} = E[(\dot{G}_x - G_x)^2] \qquad (G1)$$

Where $\dot{G}_x$ is the estimate of the true PSD, G_x. If this relation is expanded it is found that the mean square error is described by the sum of the variance for the estimate and the bias of the estimate

$$E[(\dot{G}_x - G_x)^2] = \mathrm{Var}[\dot{G}_x] + b^2[\dot{G}_x] \qquad (G2)$$

This equation in turn can be manipulated to give the root mean square of the error in terms of the standard deviation for the estimate and the bias error

$$\text{rms error} = \sqrt{\sigma^2[\dot{G}_x] + b^2[\dot{G}_x]} \qquad (G3)$$

The standard deviation for the estimate is called the standard error or random error and is defined as follows

$$\sigma[\dot{G}_x] = \sqrt{E[\dot{G}_x^{\,2}] - E^2[\dot{G}_x]}$$

which can be normalized by being expressed as the fraction of the quantity which is estimated.

$$\text{Normalized standard error:} \quad \epsilon_r = \frac{\sigma[\dot{G}_x]}{G_x} \qquad (G4)$$

In the same way the bias error can be expressed as a normalized quantity.

$$\text{Normalized bias error:} \quad \epsilon_b = \frac{b[\dot{G}_x]}{G_x} \qquad (G5)$$

The total error or rather the normalized rms error can therefore be written as

$$\begin{aligned} \epsilon &= \epsilon_r + \epsilon_b \\ &= \frac{\sqrt{\sigma^2[\dot{G}_x] + b^2[\dot{G}_x]}}{G_x} \\ &= \frac{\sqrt{E[(\dot{G}_x - G_x)^2]}}{G_x} \end{aligned} \qquad (G6)$$

For spectral density estimates the error can be compiled by defining the two relevant sources seperately and then combining it. Thus the variance of the estimate is derived from the definition of the PSD similar to (C28).

$$\hat{G}_x(f) = \frac{\hat{\Psi}_x{}^2(f, \Delta f)}{\Delta f}$$

$$\text{with } \Delta f = B_e \hat{G}_x(f) = \frac{\hat{\Psi}_x{}^2(f, B_e)}{B_e} \qquad \text{(See Appendix D)}$$

Therefore $B_e\hat{G}_x(f) = \hat{\Psi}_x{}^2(f,B_e)$, but because of the relationship defined by (B7) which is also interpreted as $R_x(o) = B_eG_x(f)$ the variance can be written as

$$\text{Var}[B_e\hat{G}_x(f)] \simeq \frac{B_e{}^2G_x{}^2(f)}{B_eL}$$

$$\text{Var}[B_e\hat{G}_x(f)] \simeq \frac{G_x{}^2(f)}{B_e\,L} \qquad \text{(G7)}$$

where L, the record length in meter, replaces the time interval T which was used in Appendix C. The effective bandwidth B_e is defined as $B_e = 1/L = \Delta f$ which is also the frequency resolution.

The bias error can be expressed by

$$b[\hat{G}_x(f)] \simeq \frac{B_e{}^2}{24}\, G_x''(f) \qquad \text{(G8)}$$

where $G_x''(f)$ is the second derivative of $G_x(f)$ with respect to f.

The total normalized mean square error of the PSD estimate $\hat{G}_x(f)$ is given by equation (G6)

$$\epsilon^2 = \frac{E[(\hat{G}_x(f) - G_x(f))^2]}{G_x{}^2(f)}$$

$$\therefore \quad \epsilon^2 \simeq \frac{1}{B_e\,L} + \frac{B_e{}^4}{576}\left[\frac{G_x''(f)}{G_x(f)}\right]^2 \qquad \text{(G9)}$$

Because the bias error is a function of the second derivative of the PSD, $G_x''(f)$, it is pronounced by peaks being present in the spectral data. The result is that if high bias error exists, high peaks in the data are underestimated. Because no sharp peaks should exist in surface roughness spectral data, the bias error component would be small with respect to the random error component. For this reason the bias error are neglected in this work and the complete normalized standard error is thus defined by

$$\epsilon = \epsilon_r = \frac{1}{\sqrt{B_e L}} \tag{G10}$$

But now, if the PSD is estimated from the FFT as explained in appendix C paragraph 4, a smoothing operation is required in the data to make the estimate consistent. An estimate obtained through FFT estimates are independent of the sample record length and is therefore an inconsistent estimate (Bendat & Piersol 1979) (see also appendix A). Two ways of smoothing can be employed to obtain a consistent estimate, the first is called time averaging. The total sample length L is devided into smaller records L' and the PSD of each smaller sample is calculated afterwhich averaging of these PSD's over every frequency takes place. The effective bandwidth B_e is now defined as $B_e = 1/L$. The length of L' are determined by the number of data points required to calculate one FFT of the sample. This number should always be a power of two because of the algorithm for the FFT as a method to calculate the DFT of a waveform (See appendix C, par 4.1). This means that the total length L should include enough points so that a number of samples L' could be extracted from it. (See appendix C, par. 5).

The second way of smoothing the data is by frequency smoothing. This process is explained in detail in appendix D, paragraph 2, which is to average the value of the PSD at frequencies in narrow bandwidths. This is usually employed if the sample length cannot be devided into smaller records in order to do time averaging, because the total sample length includes just enough data points for one PSD calculation. Mention is made by authors (Newland, 1984 , Bendat & Piersol, 1971) of a process where zeros can be added to a waveform in order to complete a second, third or subsequent sample record so that time averaging can be done. This ought to be done with care and not without a thorough knowledge of the implications involved.

If frequency smoothing is employed the effective bandwidth B_e is differently defined namely,

$$B_e = \frac{(2n+1)}{L} \qquad n = 1,2,3\ldots\left[\frac{N_x}{2} - 1\right]/2 \tag{G11}$$

where $2n + 1$ is the number of adjacent spectral values which are averaged, and N_x is the number of discrete sample values in the random history in question. The detail of one such averaging or smoothing procedure is contained in appendix D.

If either of these smoothing operations are not performed the standard error equals 1 and this implies a 100% inaccuracy (Equation (G10)). In the work discussed in this report both techniques were used because it sometimes occured that the measured terrain sample was just not long enough to do more than one FFT calculation on it. Averaging adjacent spectral values had to be done in any case to obtain a smoothed curve for the calculation of the roughness constant K.

APPENDIX H

DIGITIZING OF CONTINUOUS DATA AND ALIASING

A continuous signal can be stored digitally by observing successive values of this signal at equally spaced intervals apart. This process is illustrated in figure H1.

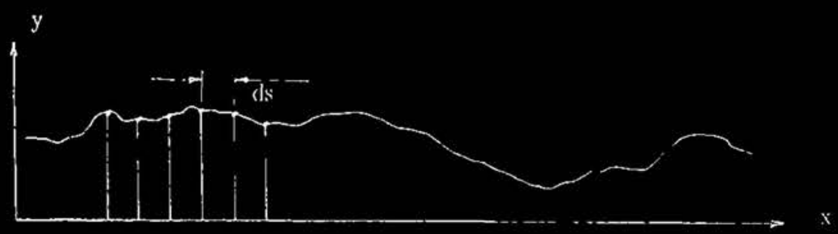

Figure H1

Sampling at points too close together will result in an unnecessary high amount of digitized values. Sampling at points too far apart will lead to confusion between the low and high frequencies in the data. It is imperative therefore to select the correct value of the sample interval 'ds'. This phenomenon is illustrated in figure H2 where the high frequency waveform is seen as the low frequency waveform when digitized. This is called aliasing.

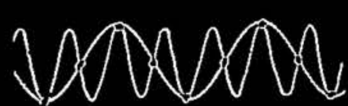

Figure H2

The sampling frequency is defined as $f_s = {}^1/_{ds}$. It is clear from figure H2 that one cycle is defined when at least two samples are made per cycle. Thus the highest frequency which can be defined when sampling at f_s is $f_s/2$. This is called the cut–off or Nyquist frequency and is defined by

$$f_c = \frac{1}{2ds} \qquad (H1)$$

From a closer study of figure H2 it can be seen that during aliasing a certain high frequency is duplicated or folded over as a predictable lower frequency. This does have a influence on the shape of the PSD as shown in figure H3a which shows the true spectrum and figure H3b which shows the aliased spectrum

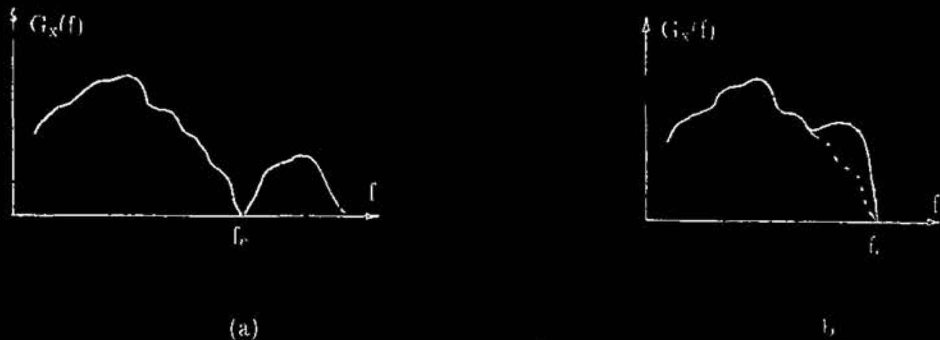

Figure H3

In order to avoid corrupting the data in this manner two solutions are possible. Firstly the cut–off frequency can be choosen so high that it is not possible for the data to contain any higher frequencies, or secondly the undigitized data can be filtered above the highest frequency of interest and then the sampling frequency is chosen twice as high. The second method is usually employed hence the use of anti–aliasing filters before digitizing

Aliasing occure, during the measurement of a surface profile with the measuring device described in this report, when the proximity switch generates pulses at steady intervals 'ds' but wavelengths smaller than 'ds' exist in the data. It is not physically possible to filter these frequencies out of the profile before measurement except when it happens in any event by the crushing effect of the towing vehicles' tyres. When the profile is unyielding the effect of aliasing ought to be considered during the analyses of the measured data with a PSD.

APPENDIX I

WIRING DIAGRAM OF MEASURING SYSTEM

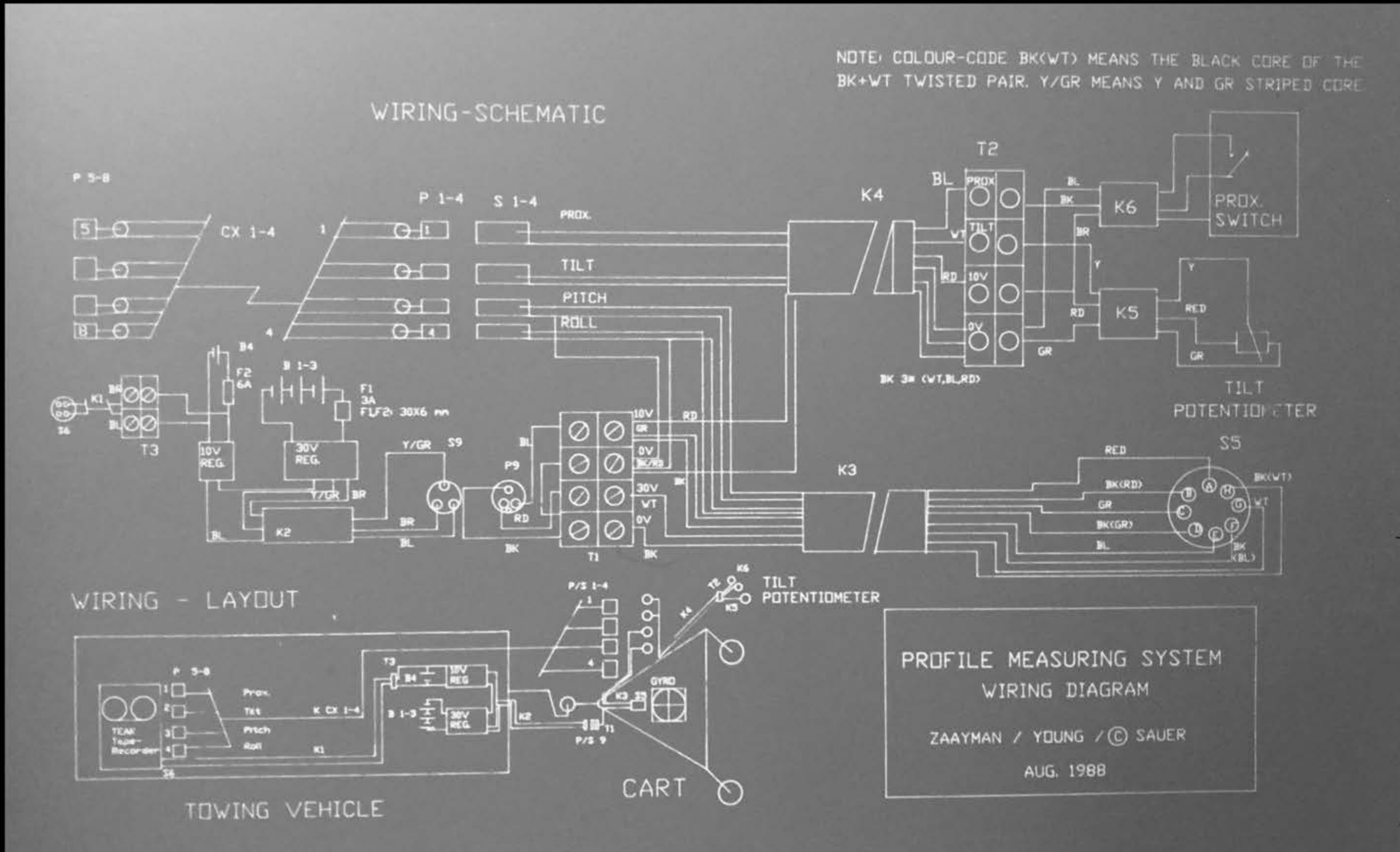
NOTE: COLOUR-CODE BK(WT) MEANS THE BLACK CORE OF THE BK+WT TWISTED PAIR. Y/GR MEANS Y AND GR STRIPED CORE
WIRING-SCHEMATIC
P 5-8
CX 1-4
P 1-4
S 1-4
PROX.
TILT
PITCH
ROLL
K4
T2
PROX
TILT
10V
0V
K6
K5
PROX. SWITCH
TILT POTENTIOMETER
BK 3= (WT,BL,RD)
S5
K3
T1
T3
10V REG.
30V REG.
K2
B 1-3
B4
F2 6A
F1 3A
F1,F2: 30X6 mm
Y/GR
S9
P9
WIRING - LAYOUT
TOWING VEHICLE
TEAK Tape-Recorder
P 5-8
Prox.
Tilt
Pitch
Roll
K CX 1-4
K1
P/S 1-4
P/S 9
TILT POTENTIOMETER
GYRO
CART
PROFILE MEASURING SYSTEM
WIRING DIAGRAM
ZAAYMAN / YOUNG / © SAUER
AUG. 1988

APPENDIX J

GUIDELINE FOR SOFTWARE USAGE

The 4 channels of data which is the output of the measuring system is stored on computer disc. Channels are allocated as follows.

Chan 1 ⇒ proximity switch pulses
Chan 2 ⇒ gyro pitch angle theta
Chan 3 ⇒ gyro roll angle beta
Chan 4 ⇒ wheelset swivel angle alfa

The data is processed by the program PROFILE to yield two arrays (right and left track) height values in mm, at equal spaced distances 'ds' mm apart. These values are in integer format so that it can be further processed by File Editor software with respect to filtering of low frequencies or trend removal. The data is then converted to real format by the program FLOATFILE. A calibration is introduced here to convert the profile heights to 'meter' values.

A type 1 data file is thus available which contain heights as REAL values. Every value is a measured profile height in meter, accurate to the mm, spaced a equal, known distance 'ds' [m] apart. This file would consist of two channels, the left and right hand track of a vehicle. The file should NOT be SHORTER than 1024 REAL values ie. 8 x 128 real w blocks
8 x 256 integer blocks (TFC blks)
16 x 128 integer blocks (HP blks)

The procedure would be as follows:

1. Calculate spatial PSD by calling SPECTRAL. All other signal analysis functions are also available. The PSD is stored in a file which is named by the user.
2. Calculate the smoothed PSD by calling SMOOTHPSD. The PSD is read out of the file which it was stored in above and the smoothed PSD is stored in another file. Use the smoothed PSD to calculate the roughness constant K, and the slope, a, in the formula G = Kn**a. This is done by the same calling program.
3. A hardcopy file can be generated at any stage in the above two steps by selecting the appropriate softkey. This hard copy file is then plotted on the plotter by calling HARDCOPY.

TO CALCULATE PROFILE HEIGHTS FROM ORIGINAL RAW DATA

Calling program: PROFILE
Load file: PROFILE.LOD
Forms: PROFILE1.FROM
Include files: FORMSDATA.INC
Subroutines: none

TO CONVERT INTEGER FILE TO REAL FILE

Calling program: FLOATFILE

TO CALCULATE PROFILE SPATIAL PSD

Calling program: SPECTRAL.FTN
Load file: SPECTRAL.LOD
Forms: SPECTRAL1.FORM main menu
SPECTRAL2.FORM menu for 1 file
SPECTRAL3.FORM menu for 2nd file
Include files: ANALYSIS.INC
FORMSDATA.INC
SPECTRCOPY.INC
Subroutines: ANALYSIS.FTN Do all spectral analysis and screen display. This subroutine includes the subroutine PLOTSPECTR in another format as below.

TO CALCULATE SMOOTHED PSD AND ROUGHNESS CONSTANT

Calling program: SMOOTHPSD.FTN
Load file: SMOOTHPSD.LOD
Forms: SMOOTHPSD1.FORM main menu
SMOOTHPSD2.FORM one file name
SMOOTHPSD3.FORM two file names
SMOOTHPSD3.FORM fitting straightline to PSD
Include files: ANALYSIS.INC
FORMSDATA.INC
SPECTR_COPY.INC
Subroutines: PLOTSPECTR.FTN

TO PLOT HARDCOPIES ON PLOTTER

Calling program: HARDCOPY.RUN (SPECTRCOPY.FTN
Load file: SPECTRCOPY.LOD
Include files: SPECTR_COPY.INC

APPENDIX K

QUALIFICATION TESTS CURVES

FIGURE K1

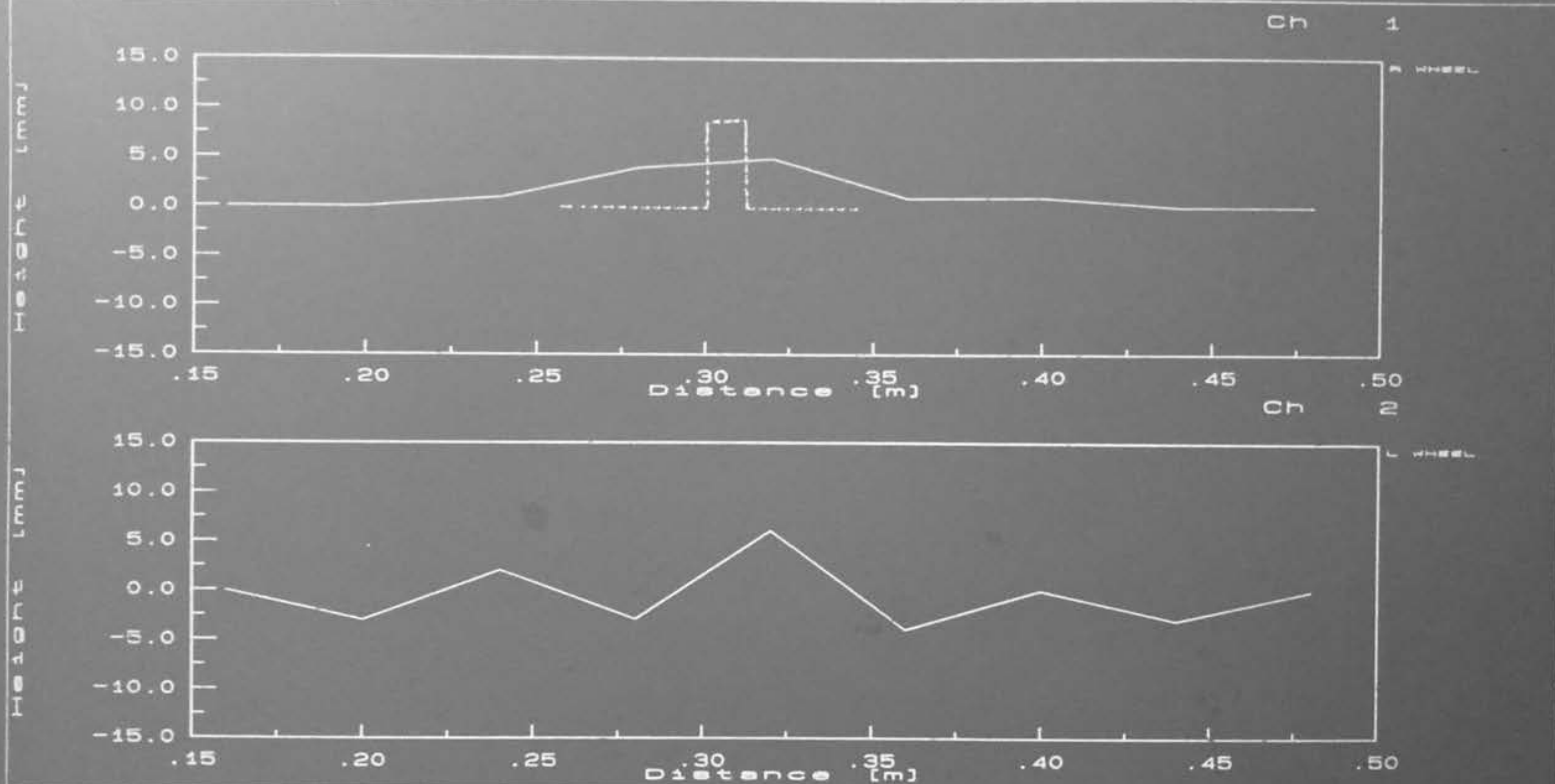

8X8 mm Square Obstacle

FIGURE K2

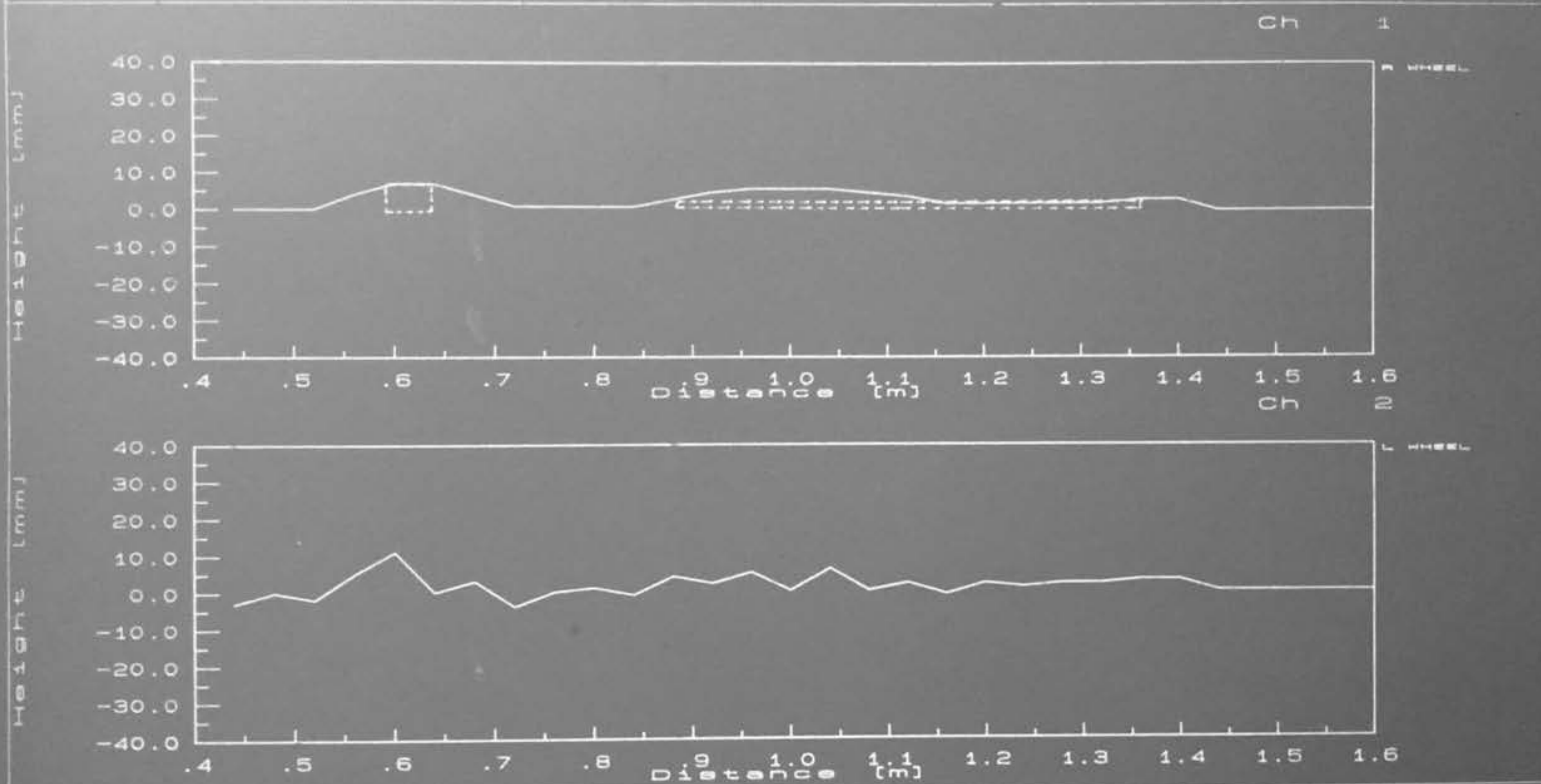

Flat Plates 7 mm & 3 mm

FIGURE K3

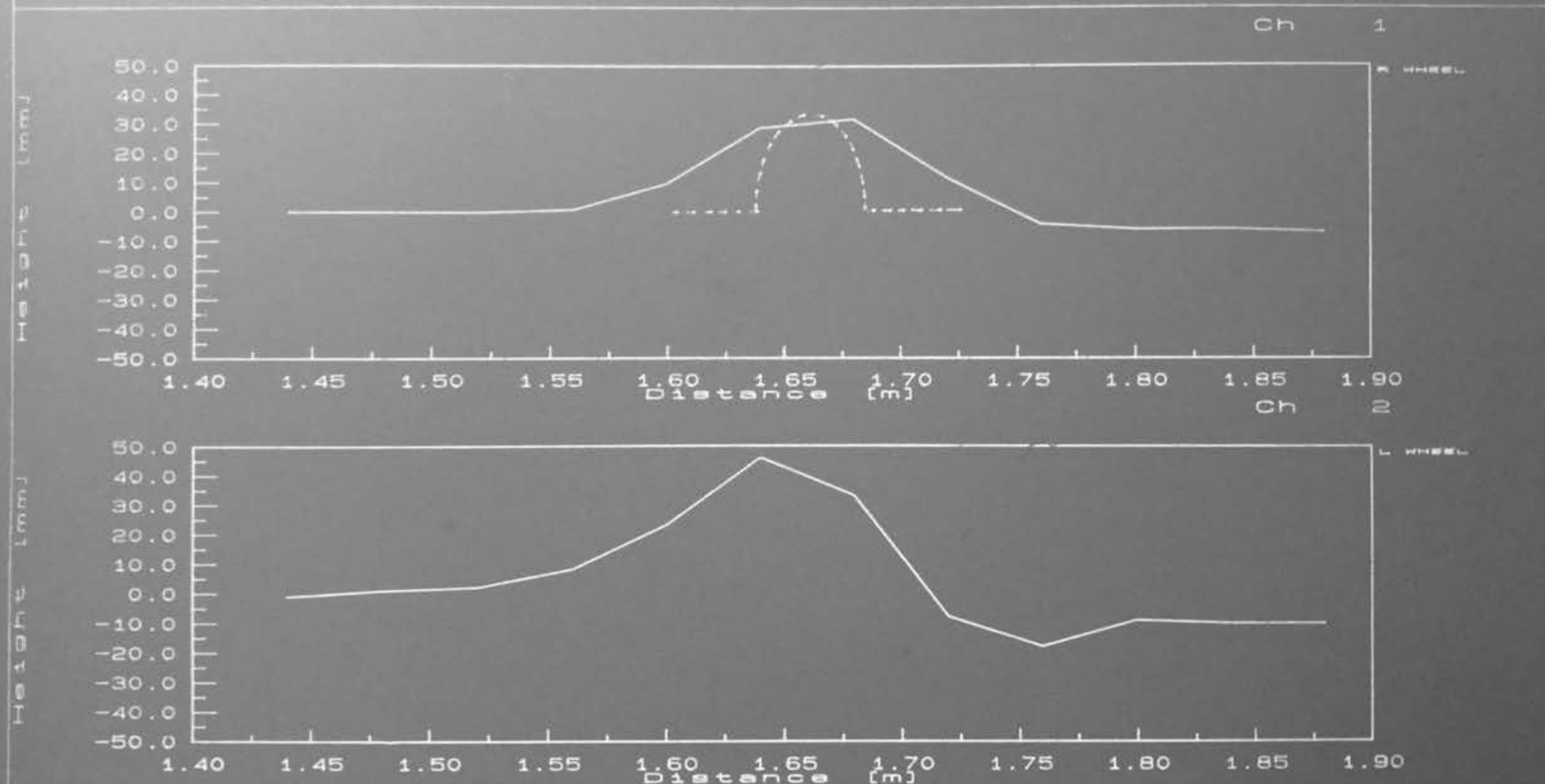

37.5 mm Half Round

FIGURE K4

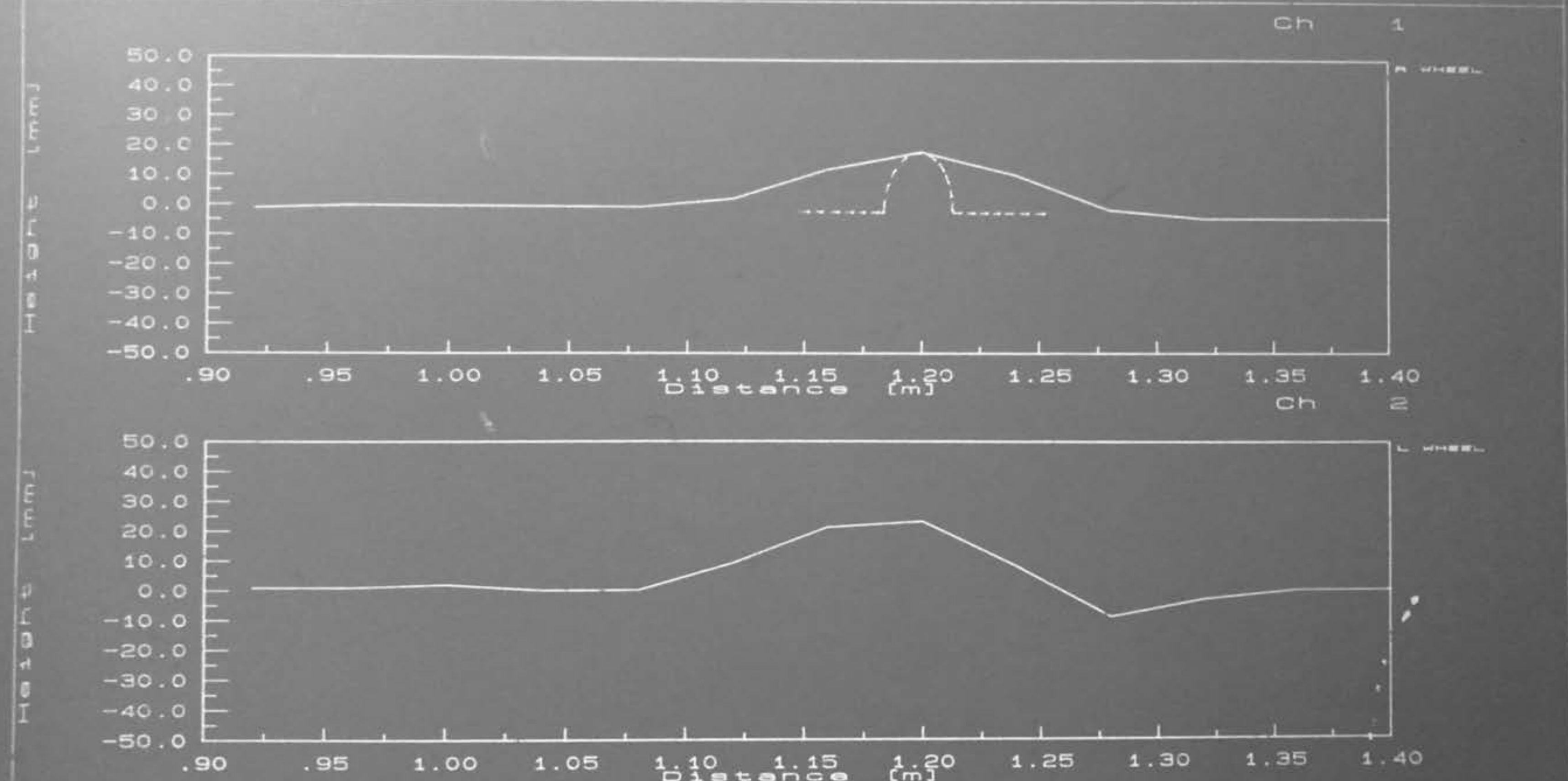

25 mm Half Round

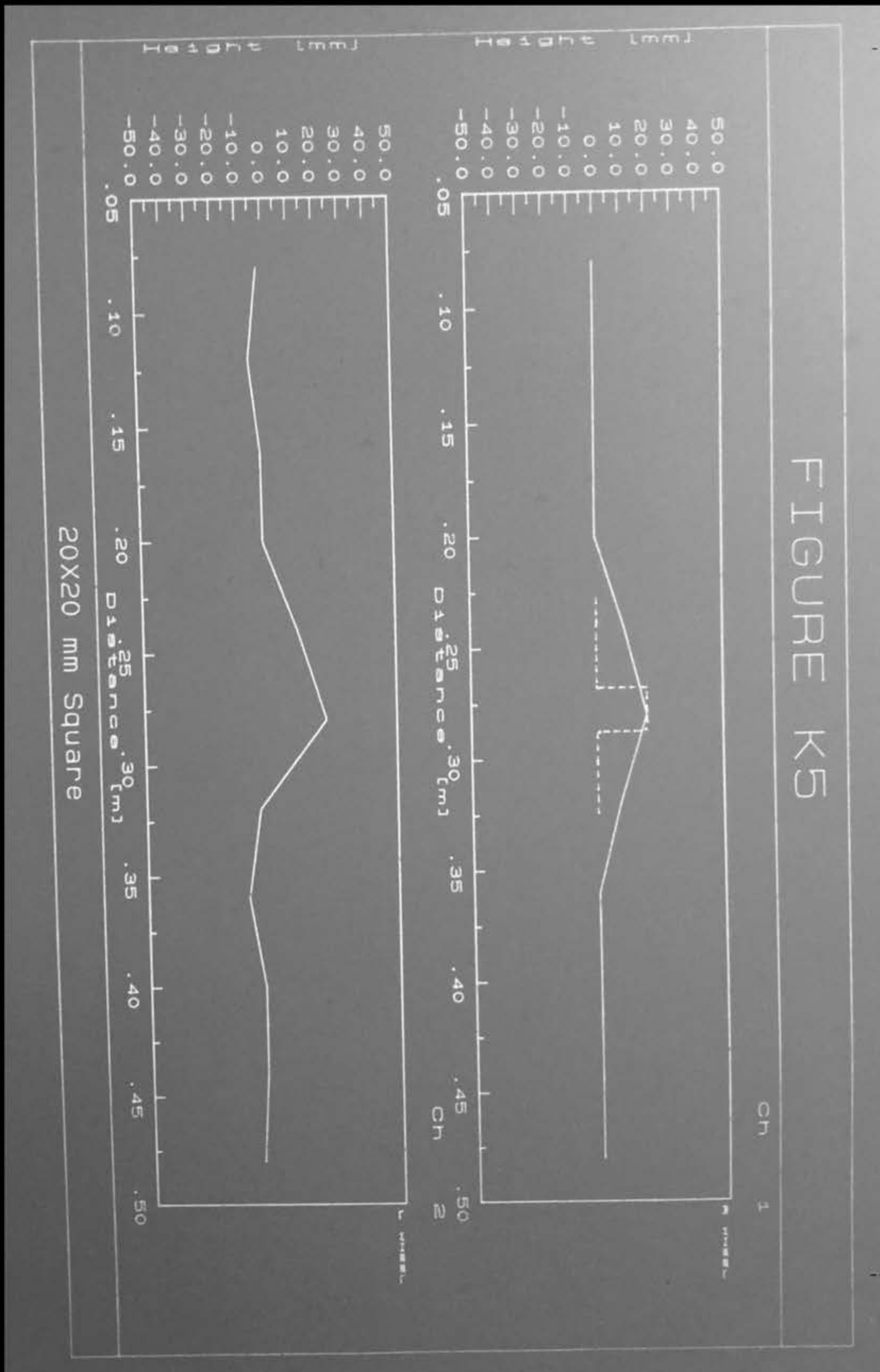
FIGURE K5
Ch 1
R WHEEL
Ch 2
L WHEEL
Height [mm]
50.0
40.0
30.0
20.0
10.0
0.0
-10.0
-20.0
-30.0
-40.0
-50.0
.05
.10
.15
.20
.25
.30
.35
.40
.45
.50
Distance [m]
20X20 mm Square

FIGURE K6

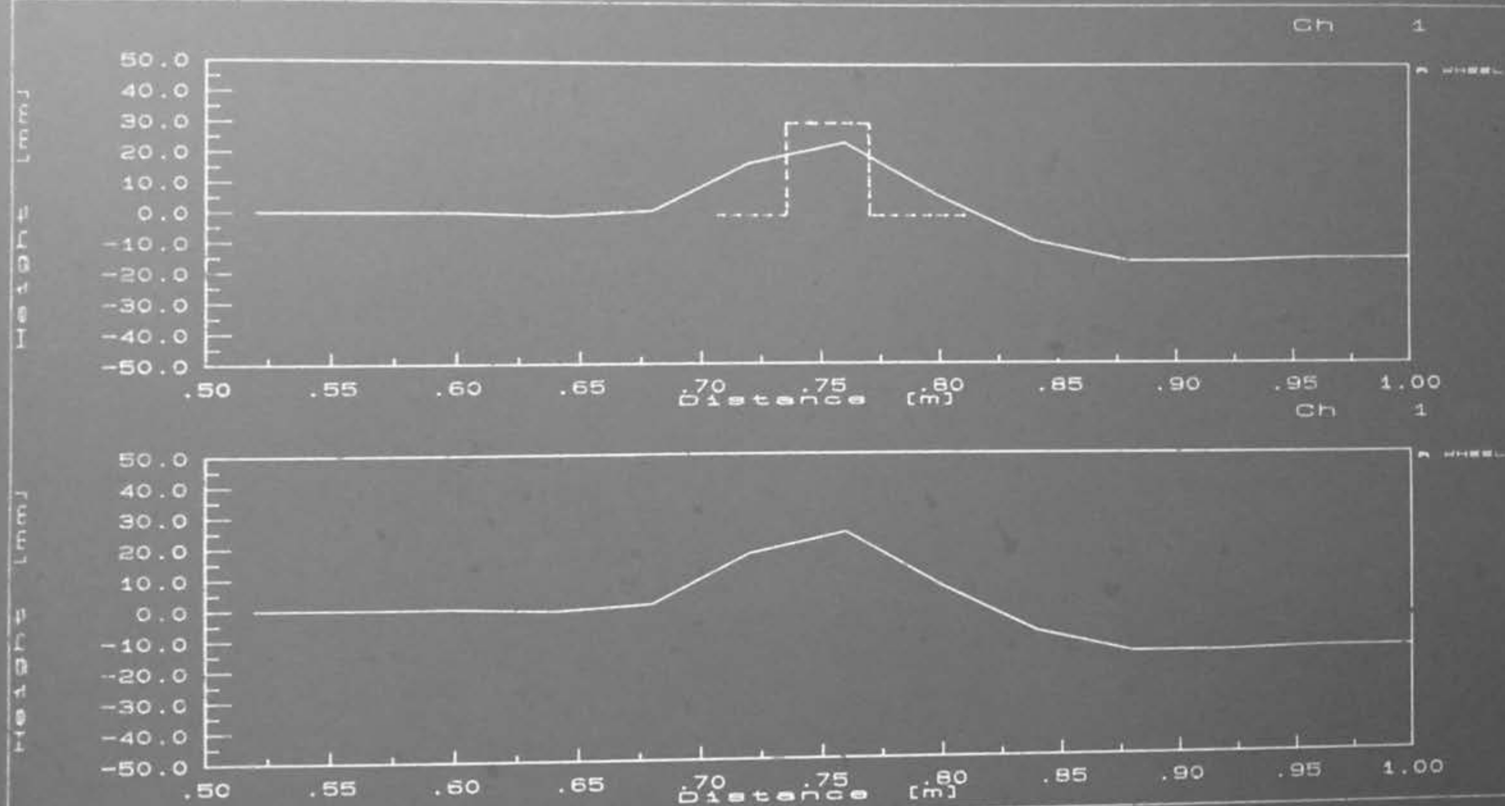

30X30 mm Square

FIGURE K7

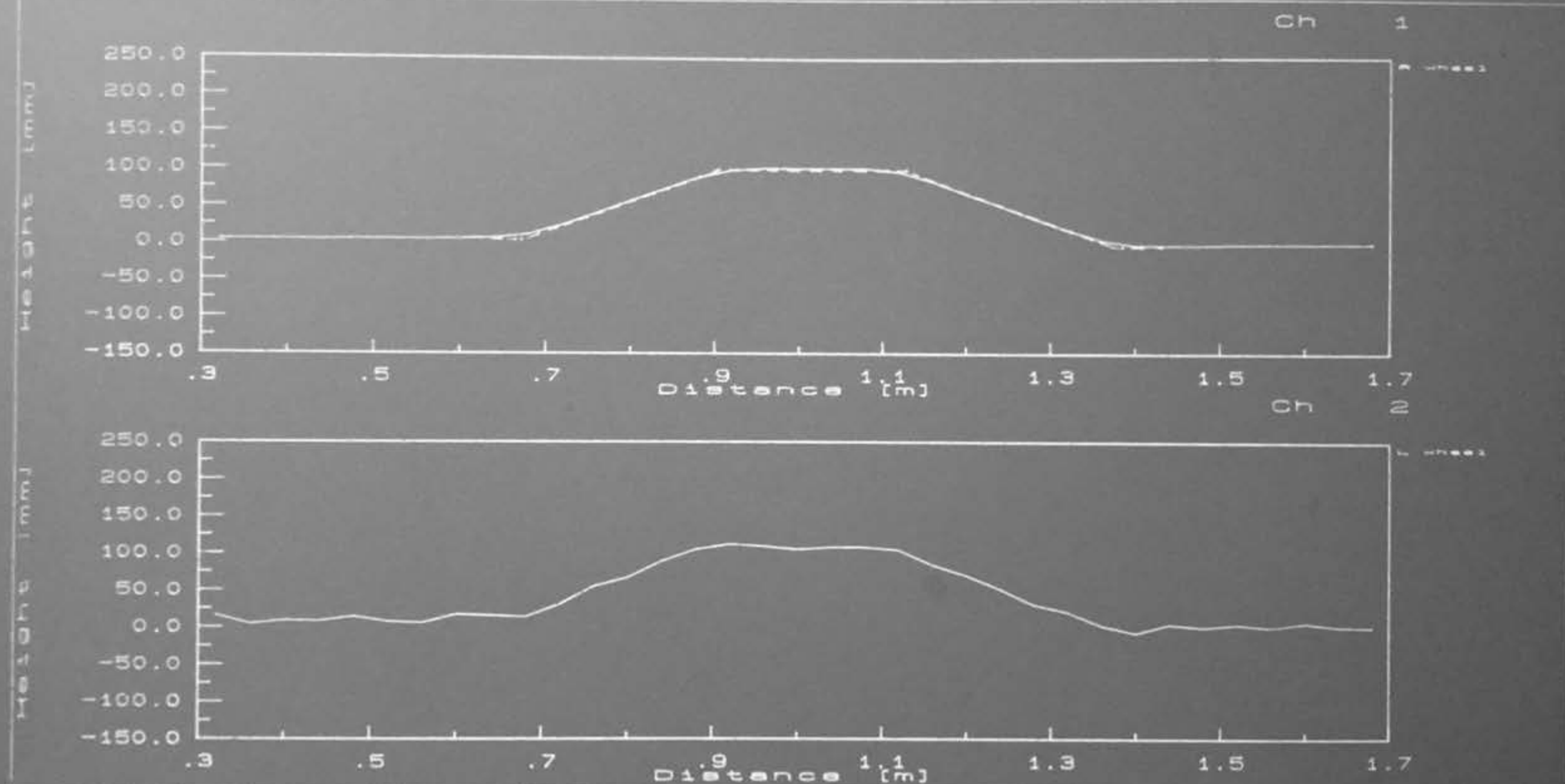

Sloped step obstacle

FIGURE K8

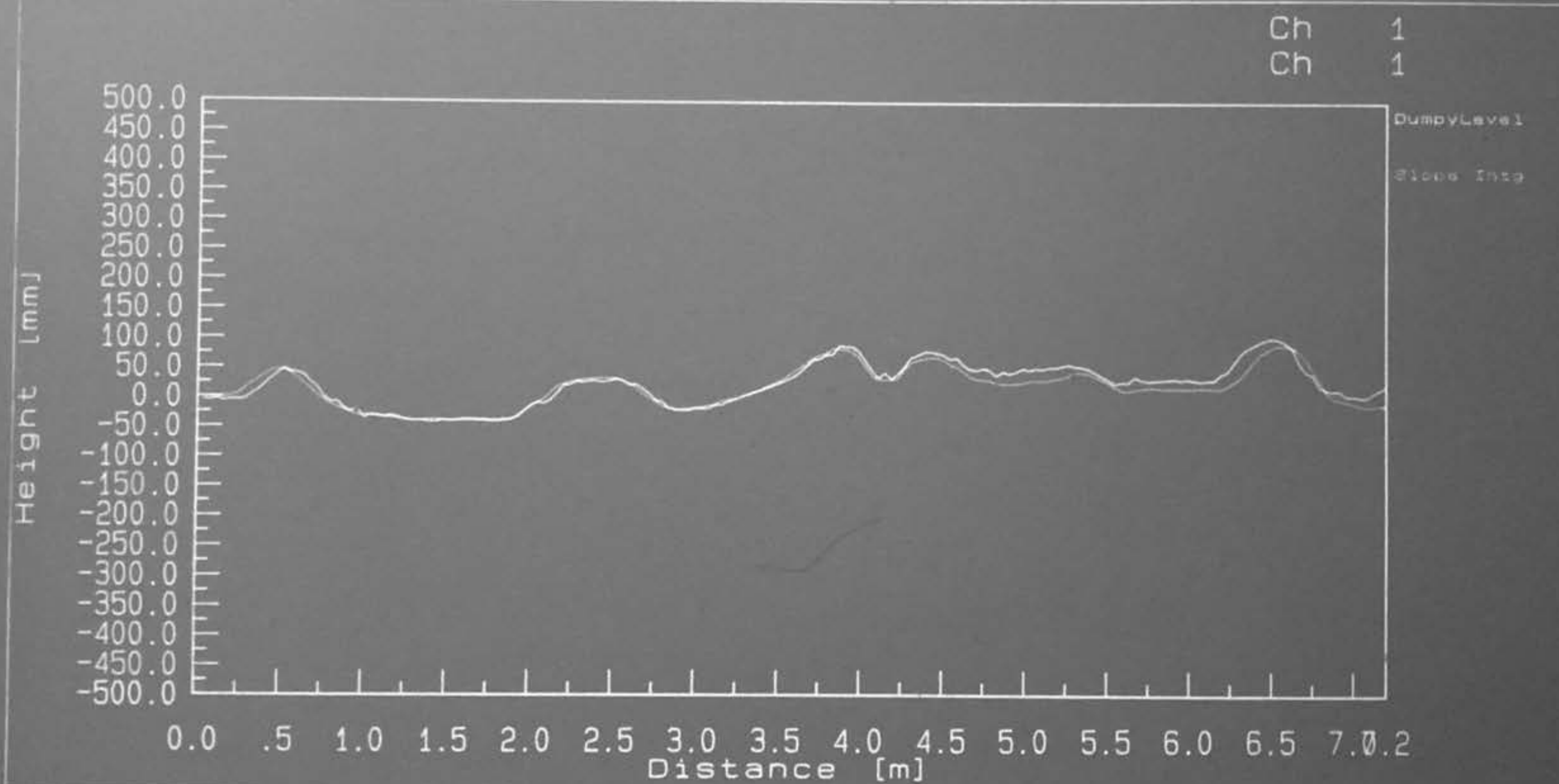

Comparison between the dumpy level & slope integration method.

APPENDIX L

FIELD TESTS CURVES

FIGURE L1

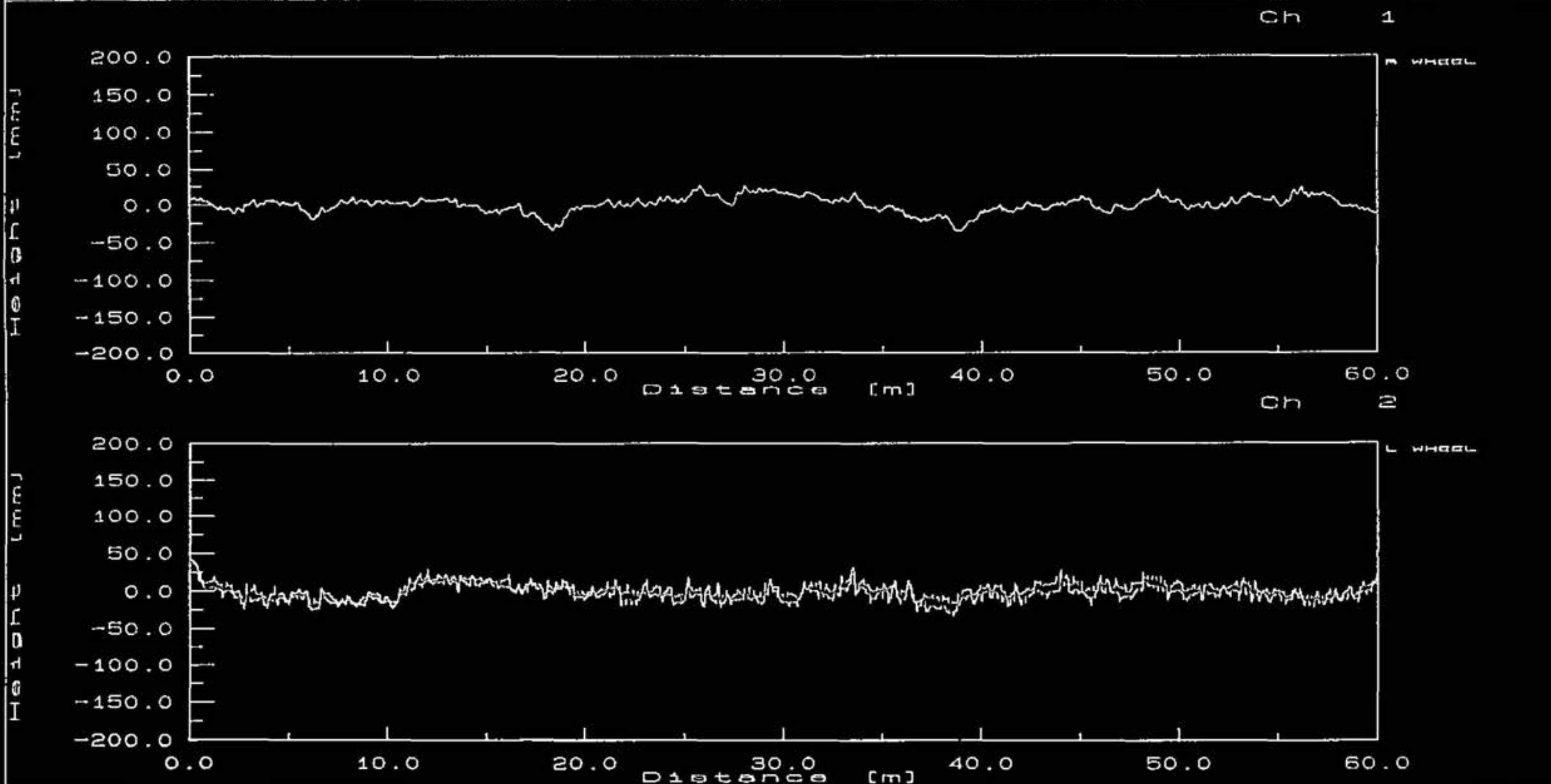

Dirt road with lose pebbles.

FIGURE L2

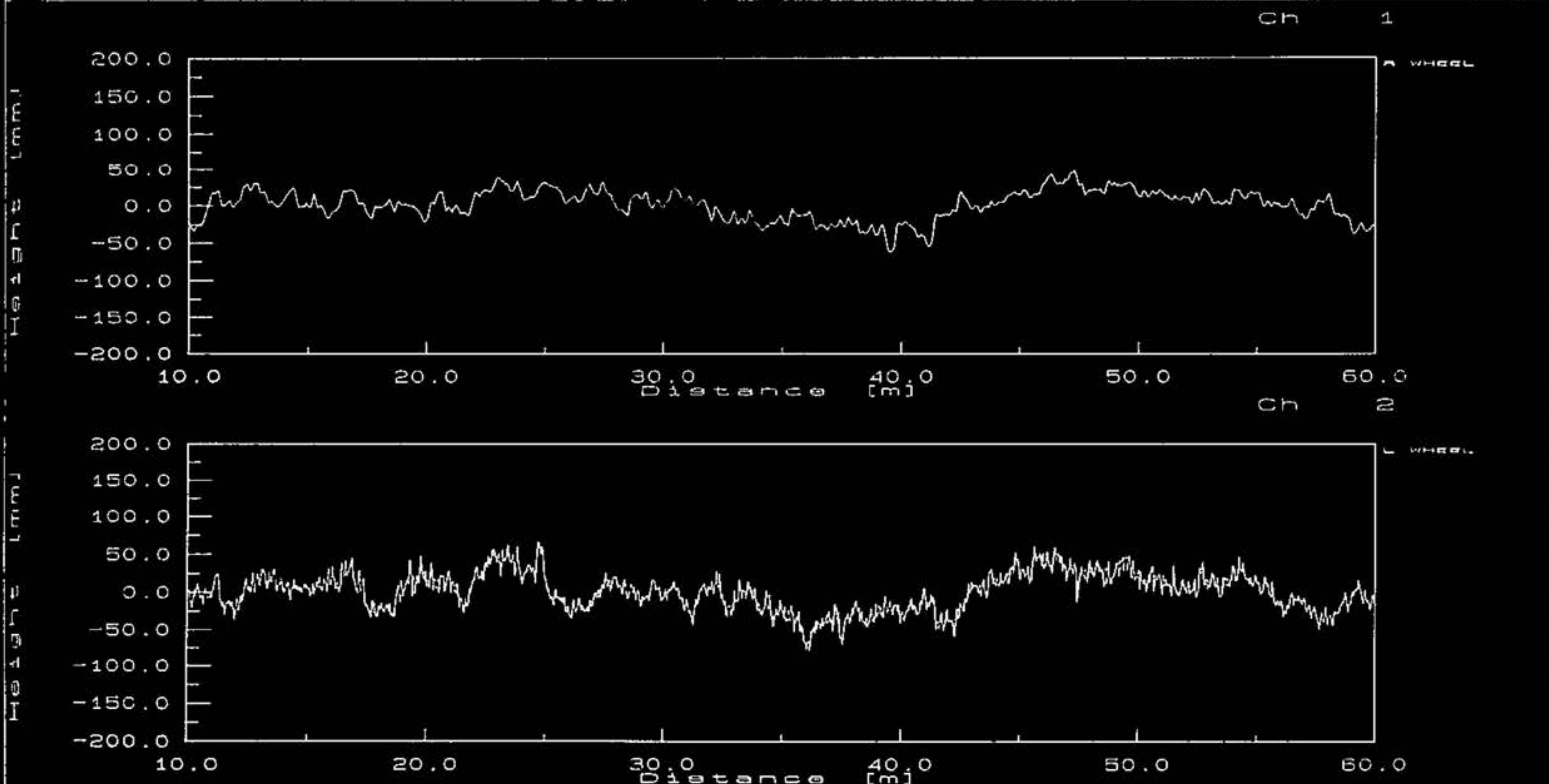

Belgian Paving

FIGURE L3

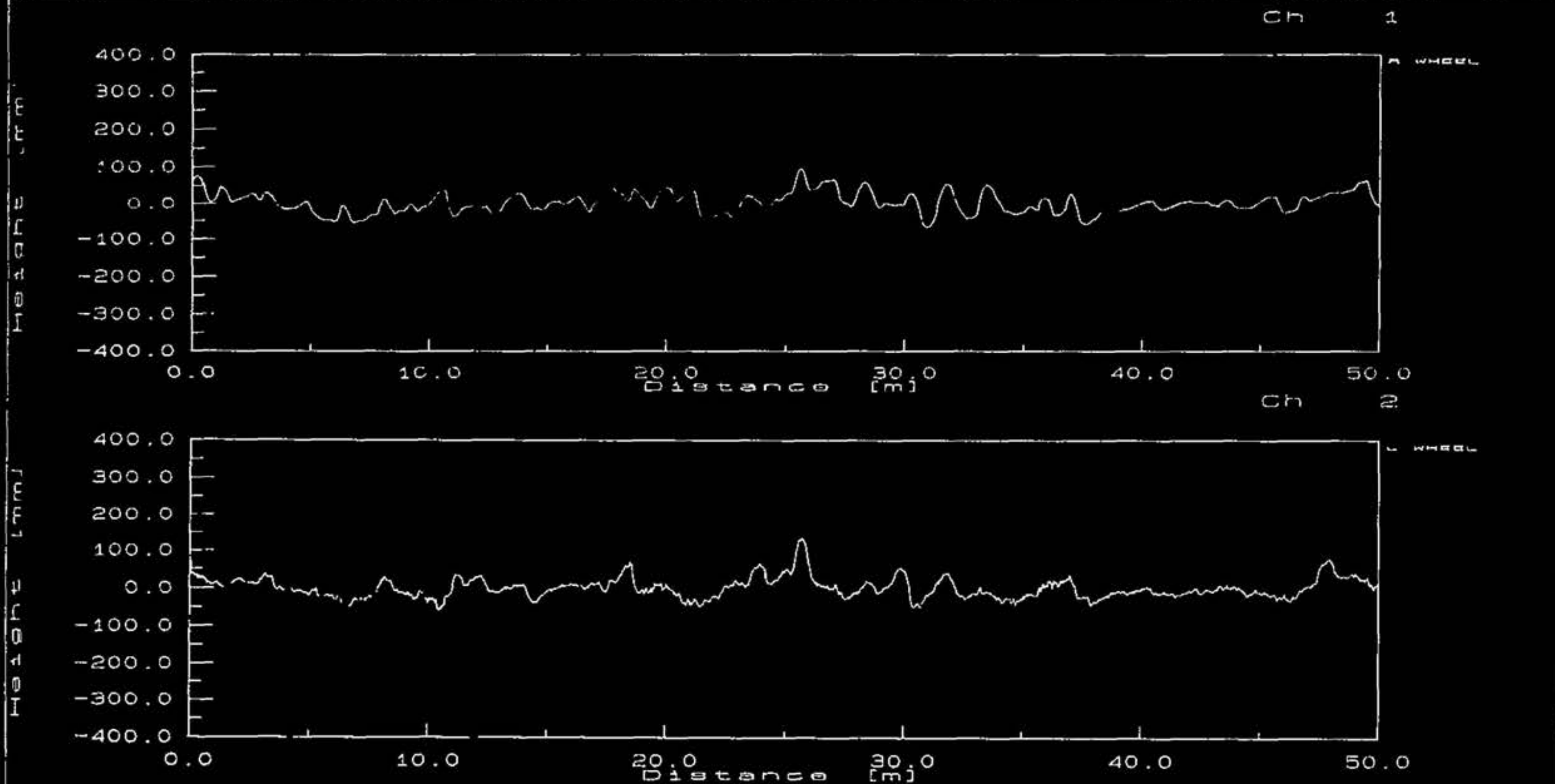

Rough concrete synthetic track copied from natural terrain.

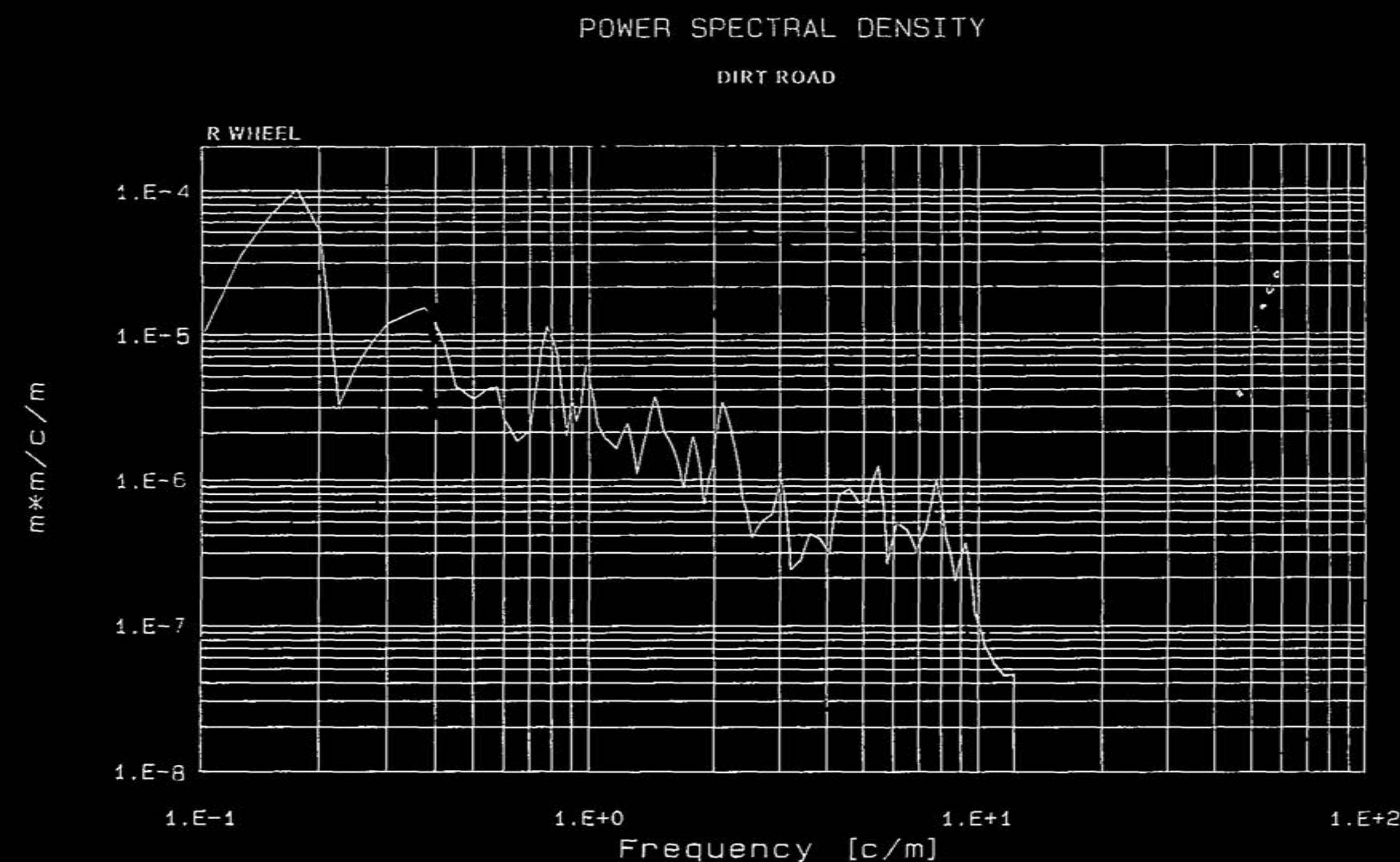
POWER SPECTRAL DENSITY
DIRT ROAD
R WHEEL
1.E-4
1.E-5
1.E-6
1.E-7
1.E-8
m*m/c/m
1.E-1
1.E+0
1.E+1
1.E+2
Frequency [c/m]

FIGURE L4

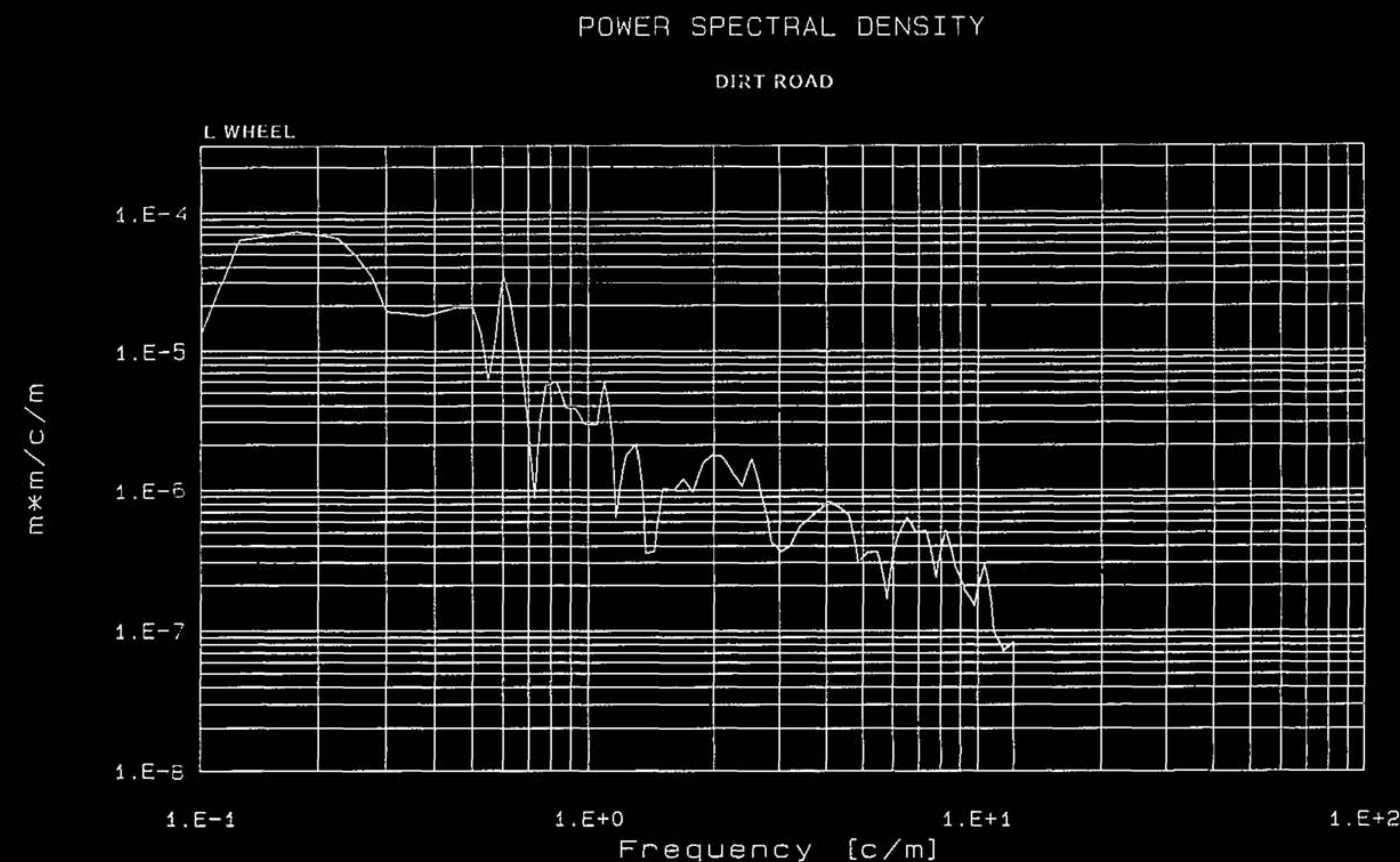
POWER SPECTRAL DENSITY
DIRT ROAD
L WHEEL
1.E-4
1.E-5
1.E-6
1.E-7
1.E-8
m*m/c/m
1.E-1
1.E+0
1.E+1
1.E+2
Frequency [c/m]

FIGURE L5

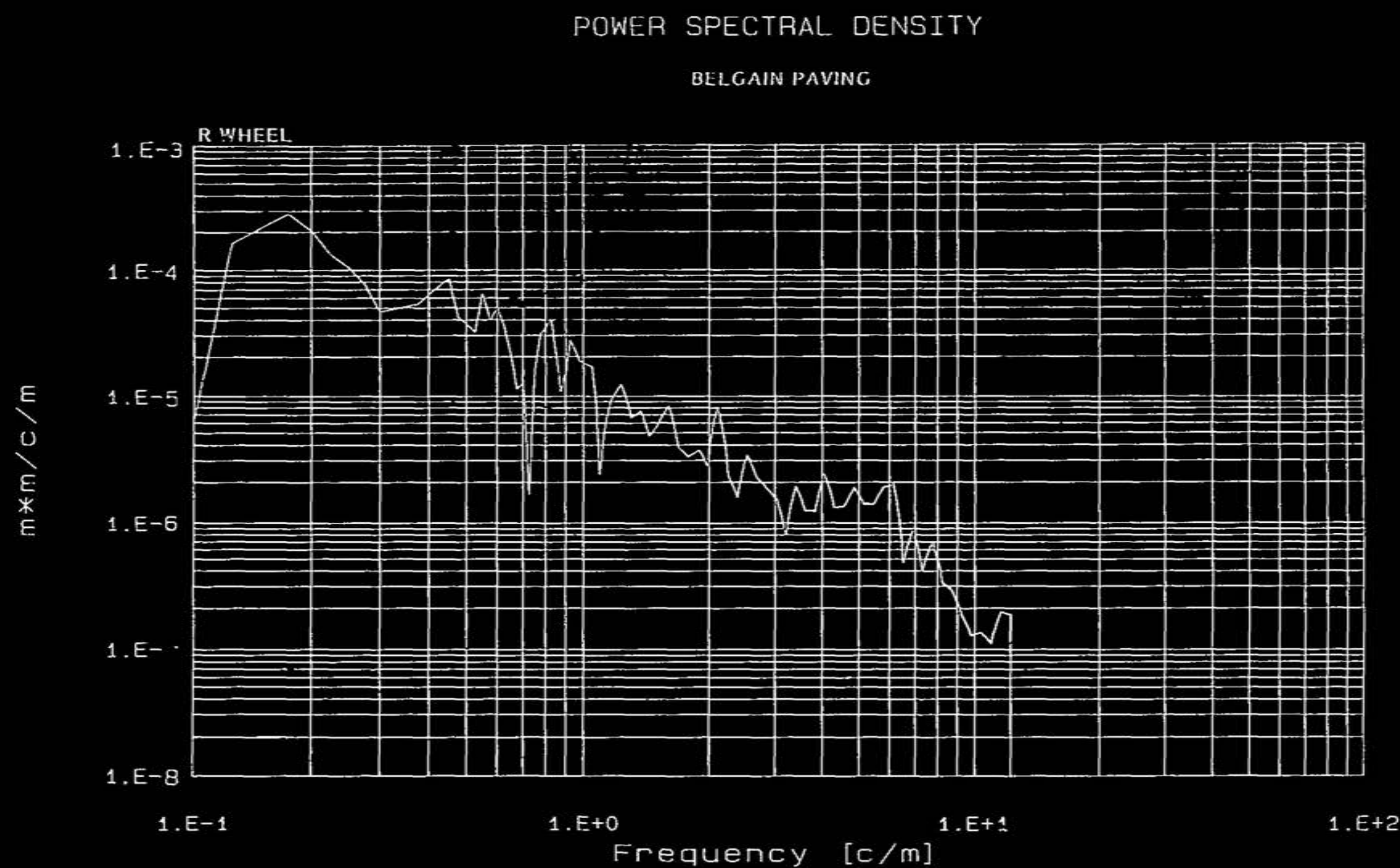
POWER SPECTRAL DENSITY
BELGAIN PAVING
R WHEEL
1.E-3
1.E-4
1.E-5
1.E-6
1.E-8
m*m/c/m
1.E-1
1.E+0
1.E+1
1.E+2
Frequency [c/m]

FIGURE L6

POWER SPECTRAL DENSITY

BELGIAN PAVING

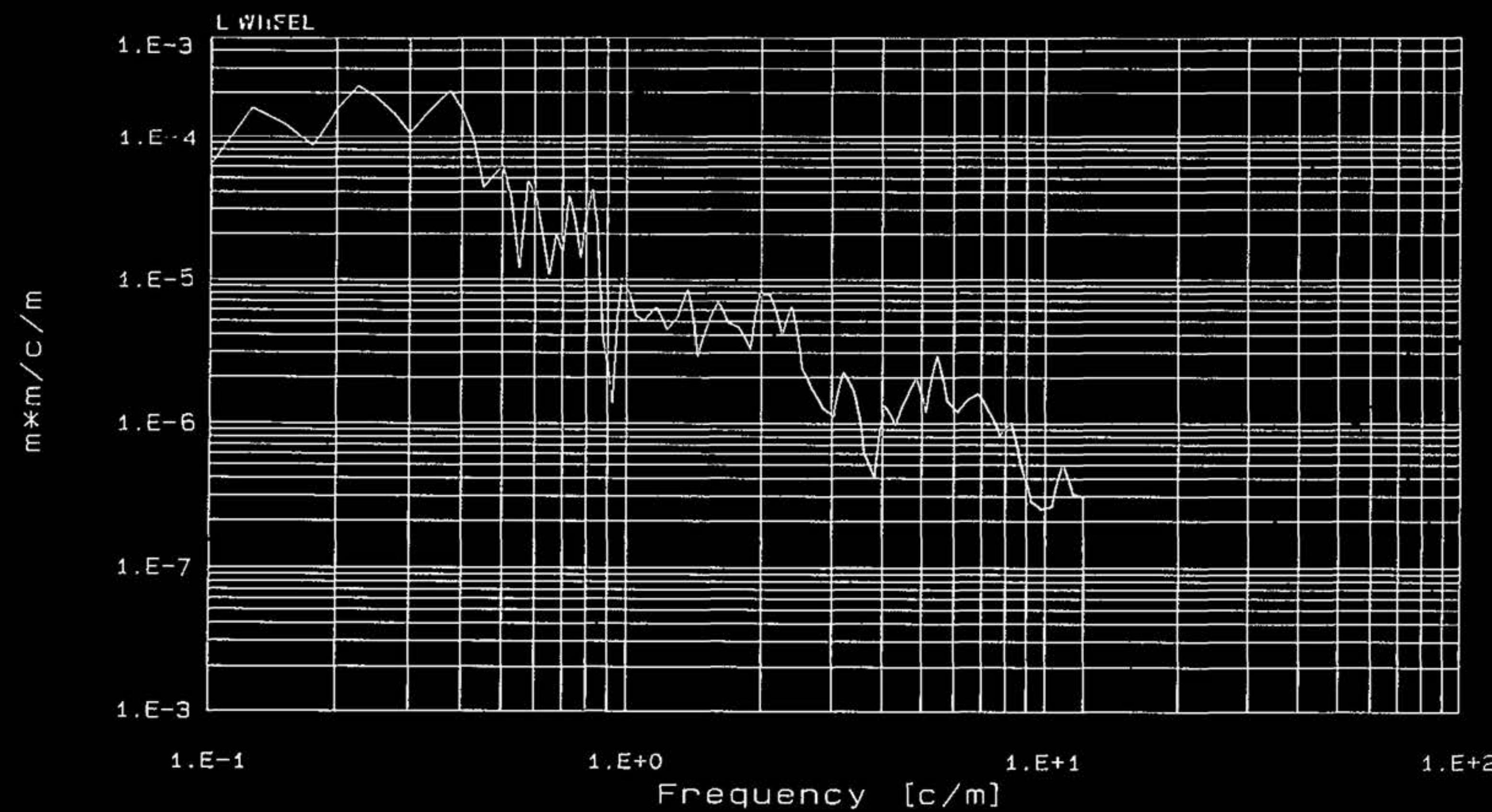

FIGURE L7

POWER SPECTRAL DENSITY

ROUGH TRACK

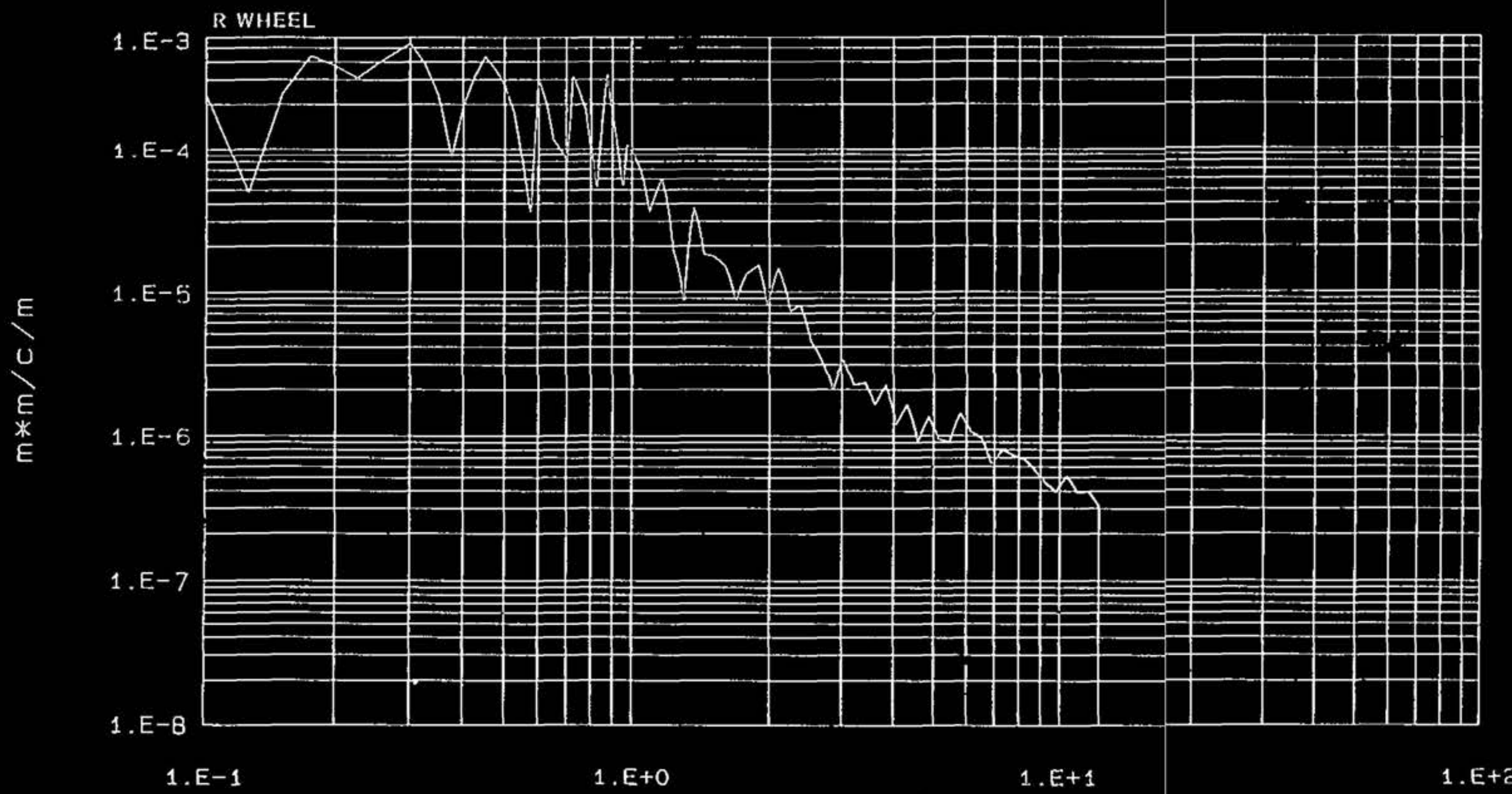

FIGURE L8

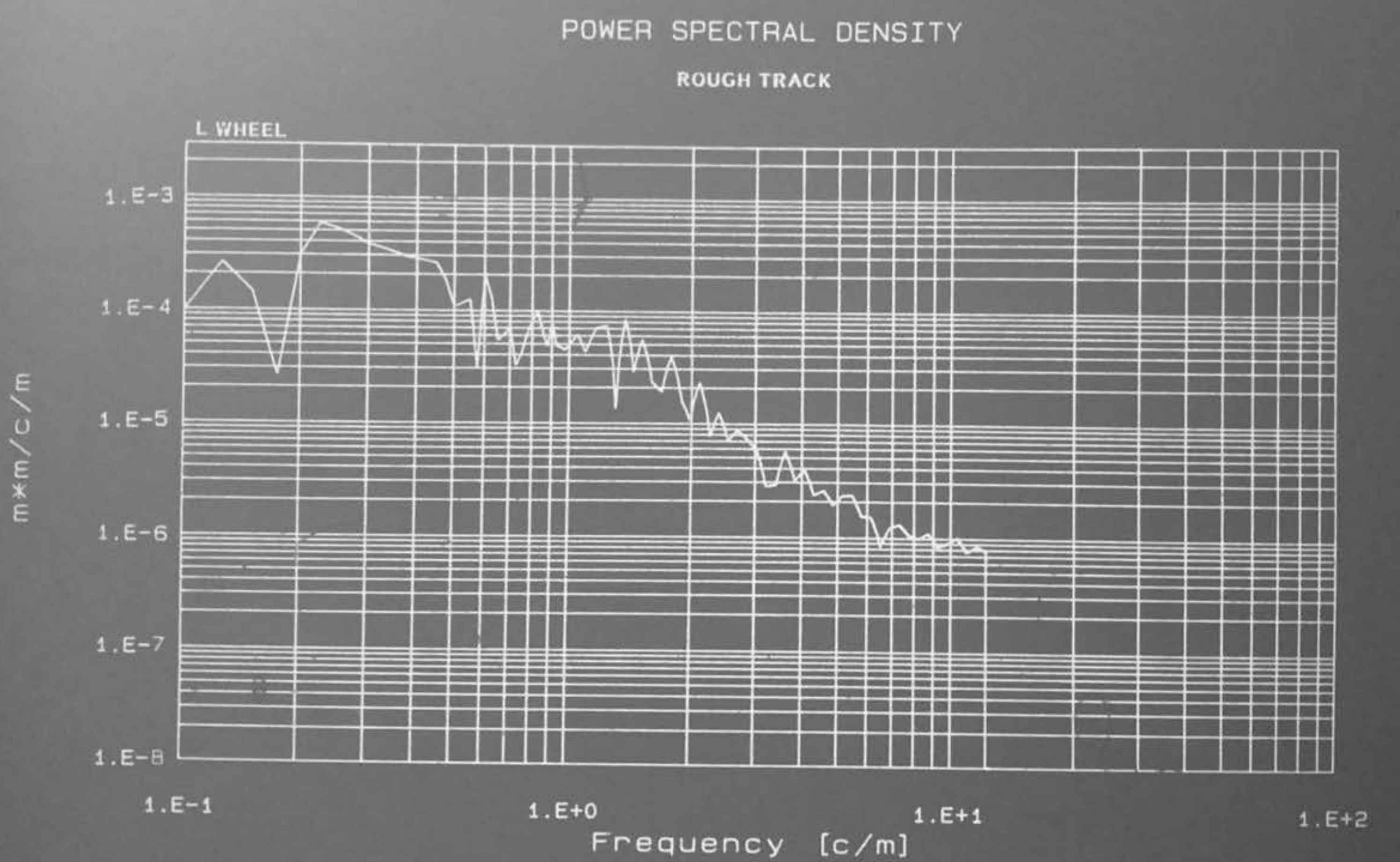
POWER SPECTRAL DENSITY
ROUGH TRACK
L WHEEL
m*m/c/m
1.E-3
1.E-4
1.E-5
1.E-6
1.E-7
1.E-8
1.E-1
1.E+0
1.E+1
1.E+2
Frequency [c/m]

FIGURE L9

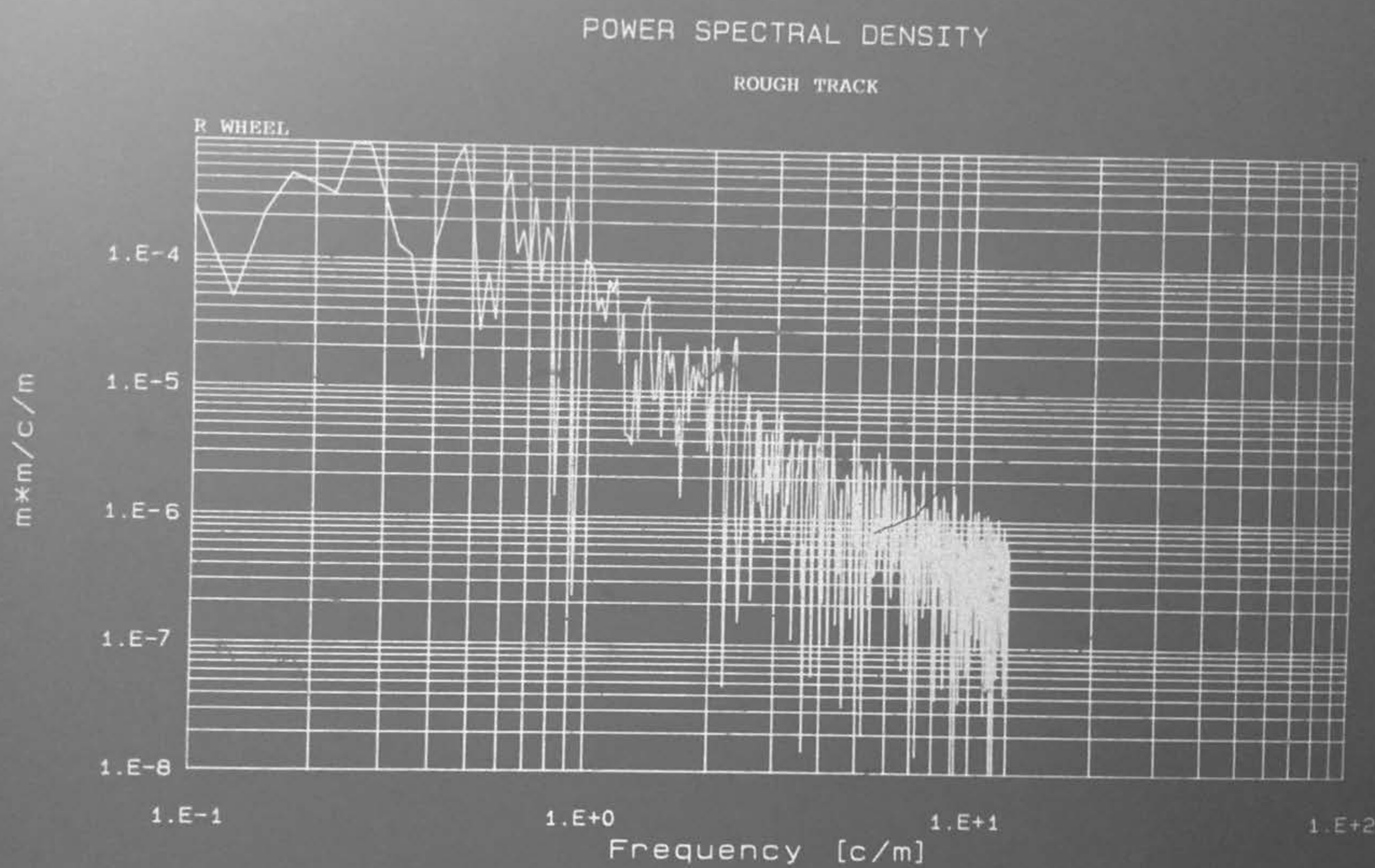
POWER SPECTRAL DENSITY
ROUGH TRACK
R WHEEL
m*m/c/m
1.E-4
1.E-5
1.E-6
1.E-7
1.E-8
1.E-1
1.E+0
1.E+1
1.E+2
Frequency [c/m]

FIGURE L10

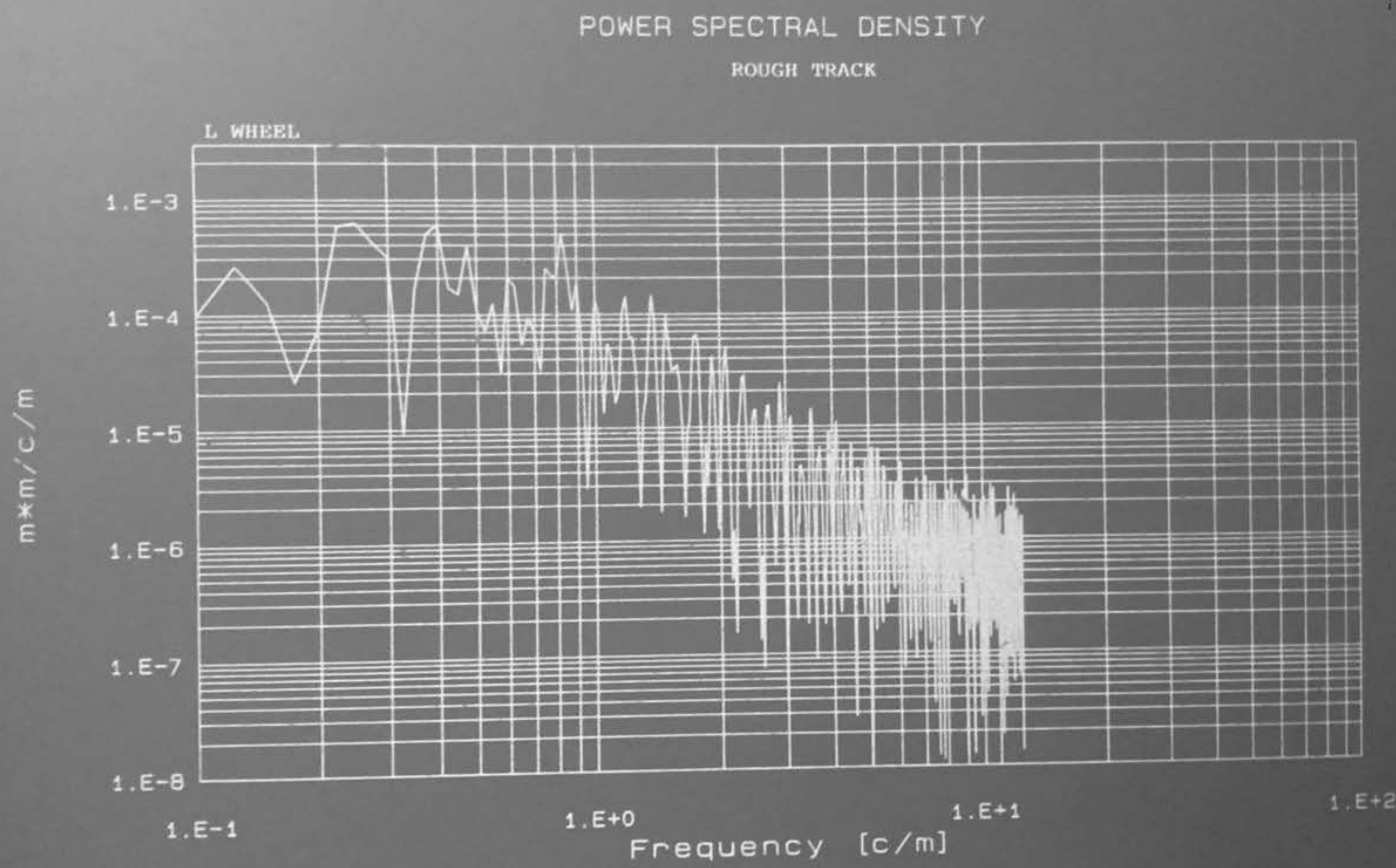
POWER SPECTRAL DENSITY
ROUGH TRACK
L WHEEL
m*m/c/m
1.E-3
1.E-4
1.E-5
1.E-6
1.E-7
1.E-8
1.E-1
1.E+0
1.E+1
1.E+2
Frequency [c/m]

FIGURE L11

APPENDIX M

THE EFFECT OF CURVES IN THE ROAD ON THE MEASURING PROCESS

Refer to figure 5.1. for a diagram of the measuring cart.

There are two obvious possibilities:

1. The wheelset is the inside wheel in the curve:

   ⇒ The wheelset, with the proximity switch mounted beside one of it's wheels, will continue to sample at 'ds' distances.
   ⇒ The other wheel will sample at longer distances because it is moving at a faster speed.

2. The wheelset is the outside wheel in the curve.
   ⇒ The wheelset will continue to sample at 'ds' distances.
   ⇒ The other wheel will sample at shorter distances than 'ds'.

Important parameters in the sampling process are:

1. The wheel diameter – This dimension is also the size of the smallest wavelength to be measured with reasonable accuracy and is therefore the lower limit of the wavelength bandwidth.
2. The sampling distance – It is necessary to sample the smallest wavelength at least twice so as to reduce the aliasing effect.

In the light of these two parameters the worst case of the two possibilities mentioned above is that where the wheelset is in the inside. The lower limit wavelength of the other wheel is the diameter of that wheel, D. The sampling pulse is generated by the wheelset wheel every 'ds_l' meter irrespective of the speed at which the wheelset wheels turn. Should the other wheel go at a faster speed then the sampling distance at this wheel would increase to say ds_o. If ds_o would increase to more than the half of the other wheel diameter, D/2 then aliasing would occure and the smallest wavelength D would be measured with error. It is necessary therefore to define the smallest curve radius which would be allowed in order to prevent this. The following parameters are defined:

Outer wheel diameter	D	[m]
Outer wheel speed	ν_o	[m/s]
Wheelset wheel diameter	d	[d]
Wheelset wheel speed	ν_l	[m/s]
Wheeldiameter ratio	$d/D = r$	

Sampling distance:

Wheelset wheel	$ds_l = \dfrac{\pi d}{r}$	[m]
Outer wheel	ds_o	[m]

($ds_l = ds_o$ with straight movement)

Track width	ℓ	[m]
Towing speed	ν	[m/s]
Curve radius	R	[m]

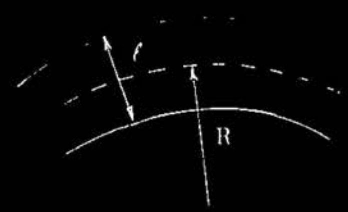

$$\text{Now } \nu_o = \frac{R + {}^{\ell}/2}{R}\,\nu \text{ and } \nu_{\ell} = \frac{R - {}^{\ell}/2}{R}\,\nu$$

$$\text{Therefore } \frac{\nu_o}{\nu_{\ell}} = \frac{(R + {}^{\ell}/2)}{(R - {}^{\ell}/2)}$$

The relationship between the sampling distances ds_o and ds_{ℓ} is as explained above and therefore it can be written that $ds_o = \frac{\nu_o}{\nu_{\ell}}\, ds_{\ell}$ where ds_{ℓ} is constant.

$$\therefore \qquad ds_o = \frac{\nu_o}{\nu_{\ell}}\,\frac{\pi}{7}\,d$$

$$\Rightarrow \qquad ds_o = \frac{\pi}{7}\,\frac{(R + {}^{\ell}/2)}{(R - {}^{\ell}/2)}\,d$$

The value of ds_o is restricted by the outer wheel diameter and should be less than D/2 as stated before. Therefore

$$\frac{D}{2} \geq \frac{\pi}{7}\,\frac{(R + {}^{\ell}/2)}{(R - {}^{\ell}/2)}\,d$$

$$\Rightarrow \quad \frac{R}{\ell} > \frac{\left[\frac{2\pi d}{14} + \frac{D}{2}\right]}{\left[D - \frac{2\pi d}{7}\right]}$$

Thus for the typical situation where $d = 0.15$ m and $D = 0{,}25$ m the condition is that the curve radius should be 1.7 times larger than the track width ℓ.

This implies a very sharp curve which is unlikely to occur in a stretch of selected for measurement. The conclusion is therefore that gradual curves with radii greater than at least two times the track width would not influence the measured data notably.

REFERENCES

1. Beamgard RS, Snodgrass KP, Stornant RF (1979)
'A Field Performance Prediction Technique for Light Truck Structural Components'
Truck and Recreation Products Operations, Ford Motor Company SAE Technical Paper 791034, 1979.

2. Bekker MG (1962)
'Theory of Land Locomotion'
Ann Arbor, The University of Michigan Press.

3. Bekker MG (1969)
'Introduction to Terrain-Vehicle Systems'
Ann Arbor, The University of Michigan Press.

4. Bendat JS, Piersol AG (1979)
'Random Data : Analysis and Measurement Procedures'
Wiley-Interscience, 1971.

5. Brüel & Kjaer
'Technical Review
No 3, 1987, No 4, 1987.

6. Brüel & Kjaer
'Digital Signal Analysis : Using Digital Filters and FFT Techniques'
Selected Reprints from Technical Review.

7. Bulman DN (1979)
'Cross Country Vehicle Ride Simulation'
Automotive Engineer, vol 4, 1979.

8. Cebon D, Newland DE
'Artificial Generation of Road Surface Topography by the Inverse FFT Method'
IAVSD Extensive Summaries.

9. Collins WI (1981)
'Failure of Materials in Mechanical Design'
Wiley & Sons, 1981.

10. Conover JC (1966)
'Simulation of Field Loading in Fatigue Testing'
SAE Technical Paper 660102.

11. Cote LJ, Kozin F, Bogdanoff JL (1965)
'Introduction to a Statistical Theory of Land Locomotion - I'
Journal of Terramechanics, Vol 2 no 2, 1965.

12. Cote LJ, Kozin F, Bogdanoff JL (1965)
'Introduction to a Statistical Theory of Land Locomotion – II – Ground Roughness'
Journal of Terramechanics, Vol 2 No 3, 1965.

13. Crolla DA, Maclaurin EB, (1986)
'Theoretical and Practical Aspects of the Ride Dynamics of Off–road Vehicles – part 2'
Journal of Terramechanics, Vol 23 No 1, 1986.

14. Dodds CJ (1972)
'The Response of Vehicle Components to Random Road Surface undulations'
PhD Thesis, University of Glasgow.

15. Dowling NE (1982)
'A Discussion of Methods for Estimating Fatigue Life'
SAE Technical Paper 820691.

16. Ewins DJ (1986)
'Modal Testing : Theory and Practice'
Research Studies Press Ltd, Hertfordshire, England.

17. Fujimoto Y (1983)
'Spectrum Analysis of Road Roughness for Earthmoving Machinery'
Journal of Terramechanics Vol 20 No 1, 1983.

18. Gillespie TD (1984)
'Developing an International Standard for Measuring Road Roughness' – An Interview'
UMTRI Reseearch Review, Vol 14 No 6, 1984.

19. Helfmann R
'World–wide Measurement of Operational Profiles and their True–time Simulation in the Laboratory'
Adam opel Ag.

20. Hofmeister WF (1959)
'Application of the Cumulative Fatigue Damage Theory to Practical Problems'
SAE Transactions, Vol 68, 1960.

21. Hunter AGM (1979)
'Characterisation of Rough Ground using an Accelerometer for Measurement'
Journal of Terramechanics, Vol 16 No 1, 1979.

22. Hunter AGM, Sm[illegible] (1980)
'Filtering Errors when a Rigid Wheel is used to Measure Ground Roughness'
Journal of Te[illegible], Vol 1[illegible], No 1, 1980

23. Jackel HR (1982)
'Design Validation Testing'
Ford Motor Company, SAE Technical Paper 820690.

24. Jenkins GM (1961)
'General Considerations in Analysis of Spectra'
Technometrics Vol 3 No 2, 1961.

25. Kaneshige I (1969)
'Application of the Probability Theory to the Design Procedure of an Endurance Test Track Surface'
ISUZU Motors, SAE Technical Paper 690111.

26. Kaplan W (1980)
'Advanced Mathematics for Engineers'
Addison-Wesley Publishing Company, University of Michigan.

27. Kozin F, Cote LJ, Bogdanoff JL (1963)
'Statistical Studies of Stable Ground Roughness'
US Army Tank-Automotive Center, Warren, Michigan.

28. Laib L
'Measurement and Mathematical Analysis of Agricultural Terrain and Road Profiles'
Journal of Terramechanics, Vol 14 No 2, 1977.

29. Landgraf RW, La Pointe NR (1974)
'Cyclic Stress-Strain Concepts Applied to Component Fatigue Life Prediction'
Ford Motor Co. SAE Technical paper 740280.

30. Michelberger P, Gedeon J, Keresztes A (1980)
'Problems and Development in Commercial Road Vehicle Fatigue and Testing'
University of Budapest, Hungary
Journal of Vehicle Design, Vol 1 no 5, 1980.

31. Murphy RW (1982)
'Endurance Testing of Heavy Duty Vehicles'
L Ray Buckendal Lecture
SAE Technical Paper 820001.

32. Nelson DV, Fuchs HO
'Predictions of Cumulative Fatigue Damage Using Condensed Load Histories'
Stanford University, based on SAE Paper 750045.

33. Newland DE (1984)
'An Introduction to Random Vibrations and Spectral Analysis'
Longman Group Ltd, Essex, England.

34. Ohmiya K (1986)
'Characteristics of Farm Field Profiles as Sources of Tractor Vibration'
Journal of Terramechanics vol 23 No 1, 1986.

35. Osgood CC (1982)
'Fatigue Design'
Pergamon Press, 1982.

36. Raasch W (1979)
'Photometric Measurement of Terrain Roughness'
Journal of Terramechanics, Vol 16 No 2, 1979.

37. Sayles RS, Thomas TR (1978)
'Surface Topography as a Non-stationarity Random Process'
Nature, Vol 271, 1978.

38. Spangler EB, Kelly WJ (1964)
'GMR Road Profilometer'
General Motors Research Laboratories. GMR-452.

39. Smith KV, Stornant RF (1979)
'Cumulative Damage Approach to Durability Route Design'
SAE Technical Paper 791033.

40. Strahler AN (1956)
'Quantitative Slope Analysis'
Bulletin of the Geological Society of America Vol 67, 1956.

41. Thomson WT, (1983)
'Theory of Vibration with Applications'
George Allen & Unwin, London, 2nd Edition.

42. Van Deusen BD
'A Statistical Technique for the Dynamic Analysis of Vehicles Traversing Rough Yielding and Non-yielding Surfaces'
Research Report, Chrysler Motor Corporation Ltd.

43. Van Deusen BD, McCarren GE (1967)
'A New Technique for Classifying Random Surface Roughness'
Chrysler Corporation, SAE Technical Paper 670032.

44. Van der Merwe CJ, Grant MC
'A Simple Instrument for the Assessment of Road Riding Quality'
Report RC/8/80, CSIR, 1980.

45. Wendenborn JG (1965/66)
'The Irregularities of Farm Roads and Fields as sources of Farm Vehicle Vibrations'
Journal of Terramechanics, Vol 3 No 3, 1966.